AD-A113 766 DAYTON UNIV OH RESEARCH INST F/G 17/2
ACCELERATED LIFE PREDICTION TECHNIQUES.(U)
NOV 81 K DAVIS, M KELLER, R MARTIN F33615-78-C-5107
UNCLASSIFIED UDR-TR-81-90 AFWAL-TR-81-4137 NL

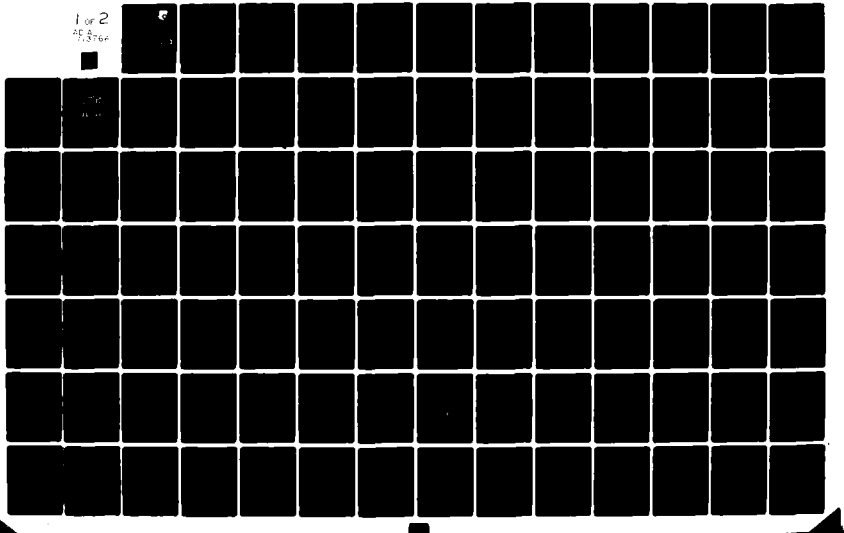

AFWAL-TR-81-4137

ACCELERATED LIFE PREDICTION TECHNIQUES

K. Davis
M. Keller
R. Martin

University of Dayton Research Institute
300 College Park Avenue
Dayton, Ohio 45469

November 1981

Final Report for Period 31 July 1978 - 31 May 1981

Approved for public release; distribution unlimited

MATERIALS LABORATORY
AIR FORCE WRIGHT AERONAUTICAL LABORATORIES
AIR FORCE SYSTEMS COMMAND
WRIGHT-PATTERSON AIR FORCE BASE, OHIO 45433

NOTICE

When Government drawings, specifications, or other data are used for any purpose other than in connection with a definitely related Government procurement operation, the United States Government thereby incurs no responsibility nor any obligation whatsoever; and the fact that the government may have formulated, furnished, or in any way supplied the said drawings, specifications, or other data, is not to be regarded by implication or otherwise as in any manner licensing the holder or any other person or corporation, or conveying any rights or permission to manufacture use, or sell any patented invention that may in any way be related thereto.

This report has been reviewed by the Office of Public Affairs (ASD/PA) and is releasable to the National Technical Information Service (NTIS). At NTIS, it will be available to the general public, including foreign nations.

This technical report has been reviewed and is approved for publication.

Wayne E. Ward

W.E. WARD, Project Engineer
Fluids, Lubricants & Elastomers Branch
Nonmetallic Materials Division

B.D. McConnell

B.D. McCONNELL, Chief
Fluids, Lubricants & Elastomers Branch
Nonmetallic Materials Division

FOR THE COMMANDER:

F.D. Cherry

F.D. CHERRY, Chief
Nonmetallic Materials Division

"If your address has changed, if you wish to be removed from our mailing list, or if the addressee is no longer employed by your organization, please notify AFWAL/MLBT, WPAFB, OH 45433 to help us maintain a current mailing list."

Copies of this report should not be returned unless return is required by security considerations, contractual obligations, or notice on a specific document.

Unclassified

SECURITY CLASSIFICATION OF THIS PAGE (When Data Entered)

REPORT DOCUMENTATION PAGE		READ INSTRUCTIONS BEFORE COMPLETING FORM
1. REPORT NUMBER AFWAL-TR-81-4137	2. GOVT ACCESSION NO. AD-A113764	3. RECIPIENT'S CATALOG NUMBER
4. TITLE (and Subtitle) ACCELERATED LIFE PREDICTION TECHNIQUES		5. TYPE OF REPORT & PERIOD COVERED Final Report 31 Jul 78 - 31 May 81
		6. PERFORMING ORG. REPORT NUMBER UDR-TR-81-90
7. AUTHOR(s) K. Davis, M. Keller, and R. Martin		8. CONTRACT OR GRANT NUMBER(s) F33615-78-C-5107
9. PERFORMING ORGANIZATION NAME AND ADDRESS University of Dayton Research Institute 300 College Park Ave. Dayton, OH 45469		10. PROGRAM ELEMENT, PROJECT, TASK AREA & WORK UNIT NUMBERS P.E. 62102F, Project No. 2421 Task 242102, Work Unit 24210204
11. CONTROLLING OFFICE NAME AND ADDRESS Materials Laboratory (AFWAL/MLBT) Air Force Wright Aeronautical Laboratories, AFSC Wright-Patterson Air Force Base, Ohio 45433		12. REPORT DATE November 1981 13. NUMBER OF PAGES 114
14. MONITORING AGENCY NAME & ADDRESS(if different from Controlling Office)		15. SECURITY CLASS. (of this report) 15a. DECLASSIFICATION DOWNGRADING SCHEDULE
16. DISTRIBUTION STATEMENT (of this Report) DISTRIBUTION STATEMENT A Approved for public release; Distribution Unlimited		
17. DISTRIBUTION STATEMENT (of the abstract entered in Block 20, if different from Report)		
18. SUPPLEMENTARY NOTES		

19. KEY WORDS (Continue on reverse side if necessary and identify by block number)

analysis	data transmission slip ring	lubrication
automated data acquisition	degradation	proximity sensor
bearing	despin mechanical assembly	satellite
chromatography	load cell	vacuum
correlation coefficient	lubricant	Vac Kote

20. ABSTRACT (Continue on reverse side if necessary and identify by block number)

Exploratory development was conducted in the area of accelerated life prediction techniques for satellite despin mechanical assembly bearings and data transmission slip ring assemblies Slip ring assemblies were instrumented and operated in a simulated space environment. Data was taken and analyzed. Bearing test rigs were set up, instrumented and operated. Studies were conducted to determine the chemical and physical properties of the commonly used space lubricant. Degradation studies of this material were also conducted.

DD FORM 1 JAN 73 1473 EDITION OF 1 NOV 65 IS OBSOLETE

Unclassified

SECURITY CLASSIFICATION OF THIS PAGE (When Data Entered)

FOREWORD

This final report was prepared by the University of Dayton Research Institute, Dayton, Ohio under United States Air Force Contract F33615-78-C-5107. This contract was initiated under Project No. 2421. The work was administered under the direction of the Nonmetallic Materials Division, Materials Laboratory, Air Force Wright Aeronautical Laboratories, Wright-Patterson Air Force Base, Ohio.

This report covers work conducted from 31 July 1978 through 31 May 1981 in accelerated life prediction techniques for satellite despin mechanical assembly bearings and data transmission slip ring assemblies.

TABLE OF CONTENTS

TABLE OF CONTENTS (concluded)

LIST OF ILLUSTRATIONS

LIST OF ILLUSTRATIONS (continued)

LIST OF ILLUSTRATIONS (concluded)

LIST OF TABLES

LIST OF ABBREVIATIONS

A/D - analog to digital
AUFS - Absorbance Units Full Scale
AVG - Average Value
d - deviation of actual values
db - decibels
D.C. - Direct Current
DEC - Digital Equipment Corporation
DEF - Brush Deflection
DODPA - Dioctyldiphenylamine
DVM - Digital Volt Meter
ECD - Electrical Conductivity Detector
FFT - Fast Fourier Transform
FID - Flame Ionization Detector
g - grams
Hz - Hertz unit of frequency equal to one cycle per second
I/O - inner to outer race resistance
IR - Infrared
KΩ - kilohms
LC - Liquid Chromatography
ml - milliliters
mNm - millinewton meters
mΩ - milliohms
mV - millivolts
N - newtons
nm - nanometers
Pa - Pascals
PK - Peak Value
RHO or R - index of correlation
RI - refractive index
SE - standard error of estimate
S/N - signal to noise
SPM - Shaft Position Marker
σ - standard deviation
TGA - thermogravimetric analysis
UDRI - University of Dayton Research Institute
UV - ultraviolet
XPS - X-ray Photoelectron Spectroscopy

DEFINITIONS OF TERMS

1. "average" data - The mathematical average value of the data during the previous 5 seconds.

2. "raw" data - A data signal from a sensor that has not been altered other than by the normal sensor signal conditioner functions of scaling, zeroing, and demodulation.

3. "peak" data - The current instantaneous deviation (plus or minus) of a data signal from its "average" value. The absolute value of the deviation is output and therefore always positive.

4. "peak average" data - The mathematical average value of "peak" data signal during the previous 5 seconds.

5. "anti-alias" data - Is "raw" data minus frequencies which can be introduced into the data by the digital part of the data acquisition system. Valid data is all raw data of less than 400 Hz.

6. "processed" data - Is "raw" data which has been processed into parameters of peak, average, minimum, etc.

7. "minimum" data - The average value of the negative-going peaks of a data signal during the previous 5 seconds.

8. "maximum" data - The average value of the positive-going peaks of a data signal in the previous 5 seconds.

SECTION I
INTRODUCTION AND BACKGROUND

1. PROJECT BACKGROUND

The objective of this contract is to develop the instrumentation and analytical techniques that are required to evaluate the mechanisms and rate of degradation of components of the despin mechanical assembly (DMA) used in satellites. The specific components of interest consist of the data transmission slip ring assembly, the bearing assembly, and the lubricants used on each assembly. The configuration of a typical satellite where these components are used consists of an electronics package built around a central shaft. An antenna is mounted on the central shaft. All data to and from the satellite is transmitted through the antenna assembly. Because of the small power usually available in the satellite's transmitters, the antenna must be highly directional and pointed to a specific point on earth towards the receiving station in order to improve the signal-to-noise ratio and insure data reliability in transmission. To accomplish this, the outer portion of the satellite is spun around the central shaft creating a gyroscope effect that will stabilize the attitude of the satellite. The antenna can then be oriented to point towards the required position on the earth. Such a satellite is illustrated in Figure 1.

The purpose of the despin mechanical assembly is to prevent the antenna and central shaft from spinning while allowing the outer portion of the satellite to rotate. Also, the DMA allows the transfer of power and/or data to and from the stabilized antenna to the rotating electronics package. The components which are the subject of this research effort consist of lubricated DMA bearing assemblies and lubricated DMA data transmission slip ring assemblies. Such a DMA is illustrated in Figure 1.

Failures of DMA components are suspected by the Air Force to have caused either partial or total loss of data from certain satellites. Degradation of both DMA bearings and DMA slip rings

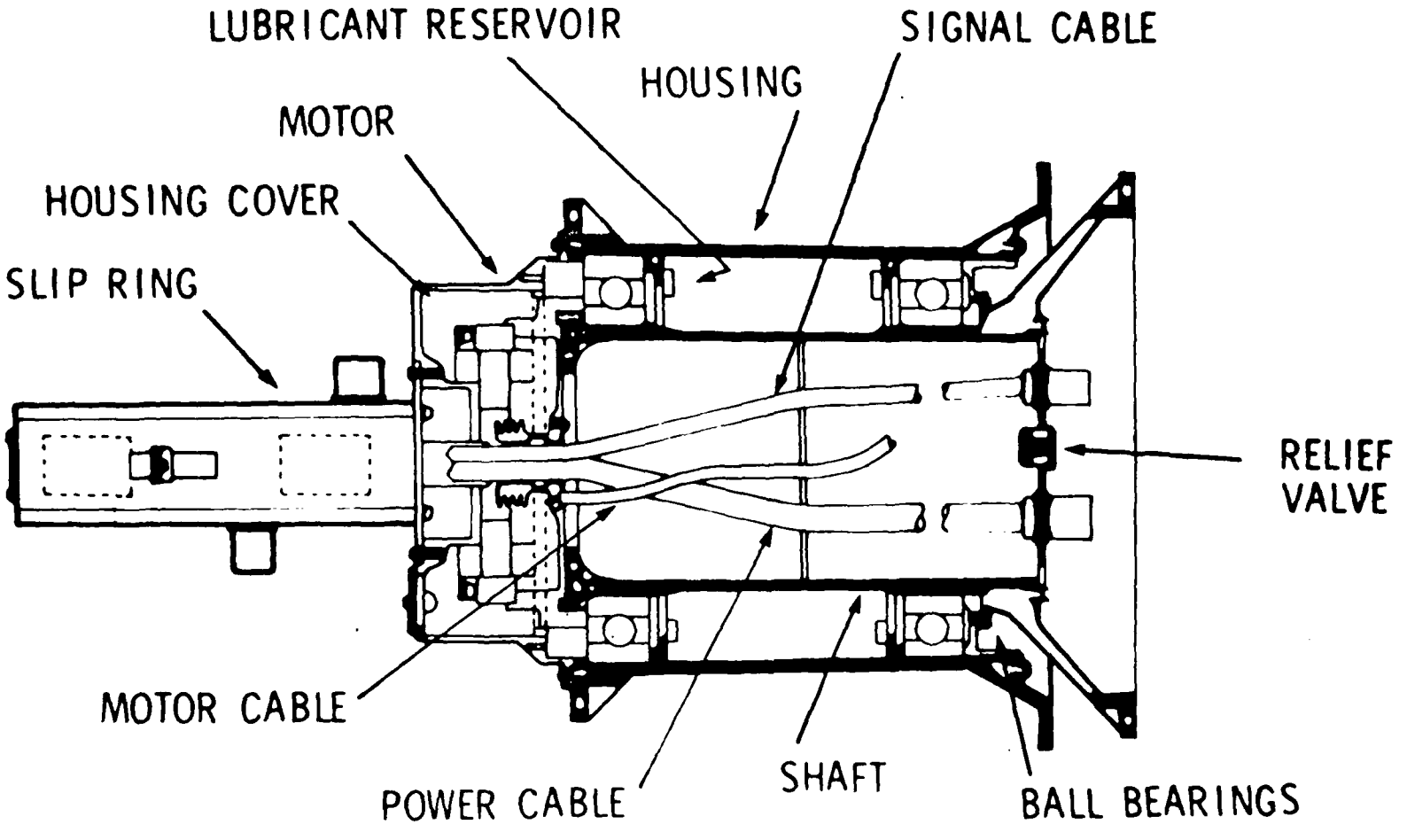

Figure 1. Despin Mechanical Assembly.

may result in degraded data transmission and reception. If the DMA bearings degrade beyond a certain point, they will cause the antenna to lock up or wobble causing an unstabilized condition which results in errors in the pointing accuracy of the antenna at the earth. If the pointing errors are small, they may cause either no loss or only a temporary loss of data or cause errors in the data transmission. However, if the pointing errors are very large, it may be impossible to regain communication with the satellite, and it may be lost completely. Degradation of the electrical contact of the data transmission slip rings and brushes may cause noise generation at the electrical contact point, therefore reducing the signal-to-noise ratio of data signal. This reduction, coupled with low transmitter power, atmosphere effects, and other interference, may cause either a temporary loss of data or errors in transmitted data. If the slip ring/brush contact degrades excessively, it may cause noise "spikes" in the transmitted data which cannot be discerned from actual data, therefore causing unrecoverable data errors.

To study the mechanisms and the rates of degradation of DMA components, the University of Dayton Research Institute (UDRI) has developed the instrumentation and experimental techniques to conduct both long-term and short-term tests on these assemblies. Results of these studies will be used as inputs to the Materials Laboratory's mathematical performance models of both slip rings and bearings. Parameters used in these models will be tested with the data provided by these instrumentation systems to verify the models' accuracy and reliability. The Air Force proposes to use these models to enable the prediction of lifetimes of DMA components under various conditions while using a wide variety of different materials and lubricants. Once this is accomplished, an optimum design of DMA components may be specified for each specific set of operating conditions encountered. This will improve the operating efficiency, reliability, and lifetime of many satellites, thus reducing the cost associated with satellite operations.

SECTION II
SLIP RING DEGRADATION STUDIES

1. SLIP RING INSTRUMENTATION

The slip ring test systems were designed and constructed to provide the measurement capability needed in order to study the slip ring/brush contact degradation referred to in Section I. The test systems developed consist of four instrumented test rigs. One of the test rigs is intended for the long-term (2 1/2) years) operation of two slip ring and brush sets, while the other three are intended for the short-term operation of a single slip ring and brush for mechanistic studies. The electronics, instrumentation, and sensors used on all slip ring test rigs are identical. These test systems have been covered in detail in previous reports.[1,2] Therefore, only a short description of the instrumentation will be presented here. A detailed discussion of long-term slip ring rig software is contained in a technical report on the subject.[3]

A. System Description

The design of the long-term slip ring data system was influenced by several factors which were considered vital to the success of the program. Factors of critical importance to the effort were the measurement of brush micromotions at the brush/ring contact, measurement of the friction force at the brush/ring contact, and measurement of the brush/ring contact resistance. Also, a system for recording moderate frequency data which would provide a permanent data record was required. Because of the length of the experiment and the number of parameters, it was imperative that the experiment and critical functions be monitored on a continuous basis and that data be recorded which exhibited significant changes in the critical operational parameters.

The system conceived to meet these objectives is shown in the block diagram of Figure 2. As shown, the analog data processing block outputs are routed to data recorders and a

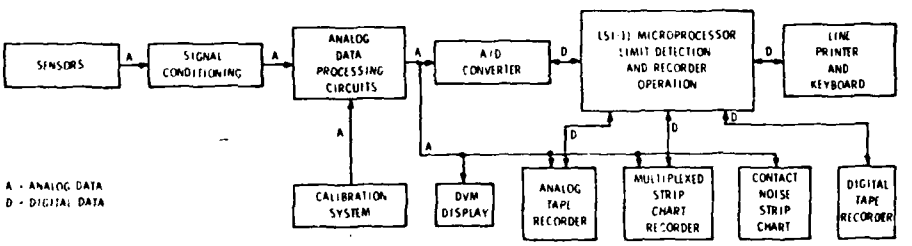

Figure 2. Slip Ring Data Acquisition System Block Diagram

microprocessor-controlled analog-to-digital (A/D) converter. Through the A/D converter the LSI-11 microprocessor compares current voltage values to limit values which are initially entered by the operator and which define a normal voltage range for each channel. When a limit value is exceeded by a respective channel, the microprocessor enables a subroutine which records a complete set of data. Average, peak, and instantaneous values of critical parameters are monitored to determine changes in various qualities of the parameters.

Signal frequencies to 10 KHz may be processed on most of the data channels and frequencies in excess of 40 KHz may be processed on selected critical data channels. The key to this system is the analog data processing circuits which greatly reduce the performance requirements of the microprocessor. These circuits process the raw high frequency sensor outputs and provide processed average and peak inputs to the A/D converters. The average and peak signal value changes are typically at less than a 100 Hz rate; a much lower frequency than the original raw sensor outputs. This hybrid processing scheme permits the use of a slower microprocessor and A/D converters and greatly simplifies software since the microprocessor does no computing; only signal value versus set limit comparisons. If a compare function detects a parameter outside of its limits, the analog and digital tape recorders are commanded by the microprocessor to record at least one slip ring revolution of each data parameter. A strip chart recorder with multiplexed data inputs is also enabled. Also, 20 data parameters may be accessed for continuous display on a digital voltmeter by the system operator. The average contact resistance at the brush/slip ring interface is continuously recorded on a strip chart recorder to provide an operational signature over extended time periods.

B. Sensor Selection and Installation

The measurement of the vertical micromotions of the brush at the slip ring/brush contact was considered to be critical

to the program. Proximity sensors of the eddy current type were selected to make this measurement. The sensor is oriented, as shown in Figure 3, to detect the movement of a 3.12 mm square nickel foil surface. This surface or "sail" is part of an assembly laser welded from .002 inch thick nickel foil. The assembly is laser welded to the slip ring brush. The sensors have a 0.5 mm full scale range, and through special gain and zeroing amplifiers are calibrated to make a position measurement to a resolution of 0.5 micron. A more detailed view is illustrated in Figure 4.

A second parameter which was considered critical to the conduct of the study of the slip ring/brush interface was the friction force at this conjunction. A load cell, having a 50 gram full scale range, was selected to measure the friction force and is used in the assembly shown in Figure 3. The load cell (3) is preloaded to 40 grams by the support springs (5) through the coupling wire (1). This preload places the operational range close to the full scale load where the linearity characteristics of the sensor are best for small load variations. The operational configuration is such that the friction force places the coupling wire in tension. In this view, the slip ring rotation is counterclockwise.

As would be expected, the determination of the electrical resistance of the test slip ring/brush conjunction is of prime importance. The determination is made by measuring the voltage developed by a constant 50 ma current which flows through the circuit. The circuit consists of four slip ring/ brush sets connected in parallel through which the current enters the circuit, and a single instrumented "data" slip ring/brush set from which the current exits the circuit. The four input sets provide a redundant input to the single "data" brush which is instrumented to measure both friction forces and vertical brush micro-motions. The slip ring/brush voltage measurement provides a continuous analog data signal of slip ring/brush contact resistance. Also a digital indication of

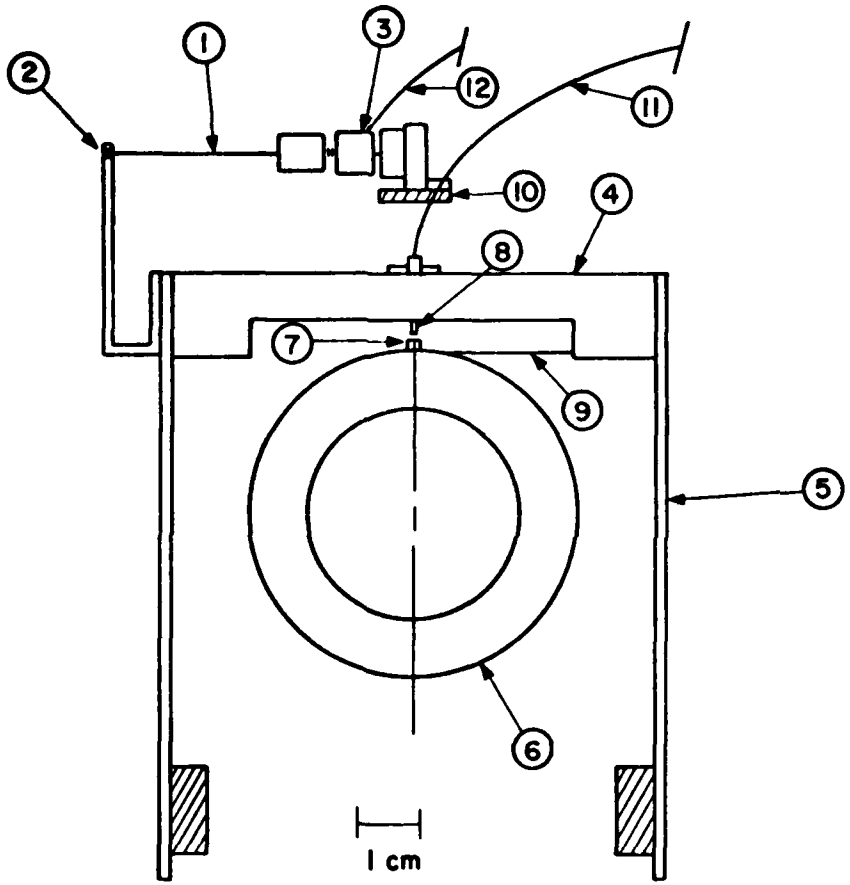

① NICKEL WIRE
② ARM
③ FRICTION SENSOR (LOAD CELL)
④ BRUSH BLOCK
⑤ SPRING
⑥ SLIP - RING
⑦ VERTICAL SAIL
⑧ VERTICAL SENSOR (PROXIMITY)
⑨ BRUSH
⑩ STATIONARY SUPPORT (CROSS SECTION)
⑪ VERTICAL SENSOR CABLE
⑫ FRICTION SENSOR CABLE

Figure 3. Slip Ring Assembly.

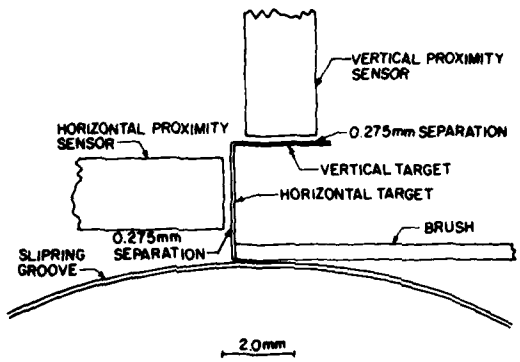

Figure 4. Details of Slip Ring Sensors and Target.

contact performance is generated by connecting a standard transistor-transistor logic (TTL) gate to the contact noise signal. Since the constant current source is excited by a +5VDC voltage source, the TTL gate generates pulses when contact resistance or brush bouncing causes a two volt or greater signal. This signal is termed "logical noise". The presence of a "logical noise" signal would indicate that the contact resistance is at a level which would cause errors in a digital data transmission through the slip ring/brush contacts. Other parameters are measured by conventional means. These include motor speed by a DC generator/tachometer, motor current by the voltage developed across a fixed resistor and the test chamber vacuum pressure to 10^{-4} pascals by an ionization gauge. Duplicate sensors and electronics have been constructed so that the performance of two "data" slip rings may be monitored in the single long-term experiment. Data slip ring/brush sets are mounted on each end of the assembly.

C. Analog Data Processing Circuits

Twelve specially designed circuit cards have been constructed to process raw sensor data for input to the A/D converter and data recorders. Each circuit card has dual circuitry to process inputs from two data slip rings. A block diagram and a schematic of one of the two data channels of the vertical deflection processing circuit card is shown in Figure 5. This is representative of a typical processing circuit card. The proximity sensor signal conditioner output is applied to the circuit input (pins 1 and 2), and then into a balanced differential amplifier which provides for scaling to engineering units of millimeters (mm) and also zeroing controls. Its output on pin 3 is termed the "raw" or "unprocessed" data parameter. Also, it outputs to the peak and antialias (A/A) circuits. The peak detector processing consists of computer controlled zeroing switches, a high pass 5-hertz filter, a full wave rectifier, a peak detector, and a low pass 400 Hz filter. The peak detector itself consists of a comparator and a sample-and-hold. The sample-and-hold consists of a diode (DI) controlled

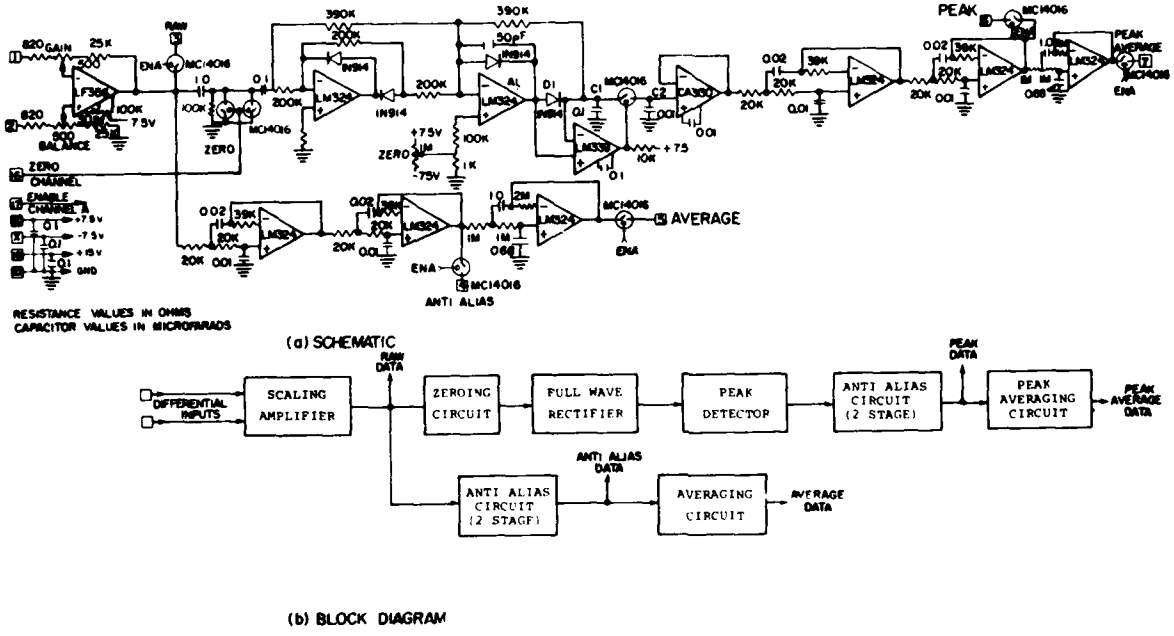

Figure 5. Schematic and Block Diagram of Vertical Deflection Processing Circuit.

comparator which compares past peak values stored on C1 to current peak values from rectifier A1. When a 0.7 volt difference is detected the new peak value is transferred by switch S2 to holding capacitor C2. The output on pin 6 is the "peak" signal. The "peak" signal is then output to a 0.5 Hz low pass filter which acts as an averaging circuit to produce the "peak average" signal on output pin 7.

The "raw" data signal is also input to the antialias (A/A) circuit which is a low pass 400 Hz filter and output on pin 4 as the A/A signal. This signal is then averaged by another 0.5 Hz low pass filter to produce an "average" data signal. The "raw" data signal is used only for high frequency analog tape recordings while all other data signals are input through the A/D converter to the microprocessor. The 400 Hz filter is necessary to prevent unwanted "alias" frequencies from being produced by the combination of data signals and the 1000 samples-per-second rate of the A/D converter. The average signal represents a trend indicating the amount of brush and ring wear. The "peak" signal represents the degree of instantaneous surface roughness on the slip ring, while the "peak average" signal indicates trends in these peak values. Table 1 indicates all parameters that are measured and processed by the sensor and analog data processing systems.

D. Data and Data Reduction

Data is recorded on the microprocessor controlled analog tape recorder from each data burst. Data channels 1, 2, 3, and 4 record logical contact noise, analog contact resistance, friction force, and brush vertical deflection continuously for seven slip ring revolutions; while channels 5 and 6 multiplex several data parameters with each being recorded for one revolution each. Channel 7 records data identification in a digital format which indicates the cause of each data burst, the hours of operation, test number, calibration reference code, and a code indicating the data parameters being multiplexed. The

TABLE 1

SLIP RING SENSOR AND DATA SYSTEM PARAMETERS

SENSOR	PARAMETER MEASURED	PARAMETERS DERIVED			
1. EDDY CURRENT PROXIMITY SENSOR	VERTICAL BRUSH MOTION	ECCENTRICITY	RAW AVERAGE ANTI ALIAS PEAK PEAK AVG.	DEFLECTION	RAW AVERAGE ANTI ALIAS PEAK PEAK AVG
2. STRAIN GAUGE LOAD CELL	BRUSH/RING FRICTION FORCE	FRICTION	RAW AVERAGE ANTI ALIAS PEAK PEAK AVG		
3. CONSTANT CURRENT SOURCE	BRUSH/RING CONTACT RESISTANCE (NOISE)	ANALOG	RAW AVERAGE ANTI ALIAS PEAK PEAK AVG	DIGITAL	PULSES PER REV. PULSE WIDTH PULSE WIDTH AVG. PULSE RATE PULSE RATE AVG
4. CURRENT SENSING RESISTOR	MOTOR CURRENT	MOTOR CURRENT	RAW AVERAGE		
5. D.C. GENERATOR/TACH	MOTOR SPEED	MOTOR SPEED	AVERAGE		
6. THERMOCOUPLE	TEMPERATURE	TEMPERATURE	RAW		
7. IONIZATION GAUGE	VACUUM PRESSURE	PRESSURE	AVERAGE		

bandwidth of the recorder is D.C. to 40 KHz on all channels except channel 1 (logical contact noise) which is to 300 KHz. The analog tape data is processed by a separate computer facility to generate a fast Fourier transform (FFT) spectrum of the parameters of contact resistance, friction force, and vertical deflection. By using the spectral data in conjunction with the other data parameters illustrated in Table 1, it is expected that a determination can be made as to whether friction forces or vertical motion is causing slip ring contact resistance (noise) variations. This can be determined both at different operational times and at different points around the slip ring. The slip ring is etched and the mark synchronized with the recorded data by an optical shaft position marker (SPM); so that at the conclusion of the experiment a surface analysis of the slip ring can be correlated with the recorded data.

2. SLIP RING DATA

Data plots of contact resistance from five slip rings are presented in Figures 6 to 13. Figures 6 and 7 are from the long-term slip ring experiment, while Figures 8 to 13 are of the slip ring unit rig experiments. The long-term rig operates at a constant 60 rpm speed, while the unit rigs operate at variable speeds.

Each of the three slip ring unit rigs has been operating first at a high rpm for either 48 or 72 hours and then at 60 rpm for two hours and then repeating. Data is recorded at both high and low rpm. The set up parameters of the slip ring rigs is as shown in Table 2. All rigs operate in a minimum vacuum of 10^{-4} Pascals (10^{-6} torr) or greater and at room temperature.

The wear-in period for long-term slip ring A (Figure 6) was 1800 hours and estimated as 1200 hours for slip ring B, although the period for B is not clearly defined by the data. Wear-in was arbitrarily defined as the elapsed time at which the initial high resistance values at the start of operation fell to a lower and stable level. The rotary drive shaft vacuum

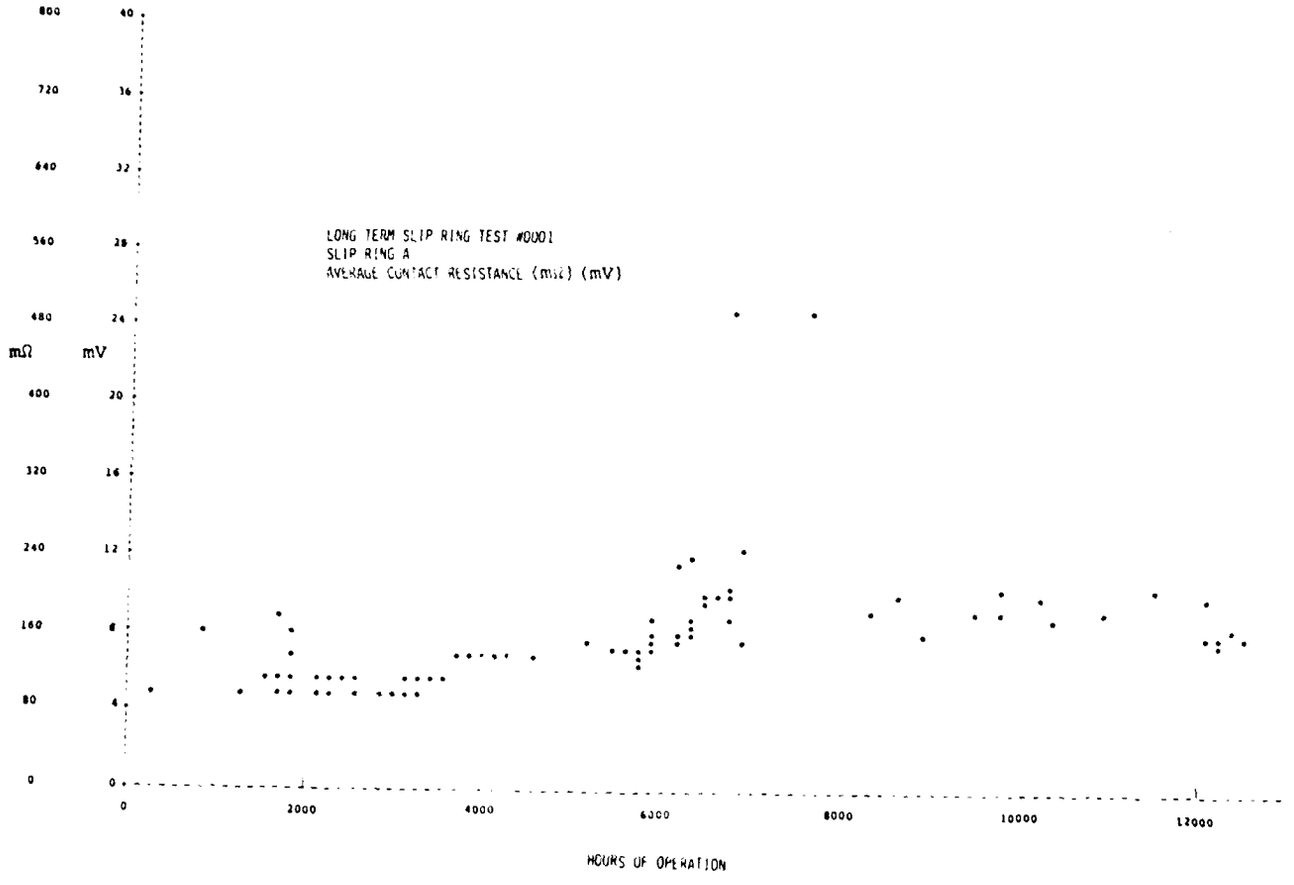

Figure 6. Average Contact Resistance, Ring A, Test 0001.

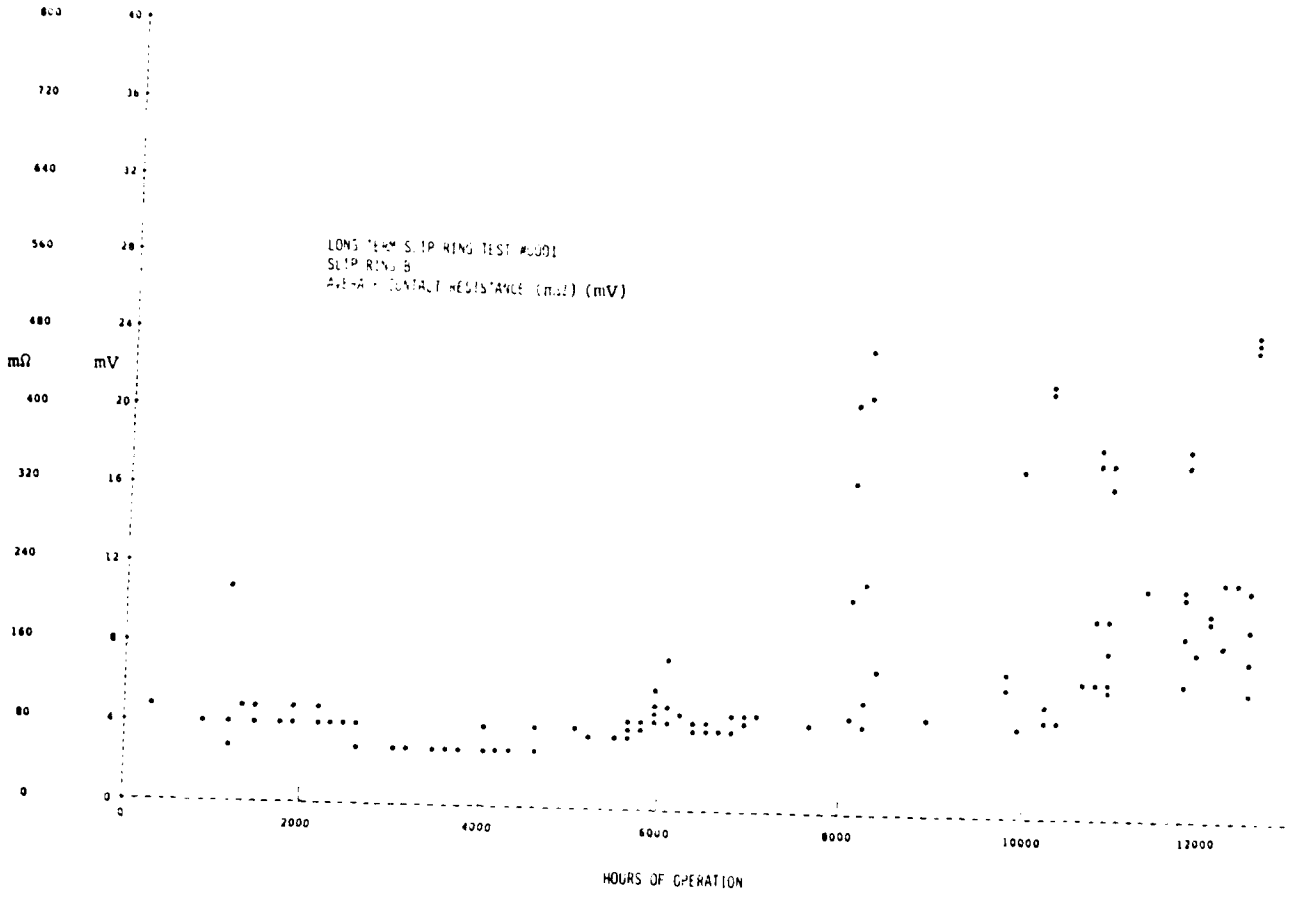

Figure 7. Average Contact Resistance, Ring B, Test 0001.

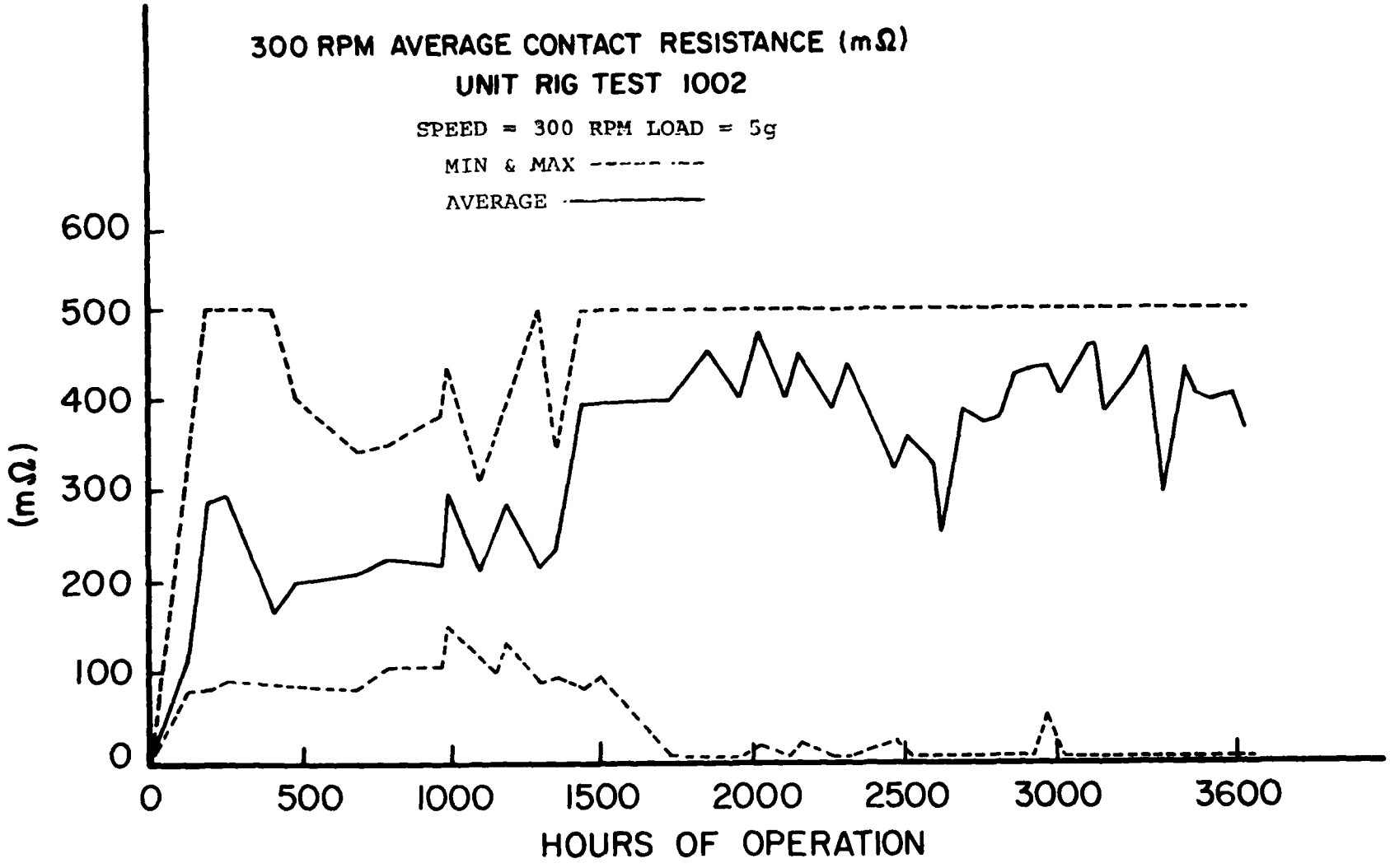

Figure 8. Average Contact Resistance, 300 rpm, Test 1002.

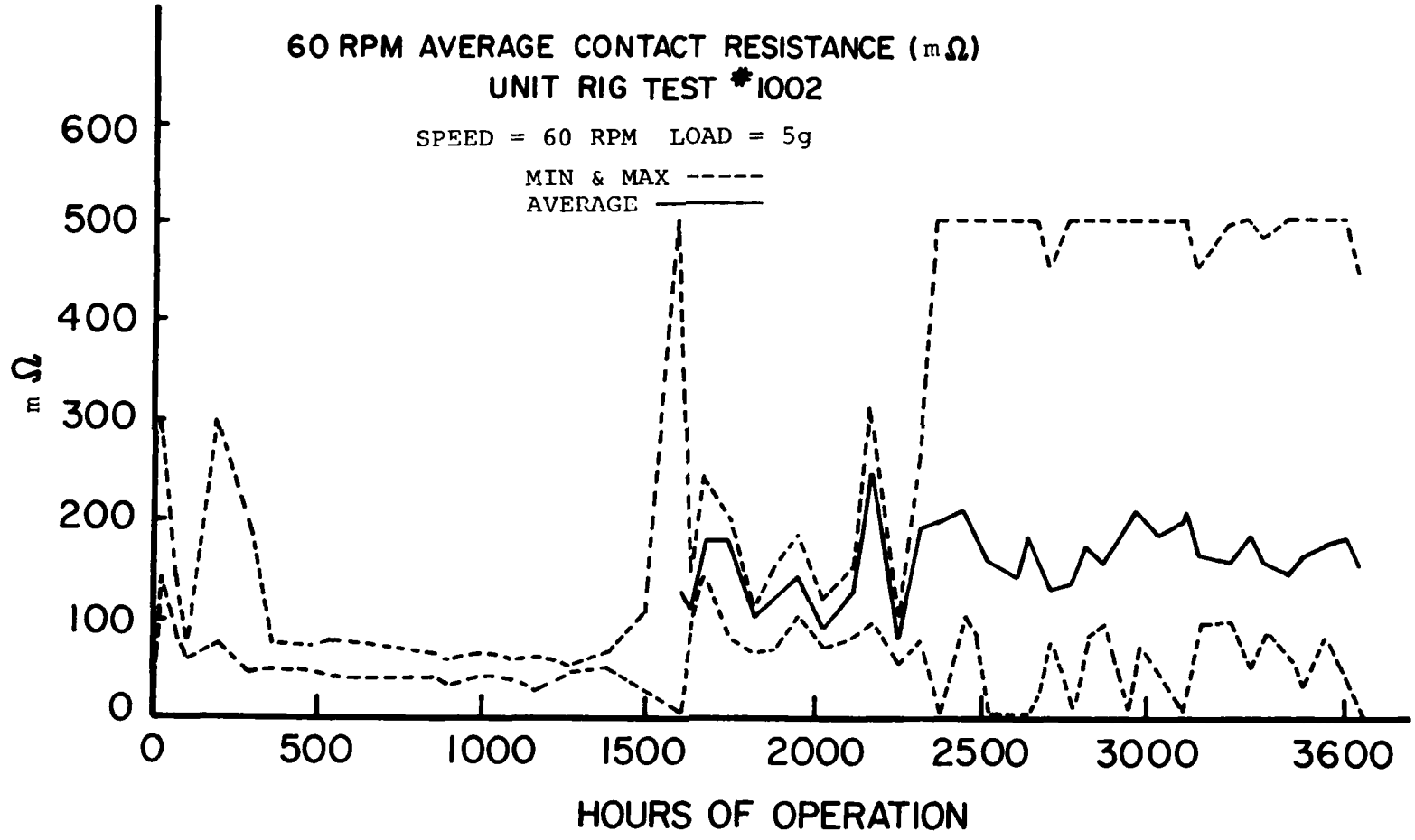

Figure 9. Average Contact Resistance, 60 rpm, Test 1002.

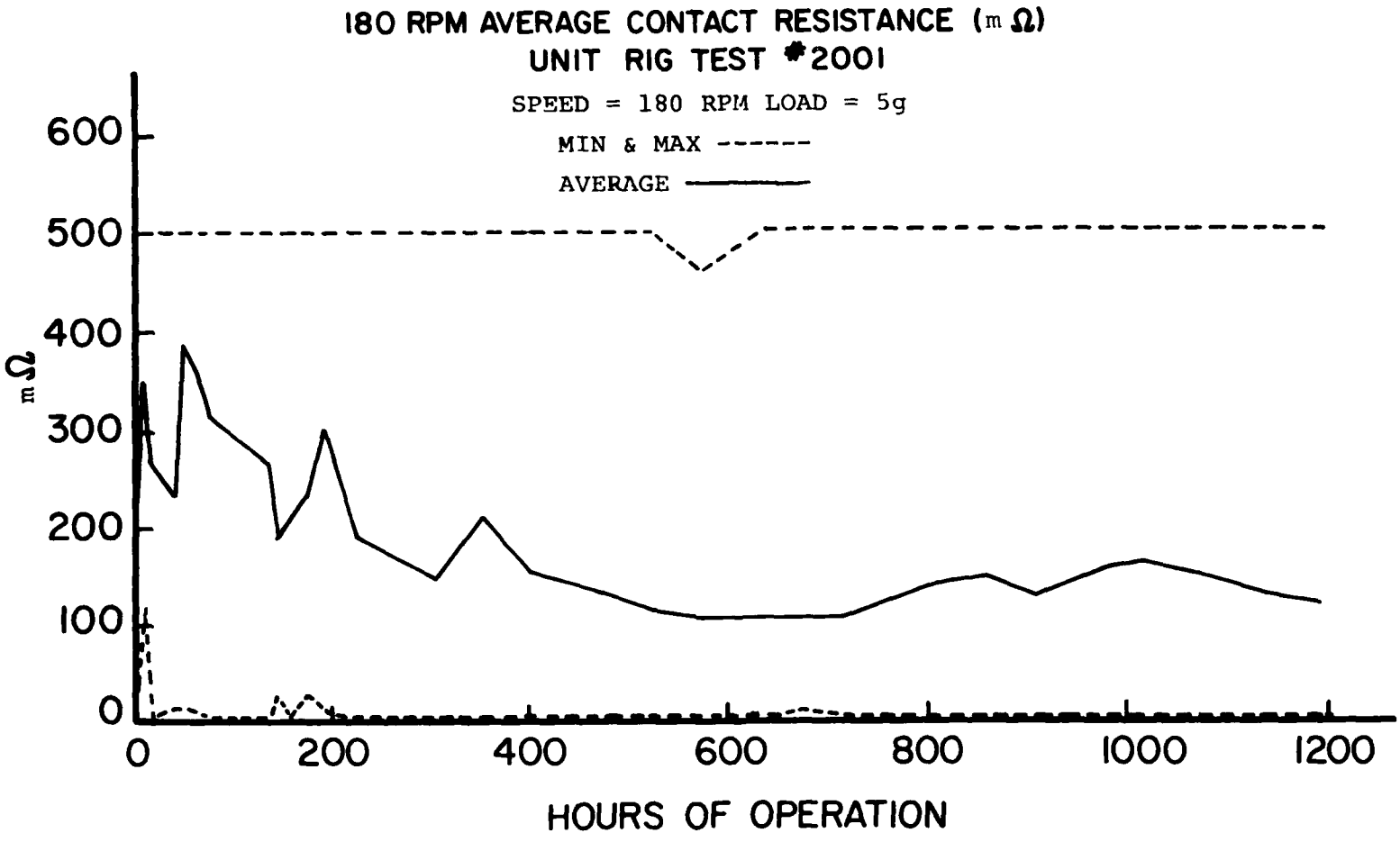

Figure 10. Average Contact Resistance, 180 rpm, Test 2001.

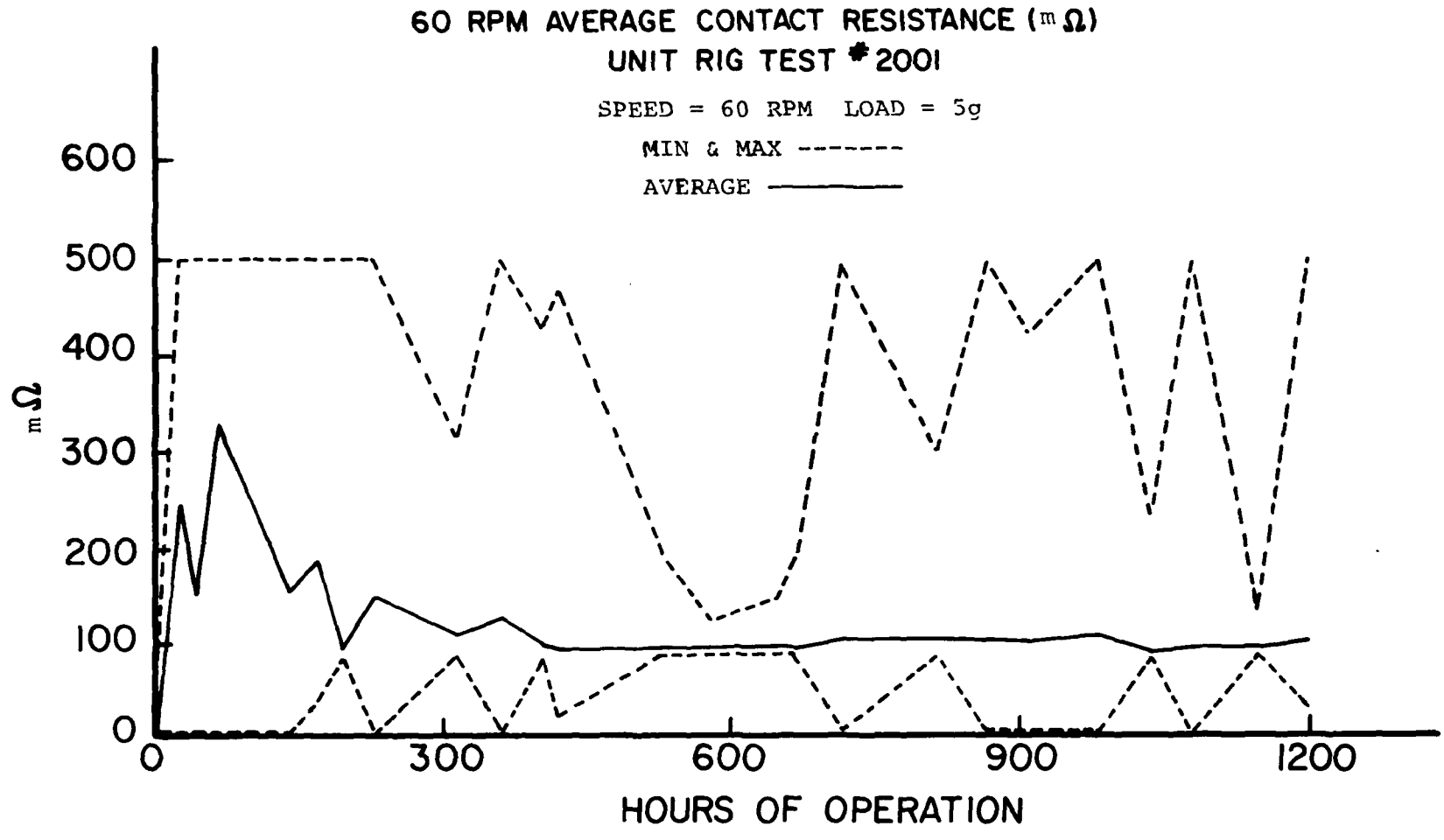

Figure 11. Average Contact Resistance, 60 rpm, Test 2001.

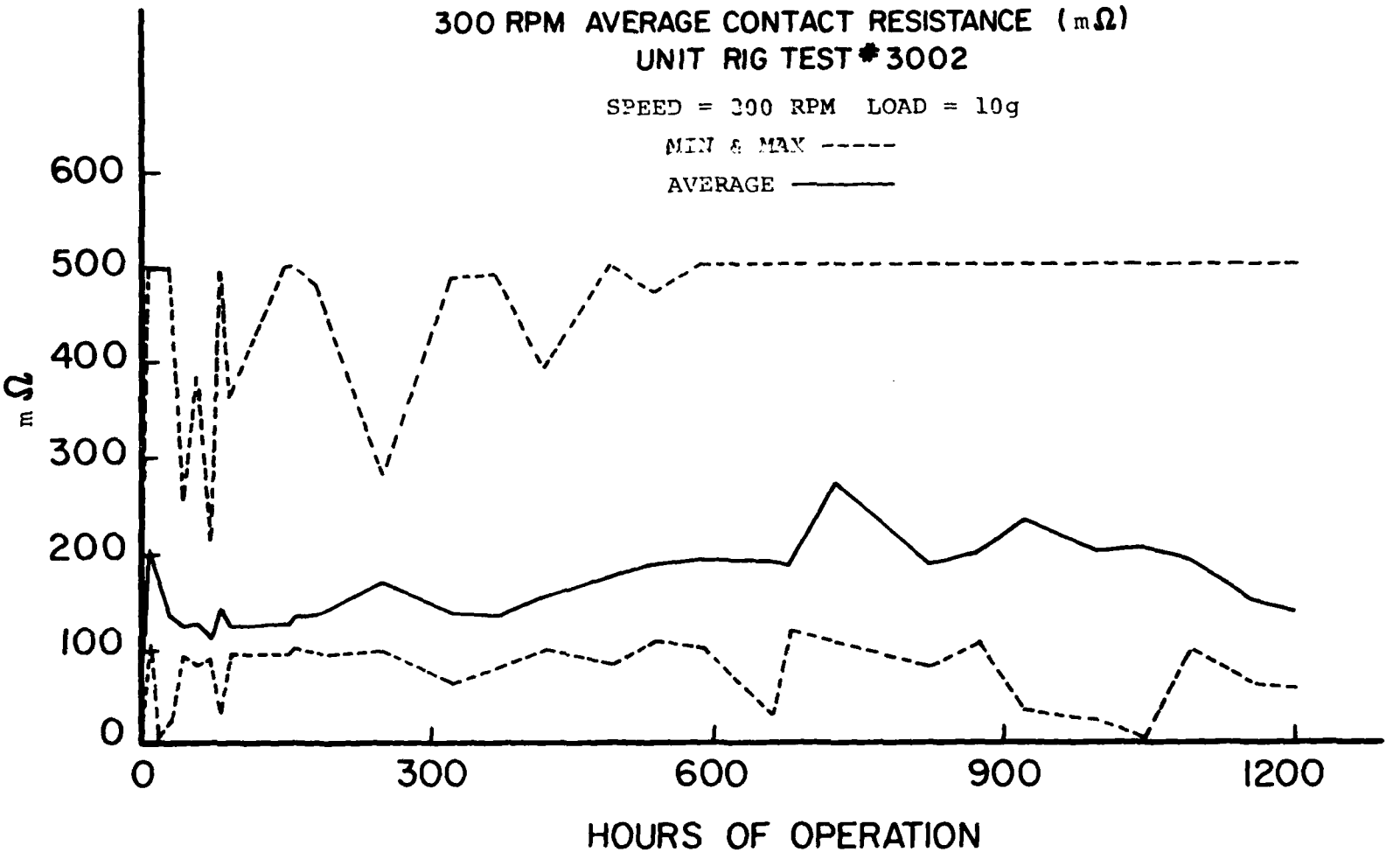

Figure 12. Average Contact Resistance, 300 rpm, Test 3002.

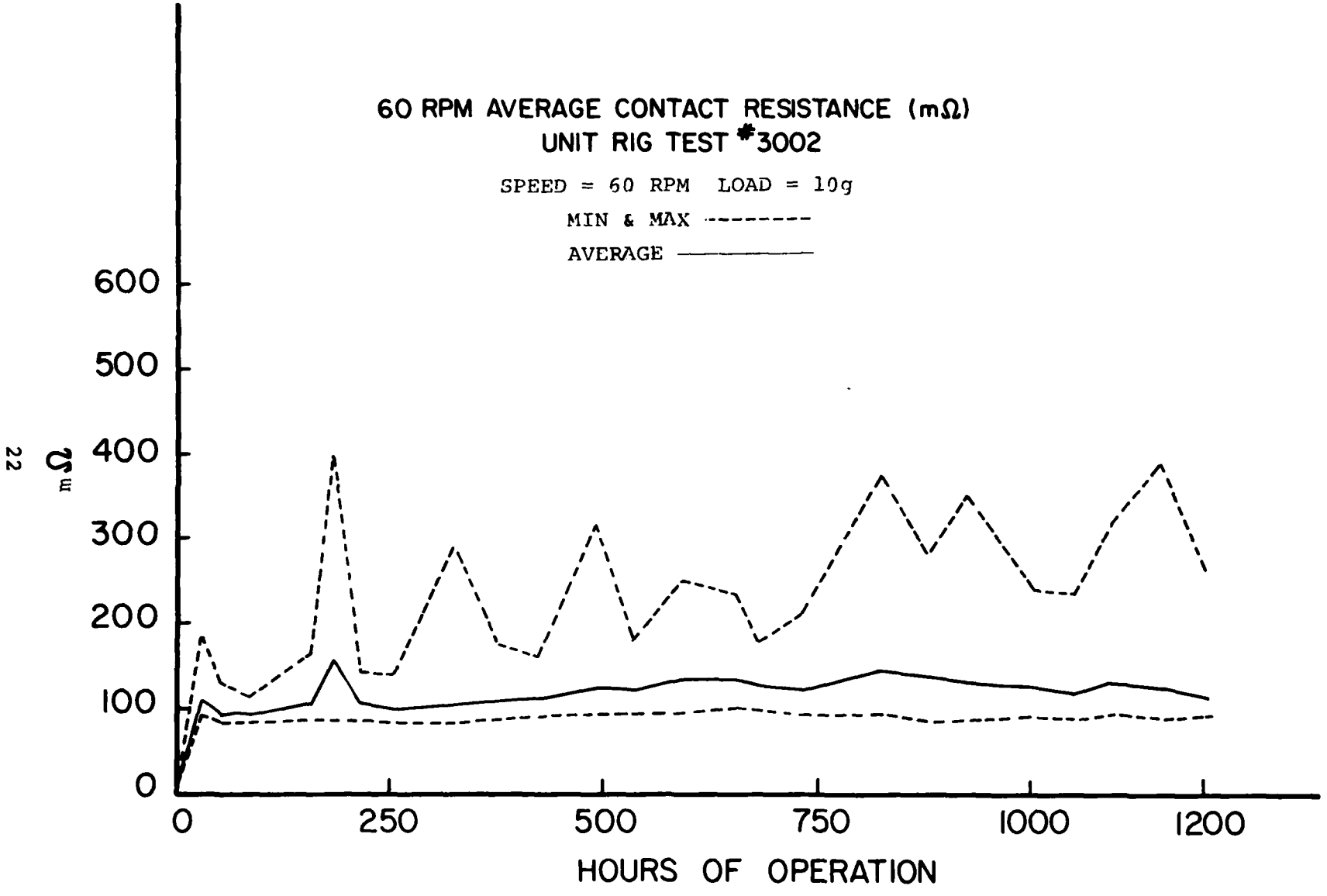

Figure 13. Average Contact Resistance, 60 rpm, Test 3002.

TABLE 2

SLIP RING RIG CONFIGURATIONS

Rig #	Test #	Brush Load (g)	High Speed (rpm)	Low Speed (rpm)	Vac Kote Qty (µl)	Total Hours
0A	0001A	5	---	60	2.8	12,700
0B	0001B	5	---	60	2.8	12,700
1	1002	5	300	60	2.8	3,750
2	2001	5	180	60	2.8	1,400
3	3002	10	300	60	2.8	1,420

feedthru failed at 5700 hours and was replaced. After replacement all parameters soon returned to their previous values. The resistance noise on ring A has been low except for the 6000 to 8000-hour period; while ring B (Figure 7) has been noisy and erratic in amplitude ever since 8000 hours and has generated a considerable number of logical noise pulses.

Figures 8, 10, and 12 show the average contact resistance at high speed of test numbers 1002, 2001, and 3002, respectively; while the low speed average contact resistance is plotted in Figures 9, 11, and 13 of each test number, respectively. The slip ring unit rigs are operated at two speeds to obtain comparable 60 rpm data with the higher speed data. The 60 rpm data is needed in order to obtain a more direct comparison to the 60 rpm long-term test data. The straight horizontal line seen on many of the MAX parameters on the graphs are due to reaching full scale.

The 300 rpm data of tests 1002 and 3002 are shown in Figures 8 and 12 respectively. Wear-in of test 1002 (Figure 8) at 300 rpm occurred at about 400 hours, and wear-in of test 3002 (Figure 12) at 300 rpm occurred at 100 to 325 hours. Test 1002 has run over 3600 hours, and data shows much more erratic operation after 1300 hours. Average resistance of test 1002 has been 300-400 milliohms. Test 3002 (Figure 12) and at 300 rpm shows different characteristics. The higher load test 3002 (Figure 12) indicates a shorter wear-in period and a somewhat more stable operation as well as a slightly lower value of overall average resistance through 1200 hours. The 180 rpm, 5 gram test 2001 (Figure 10) shows a wear-in period of 400 to 500 hours and generally lower average resistance than the 300 rpm tests.

The 60 rpm graphs of these three tests are also similar to each other. All show an average resistance through 1200 hours of about 100 milliohms, with test 1002 (Figure 9) somewhat lower at about 70 milliohms. The wear-in period at 60 rpm for test 1002

was about 350 hours (Figure 9). For test 2001 (Figure 11), the wear-in was about 410 hours at 60 rpm, and for test 3002 (Figure 10) wear-in was about 250 hours at 60 rpm. However, since the tests were actually run at 300 or 180 rpm most of the time, a conversion can be made to arrive at an equivalent 60 rpm time by multiplying the ratios 300/60 and 180/60 times the actual 60 rpm time. The equivalent 60 rpm wear-in periods, therefore, become 1750 hours for test 1002, 1230 hours for test 2001, and 1250 hours for test 3002. These compare very well with the actual 60 rpm wear-in periods experienced on the long-term slip ring test of 1200 to 1800 hours.

The maximum peaks on several of the graphs tend to be too high to be typical, perhaps because the computer picks up interference from other sources as peak data. An exception is the first 2400 hours of test 1002, where part of the computer system was inoperable and data was taken from strip charts. A fix to the maximum data problem is in progress.

While only the resistance data has been presented here, a complete set of data plots of all parameters can be found in other reports for the long-term rig experiment.[4]

3. LONG-TERM SLIP RING CORRELATION ANALYSIS

A. Correlation Analysis Techniques

The slip ring and bearing data acquisition systems used in these experiments collect many thousands of data points over a period of years. To aid in analysis of test data, statistical analytical techniques are needed in order to reduce the enormous quantity of data into functions which can be readily analyzed. Relationships between parameters versus time are some of the important characteristics that may be needed in the analysis and use of the test data.

UDRI has addressed this problem by developing special purpose computer software which computes the index of correlation between any or all pairs of test parameters over any specified

hour range of an experiment. Correlation techniques are used to measure the degree of association between two statistical series of data. A more detailed discussion of this technique is contained in the following sections of this report, but in summary, the program provides the following capabilities:

(a) The "index of correlation" between any pair of parameters.

(b) The coefficients of the equation which describes the relationship between any pair of parameters.

(c) The "standard error of estimate" of the computed relationship. This is a measure of the quality or reliability of the relationship.

(d) The "standard deviation" and "mean" values of the parameters.

The program also provides for the listing or plotting of any parameter on a computer terminal in order to view data graphically; and provides permanent mass storage of data on the computer systems disk memory.

Presented in the following sections of this report will be a brief description of the calculation and use of correlation coefficient and a presentation of correlation data and equations generated for specific hour ranges. While an analysis of the data is not within the scope of this contract, an example of possible analysis methods will be presented in order to aid future investigators of this work. These methods include the analysis of data by selecting specific hour ranges and the construction of trend tables.

This program can handle both linear and quadratic relationships between parameters, but certain assumptions are made about the parameter data. One assumption is that the data contains a "normal" statistical distribution. The other and probably most severe assumption is that the pairs of parameters are true independent variables. This is not the case, because most of the slip ring or bearing parameters that are measured interact and affect each other. However, because of the method of calculation of the index of correlation,the result is that the

correlation values are underestimated but not overestimated. Because of this particular characteristic the correlations can still be used to obtain useful relationships if these limitations are kept in mind. This is probably why many of the presented correlations are in the low correlation ranges of 0.5 to 0.8 instead of indicating high correlations in the range of 0.8 to 1.0. The use of "multiple correlation techniques" is a logical extension of this work as it allows for the presence of dependent variables in the calculation of the index of correlation.

B. Calculation and Use of Correlation Coefficient

Correlation techniques are used to measure the degree of association between two statistical series of data. Several steps are used to calculate the correlation coefficient. The first step involves pairing data points from two separate parameters. For example, pairs of friction force (grams) and contact resistance (ohms) data points, which were measured at the same point in time, are paired against each other. Then a line of regression is calculated using the method of best "least squares fit" to define an equation relating the two parameters. The form of the regression equation used is:

$$Y = a + bX + cX^2 \qquad (1)$$

Thus, if the independent variable X is friction, while the dependent variable Y is resistance, then the equation can produce an estimate of contact resistance based upon the value of any friction force.

The standard error of estimate (SE) is then calculated and used as a measure of the quality of the theoretical curve fit to the actual data. This process is similar to the calculation of standard deviation, except that standard error of estimate measures the actual data point deviation about the calculated curve, while standard deviation measures the actual data point deviation about the arithmetic mean. The form of the equation is:

$$SE = \sqrt{\frac{\Sigma(d^2)}{N}} \qquad (2)$$

where SE = standard error of estimate

d = deviation of actual values from calculated best fit curve values

N = number of data points

The lower the value of SE, the better the curve fit. Therefore, a lower value of SE also indicates that a closer relationship between the two parameters exists. An illustration of the use of SE is as follows. If the regression equation was $Y = 100 + 50X$, where Y = resistance, X = a friction force of 2 grams and SE = 5, then by substitution Y (resistance) = 200 milliohms. Using the criteria of three standard errors (3 x 5 = 15), the value of the resistance resulting from a 2 gram friction force can be estimated as being between 185 and 215 milliohms with a 99.7% probability (3 standard errors).

While SE is useful to estimate values and probabilities, it cannot be used as a comparison to the SE of other pairs of parameters because its units depend upon the units of the parameters used in the computation. Therefore, the SE value of resistance/friction cannot be compared to the SE value of resistance/vertical deflection.

The unit of measure which is used for comparison purposes is the "index of correlation (RHO)", also termed correlation coefficient. The formula is:

$$RHO = \sqrt{1 - \frac{SE^2}{\sigma^2}} \qquad (3)$$

where SE^2 = variance about the curve fit

σ^2 = variance about the arithmetic mean

The units cancel and thus RHO is nondimensional. If the curve fit is no better than just using the mean value, then $SE^2 = \sigma^2$ and RHO approaches zero indicating little or no correlation. However, if the curve fit is excellent, then SE^2

approaches zero and RHO approaches "1", indicating an excellent correlation and relationship between the two parameters. RHO can be in the range of +1 to -1. A +1 would indicate a perfect direct relationship, and a -1 would indicate a perfect inverse relationship. Zero indicates that no relationship exists. Thus, the value of RHO can be compared between various pairs of parameters to indicate the relative influence that each has on the other.[5]

C. Correlation Data

For each ring, 10 hour ranges were selected for correlation analysis. Any range can be specified however. The ranges were selected to examine correlations as follows: equal time increments; noisy versus quiet ring operation; and to bracket around the feedthru failure at 5700 hours. The selected slip ring A ranges are as follows:

```
    0 - 2000 hours
 2000 - 4000 hours
 4000 - 6000 hours
 6000 - 8000 hours
 8000 - 10000 hours
10000 - 12700 hours
    0 - 5700 hours

 5700 - 12700 hours
 5700 - 7000 hours
 7000 - 12700 hours
```

The selected slip ring B hour ranges are as follows:

```
    0 to 2000 hours
 2000 to 4000   "
 4000 to 6000   "
 6000 to 8000   "
 8000 to 10000  "
10000 to 12700  "
    0 to 5700   "
 5700 to 12700  "
 5700 to 7500   "
 7500 to 12700  "
```

Correlation data from these 20 hour ranges are presented in 20 tables in a previous technical report along with 20 tables of the corresponding equations.[6]

An example of one of the correlation tables is shown in Table 3. It lists correlations of all combinations of nine important pairs of parameters for a specific hour range. The table may be read either by columns or rows to examine the correlations (R) between any one of the parameters and all others. Note that because of space limitations the symbol R is used instead of RHO. In each box, the standard estimate of error (SE) is also indicated for the correlation. The rightmost column indicates the mean value in engineering units of the parameters listed in the leftmost column for the indicated hour range.

An example of the corresponding equation table for the same hour range is shown in Table 4. This table lists the constant and the 2 coefficients that define the quadratic equation of the parameter relationships for this hour range and also other statistics. Because of space limitations, the parameter names are coded. The legend for the code is as follows:

COLUMN 1	HOURS
COLUMN 2	FRICTION AVERAGE
COLUMN 3	FRICTION PEAK AVERAGE
COLUMN 4	VERTICAL ECCENTRICITY AVERAGE
COLUMN 5	VERTICAL DEFLECTION AVERAGE
COLUMN 6	VERTICAL DEFLECTION PEAK AVERAGE
COLUMN 7	CONTACT NOISE AVERAGE
COLUMN 8	CONTACT NOISE PEAK AVERAGE
COLUMN 9	MOTOR CURRENT
COLUMN 10	LOGICAL NOISE

Thus a 2-10 correlation would be between the parameters of "friction average" and "logical noise".

To further summarize the correlation data, Tables 5 and 6 were constructed for slip rings A and B respectively. These tables list the highest, second highest, third highest and lowest correlations found in the 20 correlation tables for each pair of parameters. The hour range from which each correlation is taken is also listed. The asterisk and double asterisk mark values that are of suspect reliability and should probably be disregarded. This includes many of the highest values. In this case the second highest value should be considered as highest. The reasons for

TABLE 3

CORRELATION COEFFICIENTS
LONG-TERM SLIP RING TEST #0001 RING A
HOURS: 0 to 2000
NUMBER OF DATA POINTS: 20

PARAMETER	FRICTION AVERAGE	FRICTION PEAK AVERAGE	VERTICAL ECC. AVERAGE	VERTICAL DEF. AVERAGE	VERTICAL DEF.PEAK AVERAGE	CONTACT NOISE AVERAGE	CONTACT NOISE PK. AVG.	MOTOR CURRENT	LOGICAL NOISE	MEAN VALUE
FRICTION AVERAGE		R=-0.28	R= 0.26	R=*0.00	R=-0.25	R=-0.39	R=-0.33	R=-0.87	R=*0.00	-0.65
		SE= 0.65	SE= 6.85	SE= 0.00	SE= 0.54	SE= 1.13	SE=17.08	SE= 0.02	SE= 0.00	
FRICTION PEAK AVERAGE	R=-0.28		R=-0.73	R=*0.00	R=-0.82	R=-0.51	R=-0.30	R= 0.58	R=*0.00	2.24
	SE= 0.65		SE= 4.85	SE= 0.00	SE= 0.21	SE= 1.05	SE=17.32	SE= 0.02	SE= 0.00	
VERTICAL ECC. AVERAGE	R= 0.26	R=-0.73		R=*0.00	R=-0.52	R=-0.31	R=-0.58	R= 0.71	R=*0.00	-2.27
	SE= 0.65	SE= 4.85		SE= 0.00	SE= 0.47	SE= 1.18	SE=14.58	SE= 0.02	SE= 0.00	
VERTICAL DEF. AVERAGE	R=*0.00	R=*0.00	R=*0.00		R=-0.22	R=-0.22	R=-0.22	R=-0.22	R=*0.00	0.90
	SE= 0.00	SE= 0.00	SE= 0.00		SE= 0.54	SE= 1.19	SE=17.87	SE= 0.03	SE= 0.00	
VERTICAL DEF. PK. AVG.	R=-0.25	R=-0.82	R=-0.52	R=-0.22		R= 0.34	R= 0.27	R=-0.42	R=*0.00	2.61
	SE= 0.54	SE= 0.21	SE= 0.47	SE= 0.54		SE= 1.15	SE=17.48	SE= 0.03	SE= 0.00	
CONTACT NOISE AVERAGE	R=-0.39	R=-0.51	R=-0.31	R=-0.22	R= 0.34		R= 0.73	R= 0.34	R=*0.00	8.15
	SE= 1.13	SE= 1.05	SE= 1.16	SE= 1.18	SE= 1.15		SE=12.42	SE= 0.03	SE= 0.00	
CONTACT NOISE PK. AVG.	R=-0.33	R=-0.30	R=-0.58	R=-0.22	R= 0.27	R= 0.73		R= 0.31	R=*0.00	13.76
	SE=17.08	SE=17.32	SE=14.58	SE=17.67	SE=17.48	SE=12.42		SE= 0.03	SE= 0.00	
MOTOR CURRENT	R=-0.87	R= 0.58	R= 0.71	R=-0.22	R=-0.42	R= 0.34	R= 0.31		R=*0.00	0.55
	SE= 0.02	SE= 0.02	SE= 0.02	SE= 0.03	SE= 0.03	SE= 0.03	SE= 0.03		SE= 0.00	
LOGICAL NOISE	R=*0.00	R=*0.00	R=*0.00	R=*0.00	R=*0.00	R=*0.00	R=*0.00	R=*0.00		0.00
	SE= 0.00	SE= 0.00	SE= 0.00	SE= 0.00	SE= 0.00	SE= 0.00	SE= 0.00	SE= 0.00		

TABLE 4

RING A CORRELATION EQUATIONS
HOURS 0.00 to 2000.00 N=20

COLUMNS	X**0	X**1	X**2	STDEV	SE	X-MEAN	Y-MEAN	RHO
2- 3	-.6676E+00	-.1165E+02	-.1072E+02	0.679	0.653	-0.65	2.24	-0.28
2- 4	-.7071E+01	-.3541E+02	-.4174E+02	7.099	6.851	-0.65	-2.27	0.28
2- 5	0.9001E+00	0.3568E-03	0.3407E-03	0.000	0.000	-0.65	0.90	*0.00
2- 6	0.9601E+00	-.6977E+01	-.6641E+01	0.554	0.536	-0.65	2.61	-0.25
2- 7	0.4273E+01	-.1480E+01	0.2060E+01	1.226	1.129	-0.65	6.15	-0.39
2- 8	0.1090E+02	0.6149E+02	0.9794E+02	18.132	17.090	-0.65	13.76	-0.33
2- 9	0.5971E+00	0.5086E+00	0.6391E+00	0.029	0.021	-0.65	0.55	-0.67
2-10	0.0000E+00	0.0000E+00	0.0000E+00	0.000	0.000	-0.65	0.00	*0.00
3- 4	0.4714E+02	-.3958E+02	0.7194E+01	7.099	4.851	2.24	-2.27	-0.73
3- 5	0.9000E+00	-.2552E-05	0.4495E-06	0.000	0.000	2.24	0.90	*0.00
3- 6	0.6510E+00	0.2037E+01	-.4781E+00	0.554	0.212	2.24	2.61	-0.92
3- 7	0.9781E+01	-.2277E+01	0.2692E+00	1.226	1.051	2.24	6.15	-0.51
3- 8	-.1022E+02	0.2157E+02	-.4459E+01	18.132	17.316	2.24	13.76	-0.30
3- 9	0.6779E+00	-.1117E+00	0.2159E-01	0.029	0.023	2.24	0.55	0.58
3-10	0.0000E+00	0.0000E+00	0.0000E+00	0.000	0.000	2.24	0.00	*0.00
4- 5	0.9000E+00	0.1314E-08	0.6811E-09	0.000	0.000	-2.27	0.90	*0.00
4- 6	0.2743E+01	-.4555E-01	-.4542E-02	0.554	0.474	-2.27	2.61	-0.52
4- 7	0.5852E+01	0.7381E-02	0.5928E-02	1.226	1.165	-2.27	6.15	-0.31
4- 8	0.4575E+01	-.5050E+00	0.1517E+00	18.132	14.578	-2.27	13.76	-0.59
4- 9	0.5269E+00	0.2683E-02	0.4650E-03	0.029	0.020	-2.27	0.55	0.71
4-10	0.0000E+00	0.0000E+00	0.0000E+00	0.000	0.000	-2.27	0.00	*0.00
5- 6	0.3850E+01	-.8498E+00	-.5931E+00	0.554	0.540	0.90	2.61	-0.22
5- 7	0.1197E+02	-.2121E+01	-.4828E+01	1.226	1.195	0.90	6.15	-0.22
5- 8	0.2480E+02	-.9682E+01	-.2869E+01	18.132	17.673	0.90	13.76	-0.22
5- 9	0.6959E+00	0.2224E-01	-.2103E+00	0.029	0.028	0.90	0.55	-0.22
5-10	0.0000E+00	0.0000E+00	0.0000E+00	0.000	0.000	0.90	0.00	*0.00
6- 7	0.5137E+01	-.6461E+00	0.3809E+00	1.226	1.154	2.61	6.15	0.34
6- 8	0.4932E+01	-.4551E+01	0.2923E+01	18.132	17.481	2.61	13.76	0.27
6- 9	0.6073E+00	-.6399E-01	0.1482E-01	0.029	0.026	2.61	0.55	-0.42
6-10	0.0000E+00	0.0000E+00	0.0000E+00	0.000	0.000	2.61	0.00	*0.00
7- 8	-.9477E+02	0.2416E+02	-.1021E+01	18.132	12.419	6.15	13.76	0.73
7- 9	0.3059E+00	0.7415E-01	-.5514E-02	0.029	0.027	6.15	0.55	0.34
7-10	0.0000E+00	0.0000E+00	0.0000E+00	0.000	0.000	6.15	0.00	*0.00
8- 9	0.5499E+00	-.1256E-02	0.2573E-04	0.029	0.027	13.76	0.55	0.31
8-10	0.0000E+00	0.0000E+00	0.0000E+00	0.000	0.000	13.76	0.00	*0.00
9-10	0.0000E+00	0.0000E+00	0.0000E+00	0.000	0.000	0.55	0.00	*0.00

TABLE 5

SLIP RING A
SUMMARY OF CORRELATION RANGES

	HIGHEST CORR.	HOURS (THOUSANDS)	2ND HIGHEST CORR.	HOURS (THOUSANDS)	3RD HIGHEST CORR.	HOURS (THOUSANDS)	LOWEST CORR.	HOURS (THOUSANDS)
FRICTION AVG. FRICTION PK. AVG.	-0.79	* 8-10	0.56	10-12.7	-0.41	7-12.7	-0.25	0-5.7
FRICTION AVG. VERT. ECC. AVG.	-0.97	* 8-10	0.66	6-8	0.54	10-12.7 5.7-7	0.26	0-2
FRICTION AVG. VERT. DEF. AVG.	0.51	* * 4-6	0.50	* 8-10	-0.49	10-12.7	0.32	2-4 5.7-12.7
FRICTION AVG. VERT. DEF. PK. AVG.	-0.81	* 8-10	0.64	7-12.7	0.50	* * 4-6	0.21	2-4
FRICTION AVG. CONTACT NOISE AVG.	0.86	* 8-10	0.56	10-12.7	-0.39	0-2	-0.15	5.7-12.7
FRICTION AVG. CONTACT NOISE PK. AVG.	0.92	* 8-10	0.57	7-12.7	-0.36	10-12.7	-0.14	0-5.7
FRICTION AVG. MOTOR CURRENT	-0.67	0-2	-0.58	8-10* 10-12.7	-0.56	7-12.7	-0.18	5.7-7
FRICTION AVG. LOGICAL NOISE	-0.56	5.7-7	-0.52	6-8	-0.27	5.7-12.7	0.12	0-5.7
FRICTION PK. AVG. VERT. ECC. AVG.	-0.73	0-2	0.71	* 8-10	0.59	5.7-12.7	0.32	5.7-7
FRICTION PK. AVG. VERT. DEF. AVG.	0.79	2-4	0.78	0-5.7	-0.73	10-12.7	0.41	5.7-12.7
FRICTION PK. AVG. VERT. DEF. PK. AVG.	-0.92	0-2	0.84	2-4	-0.74	* 8-10	0.38	5.7-7
FRICTION PK. AVG. CONTACT NOISE AVG.	0.90	10-12.7	0.65	* * 4-6	-0.60	* 8-10	0.21	5.7-12.7
FRICTION PK. AVG. CONTACT NOISE PK. AVG.	0.99	10-12.7	-0.85	* 8-10	-0.74	7-12.7	0.16	2-4
FRICTION PK. AVG. MOTOR CURRENT	0.81	* 8-10	-0.70	* * 4-6	0.63	2-4	0.24	5.7-12.7
FRICTION PK. AVG. LOGICAL NOISE	0.34	5.7-12.7 6-8	0.25	5.7-7	0.24	2-4	0.17	0-5.7
VERT. ECC. AVG. VERT. DEF. AVG.	-0.59	* * 4-6	-0.56	* 8-10	0.52	10-12.7	0.29	5.7-12.7 2-4

TABLE 5

SLIP RING A
SUMMARY OF CORRELATION RANGES
(concluded)

	HIGHEST CORR.	HOURS (THOUSANDS)	2ND HIGHEST CORR.	HOURS (THOUSANDS)	3RD HIGHEST CORR.	HOURS (THOUSANDS)	LOWEST CORR.	HOURS (THOUSANDS)
VERT. ECC. AVG. / VERT. DEF. PK. AVG.	-0.61	* 8-10	-0.59	4-6** 5.7-12.7	-0.52	0-2	0.24	2-4
VERT. ECC. AVG. / CONTACT NOISE AVG.	-0.67	* 8-10	0.51	* * 4-6	0.36 -0.36	10-12.7 5.7-7	0.16	2-4
VERT. ECC. AVG. / CONTACT NOISE PK. AVG.	-0.93	* 8-10	-0.74	7-12.7	-0.63	6-8	0.19	2-4 4-6**
VERT. ECC. AVG. / MOTOR CURRENT	0.71	0-2	0.66	* 8-10	0.62	7-12.7	0.24	5.7-12.7
VERT. ECC. AVG. / LOGICAL NOISE	-0.41	5.7-7	-0.35	6-8	-0.29	5.7-12.7	-0.16	0-5.7
VERT. DEF. AVG. / VERT. DEF. PK. AVG.	0.98	* * 4-6	0.92	0-5.7	0.89	2-4	-0.22	0-2
VERT. DEF. AVG. / CONTACT NOISE AVG.	-0.77	10-12.7	0.66	6-8	-0.63	* * 4-6	-0.20	0-2
VERT. DEF. AVG. / CONTACT NOISE PK. AVG.	-0.99	10-12.7	0.66	* 8-10	0.46	7-12.7	0.17	2-4
VERT. DEF. AVG. / MOTOR CURRENT	-0.84	* 8-10	0.70	4-6 ** 10-12.7	-0.65	7-12.7	-0.22	2-4
VERT. DEF. AVG. / LOGICAL NOISE	0.33	6-8	0.19	5.7-12.7	0.15	2-4	0.14	0-5.7
VERT. DEF. PK. AVG. / CONTACT NOISE AVG.	0.71	10-12.7	-0.65	* * 4-6	-0.51	* 8-10	-0.14	5.7-12.7
VERT. DEF. PK. AVG. / CONTACT NOISE PK. AVG.	0.86	* 8-10	0.83	7-12.7	0.63	5.7-12.7	-0.22	0-5.7
VERT. DEF. PK. AVG. / MOTOR CURRENT	-0.95	* 8-10	-0.91	7-12.7	0.61	* * 4-6	0.28	6-8
VERT. DEF. PK. AVG. / LOGICAL NOISE	0.50	2-4	0.45	0-5.7	0.41	6-8	0.16	5.7-12.7
CONTACT NOISE AVG. / CONTACT NOISE PK. AVG.	0.87	5.7-7	-0.86	6-8	0.84	* 8-10	-0.35	7-12.7
CONTACT NOISE AVG. / MOTOR CURRENT	0.72	* 8-10	-0.60	* * 4-6	0.57	10-12.7	-0.16	5.7-12.7
CONTACT NOISE AVG. / LOGICAL NOISE	0.45	5.7-7	0.41	6-8 5.7-12.7	0.12	2-4	-0.14	0-5.7
CONTACT NOISE PK. AVG. / MOTOR CURRENT	-0.98	* 8-10	-0.96	7-12.7	0.56	10-12.7	0.19	0-5.7
CONTACT NOISE PK. AVG. / LOGICAL NOISE	0.44	5.7-7	0.42	6-8	0.30	5.7-12	0.18	0-5.7
MOTOR CURRENT / LOGICAL NOISE	0.37	6-8	0.32	2-4	0.23	0-5.7	0.19	5.7-12.7

* 8-10 Thousand Hours Has Only 6 Data Points
* * 4-6 Thousand Hours Had Feedthru Failure

TABLE 6

SLIP RING B
SUMMARY OF CORRELATION RANGES

	HIGHEST CORR.	HOURS (THOUSANDS)	2ND HIGHEST CORR.	HOURS (THOUSANDS)	2ND HIGHEST CORR.	HOURS (THOUSANDS)	LOWEST CORR.	HOURS (THOUSANDS)
FRICTION AVG. FRICTION PK. AVG.	-0.63	5.7-7	-0.58	5.7-12.7	-0.41	0-2	0.17	0-5.7
FRICTION AVG. VERT. ECC. AVG.	0.51	* * 4-6	0.47	2-4	0.42	6-8	-0.13	5.7-12.7
FRICTION AVG. VERT. DEF. AVG.	0.47	5.7-12.7	0.44	5.7-7	-0.43	* * 4-6	0.34	0-5.7
FRICTION AVG. VERT. DEF. PK. AVG.	0.65	6-8	0.52	* 8-10	-0.49	5.7-12.7	0.23	10-12.7
FRICTION AVG. CONTACT NOISE AVG.	0.63	* * 4-6	0.52	6-8	-0.46	8-10	0.16	0-5.7
FRICTION AVG. CONTACT NOISE PK. AVG.	-0.49	2-4 8-10	-0.48	5.7-12.7	-0.37	6-8	-0.17	0-5.7
FRICTION AVG. MOTOR CURRENT	-0.73	0-2	0.59	5.7-12.7	-0.52	* * 4-6	-0.17	7-12.7
FRICTION AVG. LOGICAL NOISE	-0.38	8-10	-0.27	5.7-12.7	0.21	7-12.7	0.19	10-12.7
FRICTION PK. AVG. VERT. ECC. AVG.	-0.49	8-10	-0.47	2-4	-0.46	6-8	0.10	5.7-12.7
FRICTION PK. AVG. VERT. DEF. AVG.	0.90	2-4	0.79	0-5.7	-0.68	5.7-7	-0.52	* * 4-6
FRICTION PK. AVG. VERT. DEF. PK. AVG.	0.63	0-2	0.60	5.7-7	-0.56	0-5.7	0.27	8-10
FRICTION PK. AVG. CONTACT NOISE AVG.	-0.63	2-4	-0.59	10-12.7	-0.58	8-10	-0.26	6-9
FRICTION PK. AVG. CONTACT NOISE PK. AVG.	0.71	* * 4-6	0.62	5.7-12.7	-0.55	8-10	-0.14	0-5.7
FRICTION PK. AVG. MOT R CURRENT	-0.72	5.7-12.7	-0.70	5.7-7	0.64	0-2 2-4	0.28	0-5.7
FRICTION PK. AVG. LOGICAL NOISE	0.39	8-10	0.36	5.7-12.7	-0.34	10-12.7	-0.25	7-12.7
VERT. ECC. AVG. VERT. DEF. AVG.	0.38	5.7-7	-0.30	2-4	-0.29	0-5.7	0.18	5.7-12.7
VERT. ECC. AVG. VERT. DEF. PK. AVG.	0.48	6-8	0.47	0-2	-0.40	* * 4-6	0.24	5.7-12.7
VERT. ECC. AVG. CONTACT NOISE AVG.	0.48	8-10	0.38	6-8	-0.33	10-12.7	0.13	5.7-12.7

TABLE 6

SLIP RING B
SUMMARY OF CORRELATION RANGES
(concluded)

	HIGHEST CORR.	HOURS (THOUSANDS)	2ND HIGHEST CORR.	HOURS (THOUSANDS)	2ND HIGHEST CORR.	HOURS (THOUSANDS)	LOWEST CORR.	HOURS (THOUSANDS)
VERT. ECC. AVG.				6-8				
CONTACT NOISE PK. AVG.	-0.58	2-4	0.32	8-10	-0.29	10-12.7	-0.13	0-5.7
VERT. ECC. AVG.	-0.45	2-4			0-31	5.7-7		
MOTOR CURRENT	0.45	0-2	0.44	8-10	-0.31	10-12.7	0.10	5.7-12.7
VERT. ECC. AVG.				5.7-12.7				
LOGICAL NOISE	0.60	8-10	0.19	7-12.7 & 10-12.7				
VERT. DEF. AVG.								
VERT. DEF. PK. AVG.	-0.65	0-5.7	-0.56	5.7-7	-0.45	2-4	-0.17	10-12.7
VERT. DEF. AVG.						* *		
CONTACT NOISE AVG.	-0.94	0-2	-0.83	2-4	-0.78	4-6	-0.18	10-12.7
VERT. DEF. AVG.								
CONTACT NOISE PK. AVG.	-0.95	0-2	0.67	10-12.7	0.55	7-12.7	0.28	8-10
VERTICAL DEF. AVG.						* *		
MOTOR CURRENT	0.98	5.7-7	0.89	5.7-12.7	0.84	4-6	-0.22	10-12.7
VERTICAL DEF. AVG.			-0.19	5.7-12.7				
LOGICAL NOISE	0.23	10-12.7	0.19	7-12.7			0.10	8-10
VERT. DEF. PK. AVG.								
CONTACT NOISE AVG.	-0.50	6-8	0.49	8-10	0.39	0-2	-0.15	7-12.7
VERT. DEF. PK. AVG.								
CONTACT NOISE PK. AVG.	-0.61	7-12.7	0.52	5.7-12.7	-0.44	10-12.7	0.25	0-5.7
VERT. DEF. PK. AVG.								
MOTOR CURRENT	-0.64	5.7-12.7	-0.60	5.7-7	-0.38	2-4	0.17	0-5.7
VERT. DEF. PK. AVG.								
LOGICAL NOISE	-0.56	10-12.7	0.49	5.7-12.7	-0.48	7-12.7	-0.44	8-10
CONTACT NOISE AVG.								
CONTACT NOISE PK. AVG.	0.97	0-2	0.93	0-5.7	0.92	6-8	-0.49	10-12.7
CONTACT NOISE AVG.		* *	-0.55	2-4				
MOTOR CURRENT	-0.78	4-6	0.55	0-2	-0.46	5.7-12.7	0.20	7-12.7
CONTACT NOISE AVG.								
LOGICAL NOISE	0.52	5.7-12.7	0.42	8-10	0.29	7-12.7	0.26	10-12.7
CONTACT NOISE PK. AVG.								
MOTOR CURRENT	0.76	0-2	-0.56	5.7-12.7	0.50	2-4	0.17	0-5.7
CONTACT NOISE PK. AVG.								
LOGICAL NOISE	0.62	8-10	0.58	5.7-12.7	0.37	7-12.7	0.35	10-12.7
MOTOR CURRENT								
LOGICAL NOISE	-0.43	8-10	-0.39	5.7-12.7	0.20	10-12.7	-0.19	7-12.7

* * 4-6 Thousand Hours Had Feedthru Failure

the suspect data is the feedthru failure at 5700 hours and insufficient data points for reliable analysis at other hour ranges. In general, the middle hour ranges resulted in low correlations while the lowest and highest hour ranges produced the higher correlations.

A further summary of the best correlations of various parameters to the critical long-term experiment parameters of average contact noise, contact noise peak average, and logical noise are presented in Table 7. Table 8 presents the correlation data arranged in chronological order for all hours of operation of the experiment through 12,700 hours. The highest correlations occurred either during the first 2000 hours (wear-in) or in the later hours of the experiment for most parameters. The 0-2000 and 2000-4000-hour correlations are generally of quite different values, and consistent trends in most parameters can be seen thereafter.

4. RELATIONSHIP OF LOGICAL NOISE TO BRUSH MOVEMENT

The first instance of "logical noise" was recorded at the 3542-hour point of operation. The presence of "logical noise" indicates that the resistance level of the ring/brush contact has reached a point where the electrical noise that is generated creates a signal of greater than 40% of that of a +5V digital data signal. At this noise level, digital data transmission is completely obscured by the noise. In this case, it means a resistance of 40 ohms or greater, since the current used is 50 milliamperes. This is a dramatic resistance increase from the 0.1 to 0.2 ohm resistance of normal operation. Figure 14 is a plot from the analog tape recorder data for the data burst where "logical noise" pulses first occurred. It is data burst #159 and is of slip ring "A" recorded at 3542 hours, one minute, 45 seconds of operation. The computer detected an "out-of-limit" condition on the vertical brush deflection (peak averaged) data channel and initiated the data burst recording. Attention was drawn to this data burst when reduction of the computer data

TABLE 7

MAXIMUM CONTACT NOISE CORRELATIONS
SLIP RING A

PARAMETER	CONTACT NOISE AVERAGE RHO	(THOUSANDS) HOURS	CONTACT NOISE PEAK AVERAGE RHO	(THOUSANDS) HOURS	LOGICAL NOISE RHO	(THOUSANDS) HOURS
FRICTION AVG.	*0.56	10-12.7	*0.57	7-12.7	-0.56	5.7-7
FRICTION PK. AVG.	0.90	10-12.7	0.99	10-12.7	0.34	6-8
VERTICAL ECC. AVG.	*0.36	10-12.7	*-0.74	7-12.7	-0.41	5.7-7
VERT. DEF. AVG.	-0.77	10-12.7	-0.99	10-12.7	0.33	6-8
VERT. DEF. PK. AVG.	0.71	10-12.7	*0.83	7-12.7	0.50	2-4
CONTACT NOISE AVG.	--	--	0.87	5.7-7	0.45	5.7-7
CONTACT NOISE PK. AVG.	0.87	5.7-7	--	--	0.44	5.7-7
MOTOR CURRENT	*0.57	10-12.7	*-0.96	7-12.7	0.37	6-8
LOGICAL NOISE	0.45	5.7-7	0.44	5.7-7	--	--

SLIP RING B

PARAMETER	CONTACT NOISE AVERAGE RHO	(THOUSANDS) HOURS	CONTACT NOISE PEAK AVERAGE RHO	(THOUSANDS) HOURS	LOGICAL NOISE RHO	(THOUSANDS) HOURS
FRICTION AVG.	*0.52	6-8	-0.49	2-4	-0.38	8-10
FRICTION PK. AVG.	-0.62	2-4	*0.62	5.7-12.7	0.39	8-10
VERTICAL ECC. AVG.	0.48	8-10	-0.58	2-4	0.60	8-10
VERTICAL DEF. AVG.	-0.94	0-2	-0.95	0-2	0.23	10-12.7
VERTICAL DEF. PK. AVG.	-0.50	6-8	-0.61	7-12.7	-0.56	10-12.7
CONTACT NOISE AVG.	—	—	0.97	0-2	0.52	5.7-12.7
CONTACT NOISE PK. AVG.	0.97	0-2	--	—	0.62	8-10
MOTOR CURRENT	*0.55	0-2	0.76	0-2	-0.43	8-10
LOGICAL NOISE	0.52	5.7-12.7	0.62	8-10	--	--

* Second Highest Correlation

TABLE 8

CORRELATION TRENDS

CORRELATIONS TO
RING A AVERAGE CONTACT NOISE

HOURS THOUSANDS	FRICTION AVG.	FRICTION PK. AVG.	VERTICAL DEF. AVG.	VERTICAL DEF. PK. AVG.
0-2	-.39	-.51	-.22	.34
2-4	-.31	.57	.31	.34
6-8	-.27	-.30	.66	-.27
7-12.7	-.27	.53	.58	-.27

CORRELATIONS TO
RING A PEAK AVERAGE CONTACT NOISE

HOURS THOUSANDS	FRICTION AVG.	FRICTION PK. AVG.	VERTICAL DEF. AVG.	VERTICAL DEF. PK. AVG.
0-2	-.33	-.30	-.22	.27
2-4	-.22	.16	.17	.38
6-8	.28	.44	-.34	.41
7-12.7	.57	-.74	.46	.83

CORRELATIONS TO
RING B AVERAGE CONTACT NOISE

HOURS THOUSANDS	FRICTION AVG.	FRICTION PK. AVG.	VERTICAL DEF. AVG.	VERTICAL DEF. PK. AVG.
0-2	.33	-.29	-.94	.39
2-4	-.39	-.63	-.83	-.25
6-8	.52	-.26	.25	-.50
8-10	-.46	-.58	.44	.49
10-12.7	.21	-.59	-.18	-.16

CORRELATIONS TO
RING B PEAK AVG. CONTACT NOISE

HOURS THOUSANDS	FRICTION AVG.	FRICTION PK. AVG.	VERTICAL DEF. AVG.	VERTICAL DEF. PK. AVG.
0-2	-.28	-.28	-.95	.36
2-4	-.49	.46	.33	-.41
6-8	-.37	-.36	.34	-.37
8-10	-.49	-.55	.28	-.42
10-12.7	-.36	-.37	.67	-.44

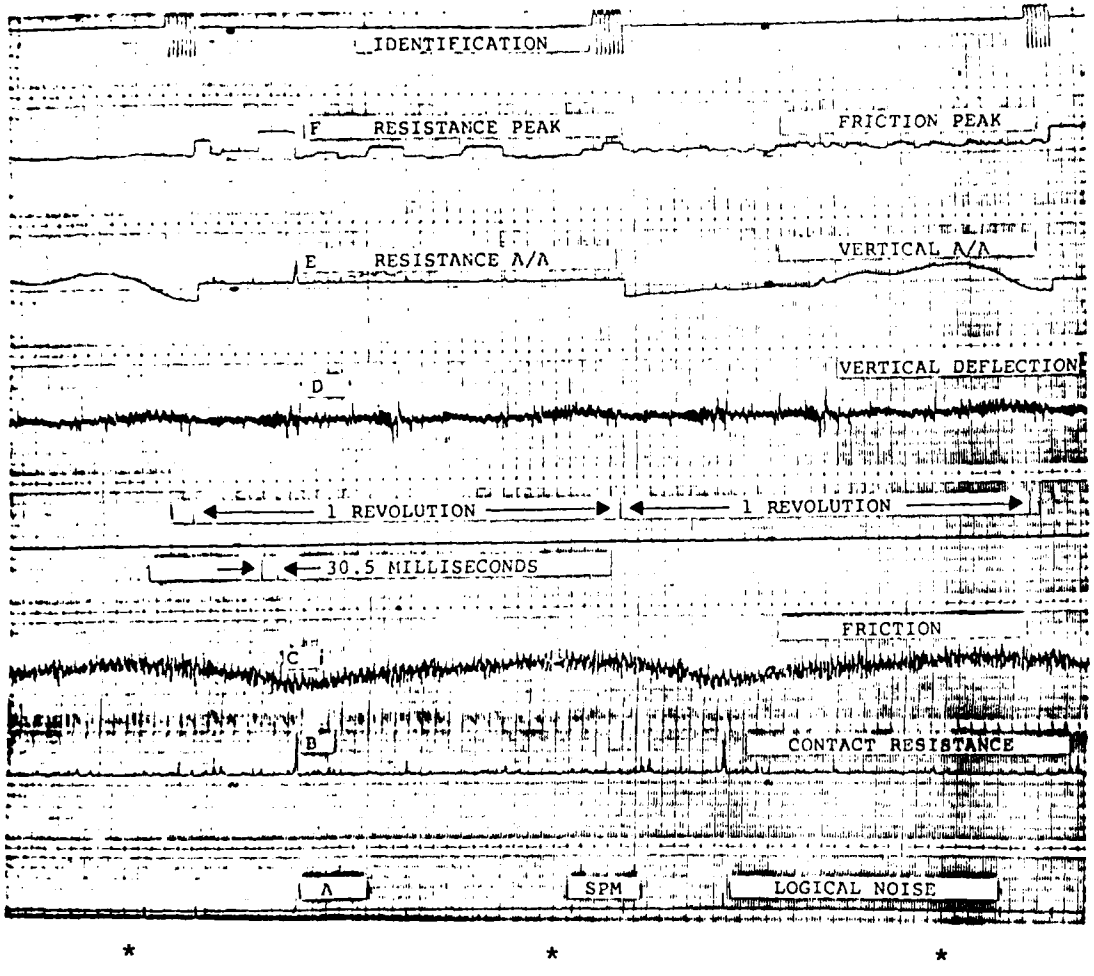

Figure 14. Long-Term Slip Ring Data Burst #159.

showed that three logical noise pulses were present on each slip ring revolution and that they correlated with the vertical brush movement. Figure 14 was generated by a computer plotter operating at 12,000 readings per second and includes two complete slip ring revolutions which show a repeating pattern on each revolution on logical noise, contact resistance, friction, and vertical deflection data channels. An asterisk marks the start of a revolution as indicated by the shaft position marker (SPM) pulses. The logical noise is indicated by point "A" on the figure. The pulses are not resolved well on this plot, but other data show that three pulses are present consisting of two pulses, each one about a millisecond wide separated by two milliseconds. They were followed by a third one millisecond wide pulse seven milliseconds later. Point "B" on the plot shows a corresponding full scale "analog" contact resistance of 500 milliohms. The pulses do not appear full scale because of lower frequency response of this data channel. Point "C" on the friction force data shows a force change indicated by a phase reversal of the resonant frequency signal although it is difficult to see at this scale. Point "D" indicates brush vertical movement of 28.5 micrometers (.0011 inch) associated with the logical noise pulses. Point "E" on the filtered version of the resistance data more clearly shows the three pulses, and point "F" on the resistance peak detector data channel shows detection of the peak value.

In summary, the data plot indicates that a surface discontinuity caused the contact resistance to increase from a nominal 0.1 ohms to an excess of 40 ohms for a period of milliseconds, and that this apparently caused a vertical movement of the brush of 28.5 micrometers. This condition persisted on each rotation for a time period in excess of 12 minutes. The significance of the event is that it indicates a relationship between contact resistance and vertical brush movement, and also verifies the electronics and computer data reduction procedures used to detect millisecond events destructive to slip ring data transmission. The events just described have now been detected

and recorded on dozens of more recent data bursts. In many of the later data bursts, the cause of logical noise pulses was due to high friction forces and not vertical brush movement.

5. RESONANT FREQUENCY ANALYSIS

A resonant frequency analysis experiment was conducted on a duplicate of the long-term slip ring brush block and sensor assembly. This was done in an effort to understand the presence of unexpected high amplitude variations on both the friction and vertical slip ring parameters. This is of concern especially on the friction parameter, because with a brush loading of 5 grams and a probable coefficient-of-friction in the range of 0.2 to 0.6, the maximum friction force should be 1 to 3 grams. However, in the fast fourier transform (FFT) analysis, the friction parameter is shown to consist of a wide range of frequencies with amplitudes of very small fractions of a gram, with the exception of the frequency of 245 hertz which has an amplitude of 5 to 10 grams. The total force in grams must be known in order to calculate the gram force at each frequency.

In summary, the large 245 hertz frequency of the friction parameter is definitely due to a resonant frequency condition of the entire slip ring assembly and sensor system and is not due to slip ring operation. The experimental value determined was 238 hertz. Now that this has been determined, this effect can be discounted from the "real" slip ring data by either graphical methods or by digital filtering in the computer data reduction programs. The resonant frequency has no effect on the "average" friction parameter because the average value of a complete sine wave is zero to these circuits. However, real "peak" values due to slip ring operation must be taken from the analog tape recorder data after discounting the 245 hertz. A resonant frequency test on the vertical parameter yielded a resonant frequency of 119 hertz. This does not correspond to the large 655 hertz frequency shown in the FFT analysis of the vertical parameter. The large value is, therefore, thought to be due to actual slip ring/brush action. Also, the 655 hertz does not

consistently appear in the data as a resonant frequency would. An FFT plot of slip ring data showing these resonant frequencies during test operation is shown in Figure 15. The y-axis amplitude units on this figure is the ratio of the energy of each specific frequency to the total energy of the signal.

Tests were also conducted to determine how to raise the resonant frequencies above the range of slip ring data. Different materials and sizes of parts of the slip ring assembly were substituted for the original parts. Changes were made in the brush preloading, brush blocks, brush block support springs, the friction "arm", and load cell connector. It was found that, with the various combinations, the friction resonant frequency could be varied over a range of 200 to 500 hertz.

6. SATELLITE TELEMETRY NOISE REQUIREMENTS

Information presented at the 1981 Instrument Society of America's Aerospace Conference may prove useful in linking contact resistance data from the slip ring experiments to actual satellite telemetry data reliability.[7] Included was the noise requirements and corresponding limits of telemetry systems for reliable operation. The allowable noise levels depend upon the design and type of system (AM or FM), the point in the system where the noise is introduced, the noise type (pulse or white noise), and the actual reliability figure of the data that is required. The key is the signal-to-noise (S/N) ratio. Allowable ranges of the S/N ratio vary from 10 to 40 decibels (db) depending upon the factors previously mentioned. Higher db values indicate a probable greater data reliability. Long-term slip ring B has, at times, exhibited an average contact resistance of 0.5 ohm for hundreds of hours corresponding to about 52 db. Some unit rig tests have shown only 40 to 46 db, and peaks on all slip ring tests have indicated a S/N ratio as low as 6 to 10 db at various times. Clearly, performance at these low levels is marginal or, during peaks, absolutely destructive to telemetry transmission. It means that slip ring noise alone could deteriorate the required

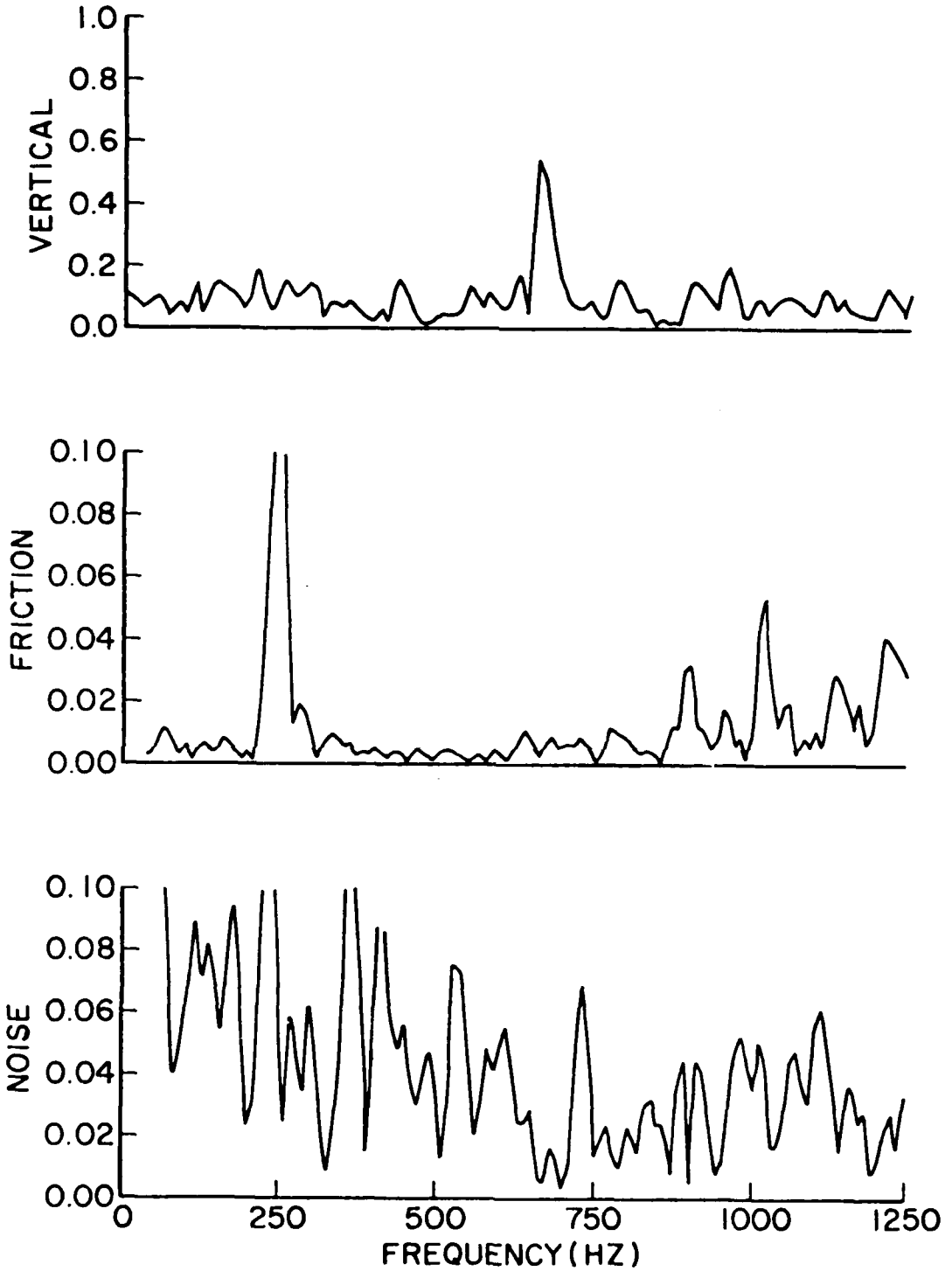

Figure 15. Representative Spectrum Plot of Long Term Rig Parameters.

S/N ratio all that it is allowed. This doesn't allow for any S/N ratio reduction due to atmospherics, power noise, other radio interference, etc. which are normally encountered.

The situation may be even worse than indicated by the S/N ratios just quoted. The slip ring experiment's S/N ratio is computed based on a signal input which is a constant D.C. current. If the one million bits per second rate (or higher) of a telemetry system was input, the S/N ratio would surely be even lower due to high frequency noise generation components being added to the constant D.C. level.

To determine the relationship of contact resistance to S/N ratio, experiments would have to be performed duplicating telemetry system operation, probably on one of the unit rigs. A repeating code at one million bits per second (one megabaud) could be input to the slip ring with the S/N ratio and D.C. resistance measured simultaneously. Also, the number of digital bit errors per second should be measured to determine the resulting reliability figure or error rate. Such a system would require considerable time and cost to set up but would provide the needed link between experimental data and actual telemetry reliability.

7. CONCLUSIONS

The following is a summary of preliminary results determined from the long-term slip ring and slip ring unit rig data to date. While these implications are indicated by the available data, they are subject to further analysis and future slip ring test data on each point. The following slip ring characteristics are indicated.

(a) In periods of generally low contact resistance noise levels, vertical brush deflection peaks appear to be the primary factor in the cause of high resistance peaks and logical noise. The friction force level may determine only the baseline resistance level.

(b) In periods of generally high contact resistance noise, friction appears to be the driving force and causes the high level resistance peaks and logical noise. Vertical brush deflection peaks now cause either low or high resistance levels and peaks.

(c) In periods of generally high contact resistance noise, the FFT spectrum of all three parameters of contact resistance, vertical deflection, and friction shift their primary frequencies to equal the mechanical resonant frequency of the friction parameter, thus indicating friction as the primary driving factor.

(d) Only slight baseline changes are seen in the values of contact resistance noise, vertical brush deflection, and friction; but there are dramatic changes in peak values.

(e) Erratic contact resistance variations last for periods of minutes to months. Erratic variations at generally low resistance levels occur only at a few specific points on the slip ring. However, high levels of friction cause erratic resistance levels around the entire slip ring circumference.

(f) Striking debris or surface discontinuities on the ring appears to cause the brush to bounce or oscillate.

(g) Correlation coefficient data verifies quantitatively the statements (a), (b), (c), and (d).

(h) The correlation data indicates that definite trends toward either higher or lower correlations exist for certain parameters as the number of test hours increases.

(i) The correlation program can be used to generate a valid equation relating any two parameters over a specified hour range in many cases.

SECTION III
BEARING DEGRADATION STUDIES

1. BEARING TEST RIG DESIGN

The design of the data acquisition, experiment control, and data analysis system for the bearing test rigs has been completed. The heart of the system is the LSI-11/23 microprocessor manufactured by Digital Equipment Corporation (DEC). It uses many peripheral interfaces, output devices, and specialized analog data circuits to form a comprehensive data test system. The goal of the system design was to provide a computer controlled data acquisition system which would allow measurement of the required parameters needed to determine the causes of bearing degradation discussed in Section I.

A. Computer System

The LSI-11/23 microprocessor which will be used in this system is the latest technological development in microprocessors. It is essentially a PDP-11/34 minicomputer reduced in physical size and adapted to the LSI-11 computer series bus structure. It is 2 1/2 times faster, has six times the memory, and a larger instruction set than the LSI-11/03 used on the current slip ring experiments. Most importantly, it uses the DEC RSX-11M real-time multi-user software operating system. This is a time-share system which can execute up to 32 software programs simultaneously. It will result in increased capability and allow the following tasks to be performed simultaneously by the LSI-11/23, where before a dedicated LSI-11/03 would be required for each task.

(1) Perform data acquisition and experiment control of all four bearing test rigs and four slip ring test rigs. Data acquisition may be triggered by operator command, at preset time periods, or when the computer detects that any parameter data channel has exceeded preset limits. Data will be stored on a dual 5M byte disk

memory. Experiment control includes automatic setting of drive motor speed.

(2) Perform analysis on data stored in the disk memory. Analysis may include averaging, sorting, fast fourier transform (FFT), correlation, scaling to engineering units, quadratic curve fitting, linearization of data, and basic statistical functions.

(3) Plotting of all data and data analysis results on a digital printer/plotter. This will include data, text, graphs, charts, formulas, etc. All graphs and charts will be completely labeled and will be of a quality suitable for reproduction and reports.

(4) Control, modification, and status of all experiments will be displayed on the CRT terminal or printed by the printer/plotter.

Although construction of the system is not yet complete a block diagram and basic interconnections of the anticipated system components are shown in Figure 16.

B. Sensor Description

A temporary, manually-operated data system is currently in use. The temporary system utilizes all of the same mechanical apparatus, sensors, and signal conditioning as the final computer-operated system. The only difference is in the amount of data processing capability. All sensors are calibrated "in place" in the test system. Accuracies are listed as the allowable % deviation from each sensor over the range of that parameters useful scale.

Sensors provided in the bearing rig instrumentation system are as follows:

(1) A 250-gram strain gauge load cell is used to measure bearing torque. It is loaded by an arm extending from the inner race of the bearing to the cell. The output is calibrated in millinewton meters. Accuracy is $\pm$1%.

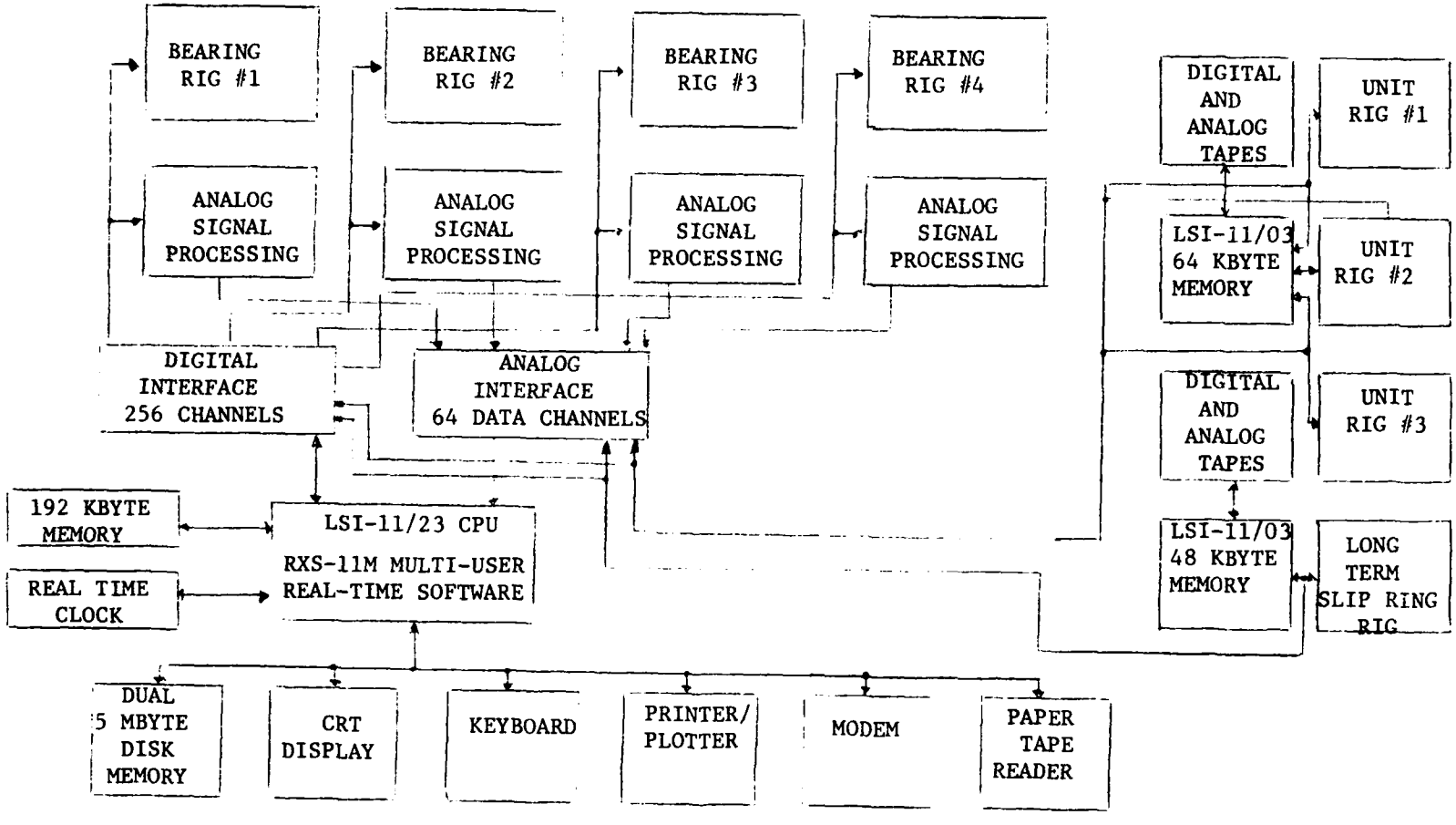

Figure 16. Block Diagram of Bearing and Slip Ring LSI 11/23 Test Data System.

(2) A 300-lb. strain gauge load cell mounted on the inner race of the bearing and loaded by the bearing load arm measures bearing load. The output is calibrated in newtons. Accuracy is ±1%.

(3) A micro-ampere constant current source with the current fed from inner to outer race and with the resulting voltage developed across the races measured and calibrated in kilo-ohms of resistance measures Inner-to-Outer (I/O) race resistance. This is a measure of race to ball contact. Accuracy is ±1%.

(4) Shaft or outer race drive speed is measured by a timer and a once-per-revolution shaft position marker (SPM) sensor. The sensor is an optical interrupter circuit aimed at a small tab on the shaft. The timer's output is calibrated in rpm. Accuracy is ±0.01 rpm.

(5) Retainer or ball speed is measured by a timer and a proximity sensor aimed at a small metal target mounted on the retainer which provides a once-per-revolution pulse. The timer's output is calibrated in rpm, and the accuracy is ±0.01 rpm.

(6) Motor current and power are measured by a 0.1Ω current-sensing resistor in the power circuit from which a voltage measurement is calibrated in both amperes and watts. Accuracy is ±1%.

2. BEARING TEST 4001 DATA

A. Test Set-Up Conditions

The first bearing rig test was designated as test #4001 and was begun at atmospheric pressure. The test bearing is a 100 mm bore bearing with a phenolic retainer and Vac Kote lubrication. It is operated at a constant speed of 60 rpm and constant load of 133.7N. The average, minimum, and maximum values of the parameters listed in section III I.B. were recorded manually from digital meters.

This bearing was previously run by Southwest Research Institute at a higher rpm and load than in this experiment.

B. Data Plots

The test can be divided into four separate periods for discussion. First is the initial wear-in period in atmosphere from 0 to 334 hours. Next is the period of stable operation in atmosphere from 334 to 1558 hours. Then comes the period of vacuum transition from 1558 to 1656 hours. Lastly is the period of stable vacuum operation from 1656 to 3700 hours. Plots of bearing test #4001 data are shown in Figures 17 through 22 for the time period of zero to 3700 hours of operation. Most of these plots were computer generated. Note that Figures 18 and 20 have a logarithmic hours scale.

The criteria used for the completion of the wear-in period is the hours at which the minimum I/O resistance level reaches a maximum value and then stabilizes. As other bearing test results are obtained, this criteria may be quantified. The hours at which the minimum I/O resistance level reaches within either one, two, or three standard deviations of its eventual peak value may be used.

The initial bearing wear-in period of 0 to 334 hours was characterized by a 40% drop in torque (Figures 17 and 18), a rise in inner-to-outer (I/O) race resistance (Figures 19 and 20), a steady drop in motor current (Figure 22), and nearly constant values of outer race rpm and retainer rpm (Figure 21). Outer race (drive) rpm and load are held constant in this test except for small daily variations which are primarily due to room temperature variations. During the wear-in period, minimum to maximum (peak-to-peak) torque values also decreased by about 50%.

The I/O race resistance values shown in Figure 20 show an initial small drop in resistance and then a dramatic resistance increase as the torque values decreased during the wear-in period. Note the dramatic change in the minimum values at 250 to 334 hours. Torque and I/O resistance vary inversely. The described resistance changes are apparently a good

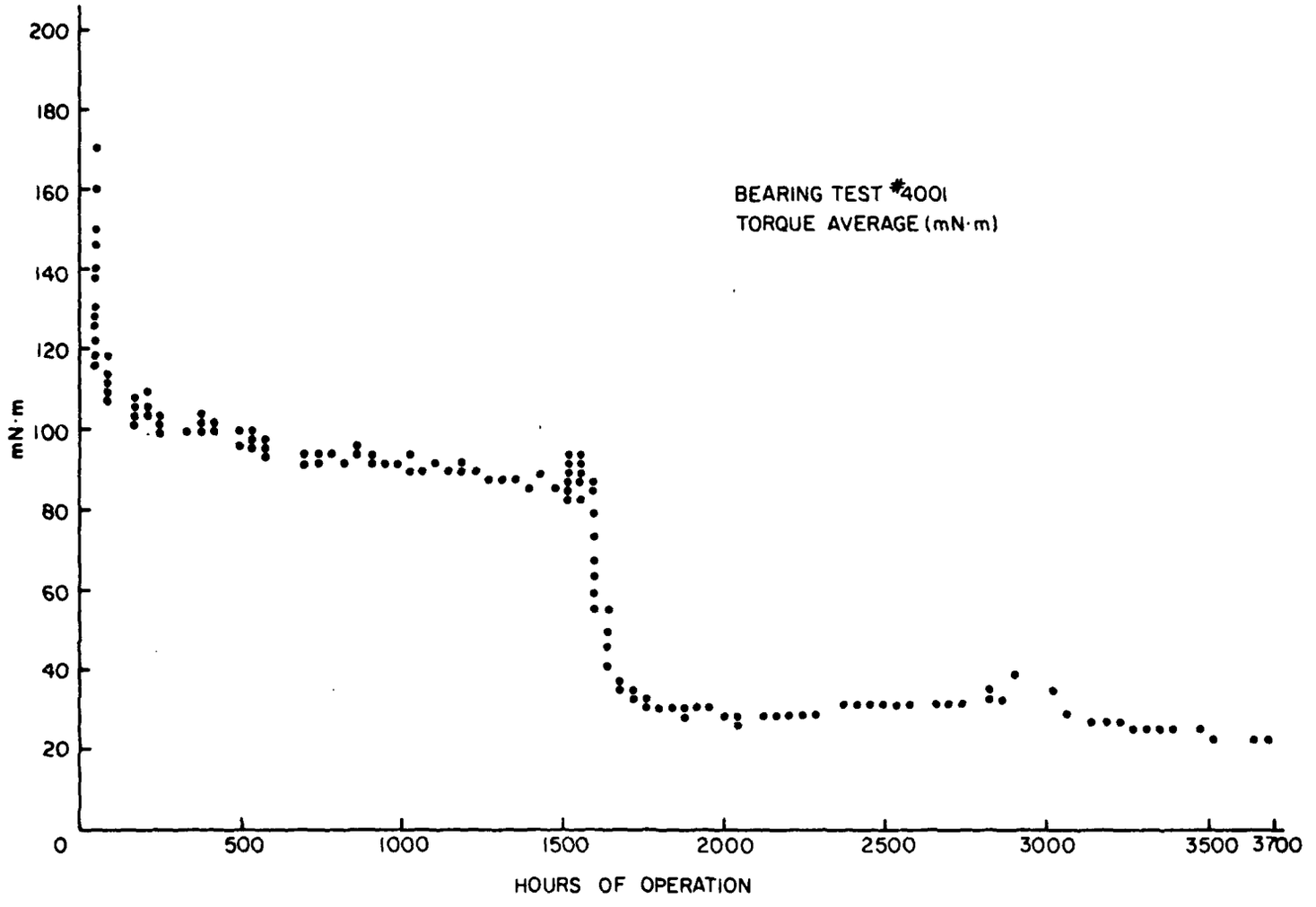

Figure 17. Computer Plot of Torque Average.

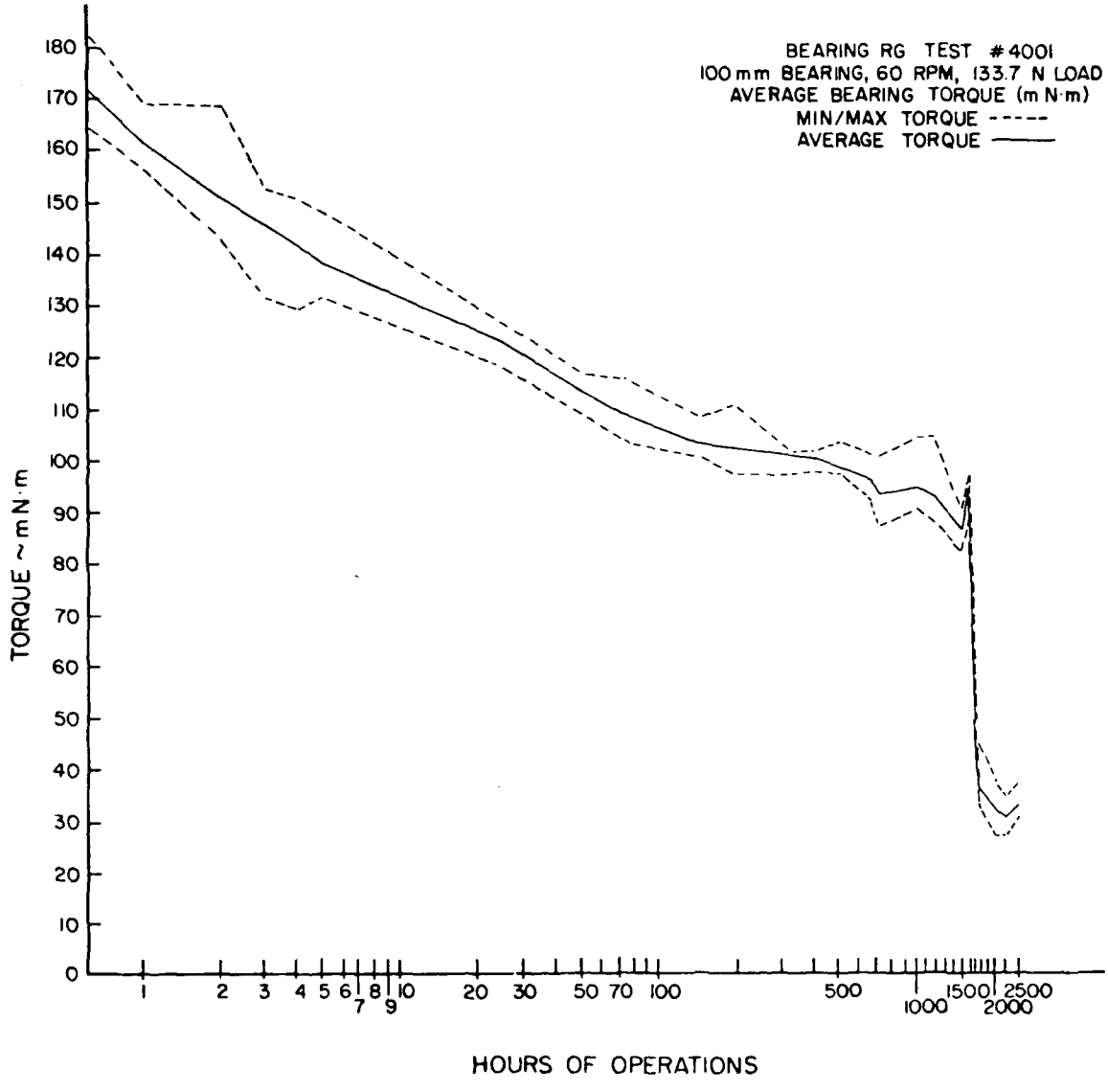

Figure 18. Torque Test 4001.

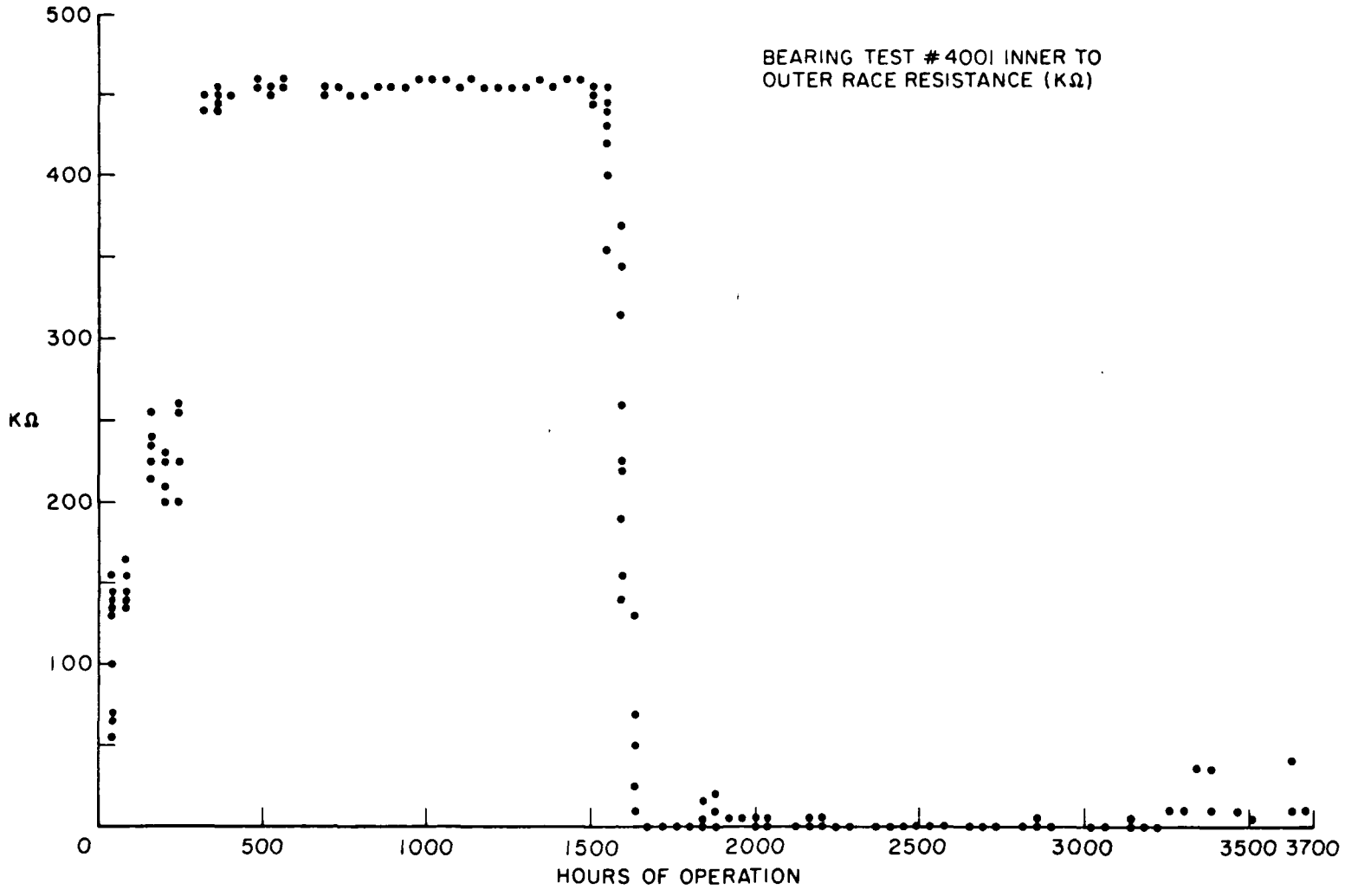

Figure 19. Computer Plot of I/O Race Resistance Average.

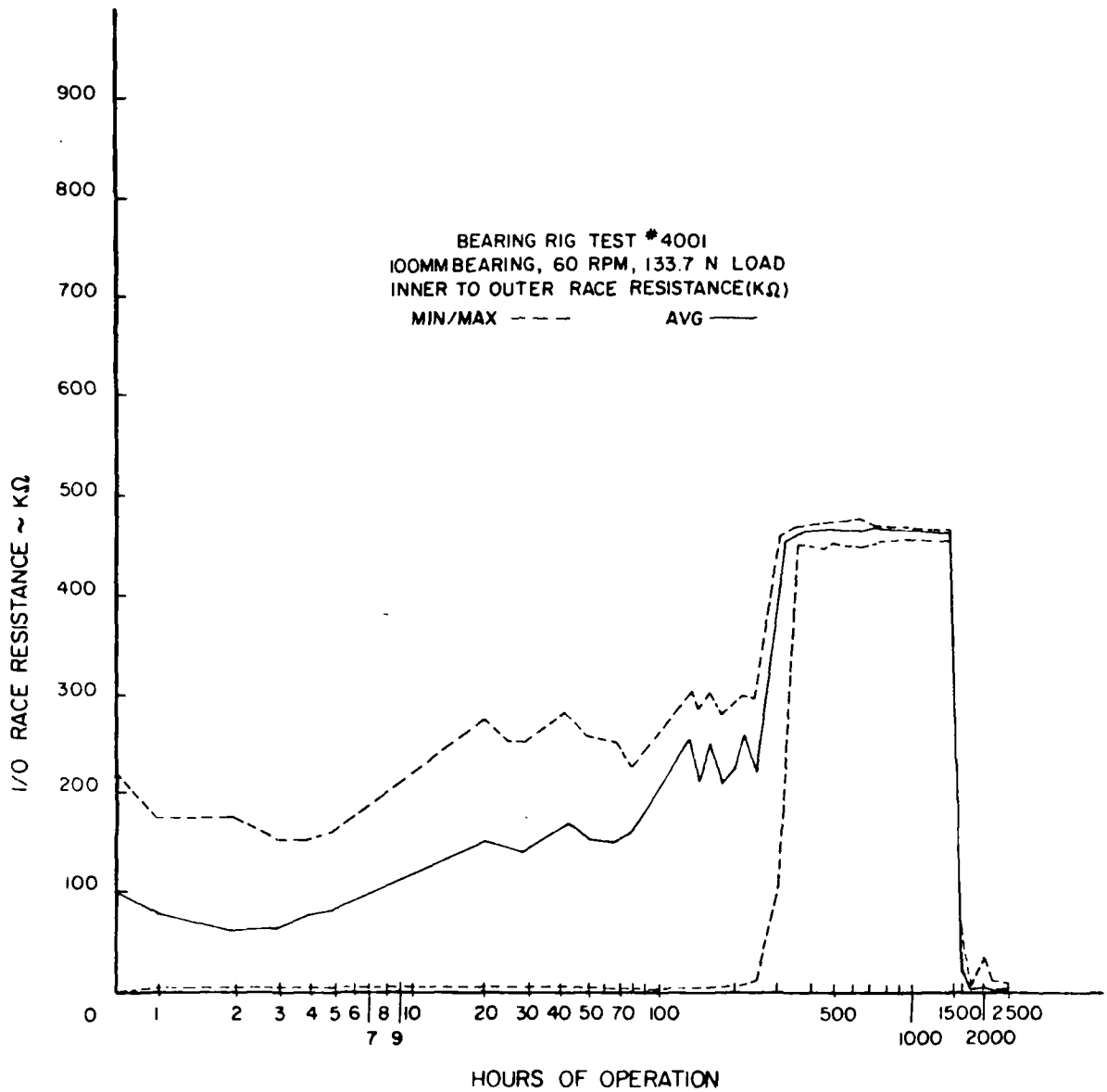

Figure 20. Inner to Outer Race Resistance, Test 4001.

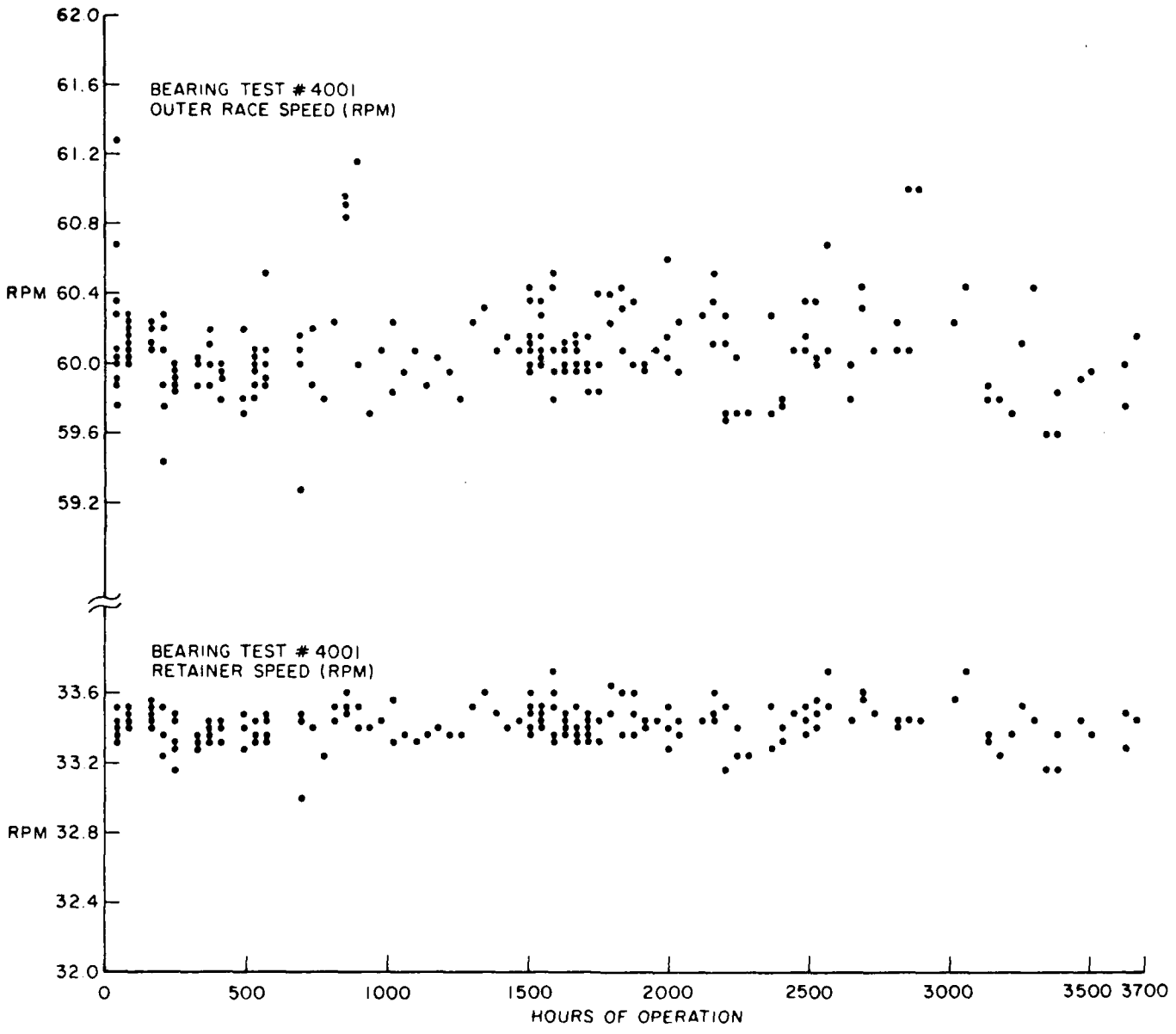

Figure 21. Outer Race and Retainer RPM, Test 4001.

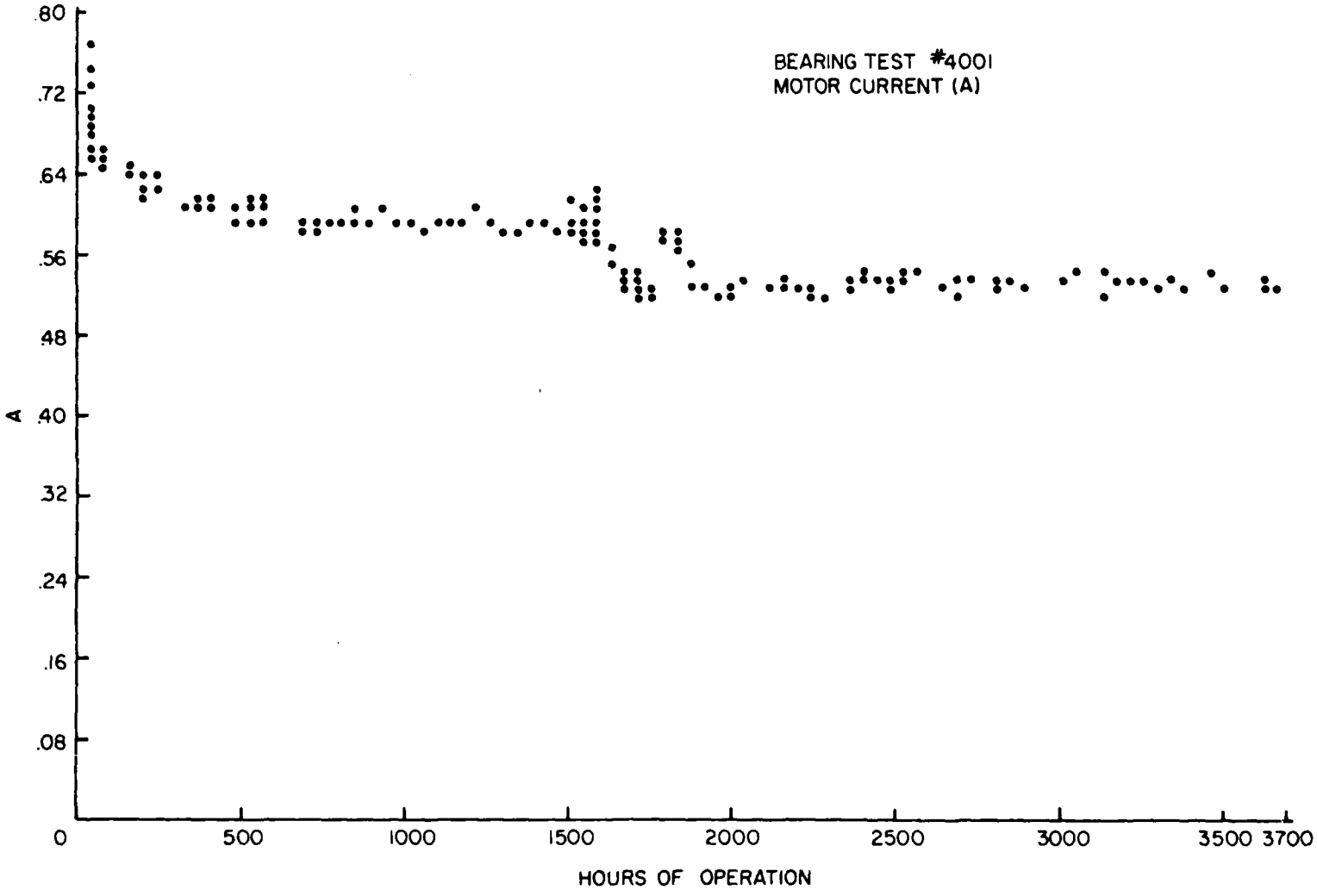

Figure 22. Motor Current, Test 4001.

criteria to determine the wear-in period. Low resistance is apparently caused by a high amount of direct ball-to-race contact (metal-to-metal) due to asperities on the metal parts. As these peaks wear down, the ball makes less contact with the race and rides on the lubricant film. This, in turn, causes a large rise in the resistance values, especially minimum resistance values, and also results in lower torque values.

Figure 22 shows the motor current, which is proportional to motor power, delivered to the bearing drive motor. Note the gradual and fairly steady decrease of the drive power. It shows no large change at 250 to 334 hours or at any other point. Apparently, the decreased power (torque) required by the motor is due to wear-in of the motor and rotary vacuum feedthru bearings and is not related directly to wear-in of the test DMA bearing. This is verified by using a conversion of the units of watts; that is, 1N·m/s = 1 watt. Therefore, if the bearing torque in mN·m is divided by the integration factor of 1 second, the result is bearing power in milliwatts. In other words, it would require 100 milliwatts of motor power to drive a bearing torque level of 100 millinewton-meters. Therefore, at the start of the test, the 172 mN·m of torque translated to requiring 0.172 watts of power from the motor drive. Since 6 watts of motor power was measured at that time, the proportion of the test bearing torque contribution to total motor current or power was only 1/35. Also, much later in the experiment at 2500 hours and later, the ratio of test bearing torque to total motor power was 1/144. Clearly, a different test rig configuration is needed in order to compare these experiments motor currents to actual spacecraft motor current. Motor current is important because it is one of the few parameters measured on actual spacecraft. A drive motor located in the vacuum chamber, which would eliminate the rotary vacuum feedthru, may be a solution. However, the motor current parameter is still useful in monitoring the health of the drive system.

The stable period of atmospheric operation from 334 to 1558 hours is characterized by only a change of a few percent in both torque and I/O race resistance. Peak-to-peak variation levels were also nearly unchanged. I/O resistance and torque continue to be inversely related.

The vacuum transition period from 1558 to 1656 hours includes the period of pressure changes of from 10^5 Pa (atmosphere) to $8x10^{-5}$ Pa ($6x10^{-7}$ torr) and is shown in detail in Figure 23. When vacuum operation began, both torque and I/O resistance began to decline. The cause of this change from the previous inverse relationship is not known but may possibly indicate a chemical or conductivity change in the lubricant, which results in decreased electrical resistance. The cause of the torque drop at initial vacuum operation is also unknown. However, the cause is not wind or air resistance, or the lack of; because torque did not start to drop until about 23 hours after high vacuum operation was initiated. The time-delay period might indicate that the torque drop is related to the outgassing of a mid-range weight molecule which occurred between the ion pump pressures of $1x10^{-6}$ and $6x10^{-7}$ torr although more testing is needed to validate this. Outer (drive) race rpm and retainer rpm shown in Figure 21 seem unaffected by vacuum operation. The quoted pressures are measured at the ion pump, so the bearing chamber pressures may be slightly higher. The ending of the vacuum transition period was arbitrarily defined as the time (hours) at which the torque frequency spectrum shifted. Spectra will be covered in the next section.

The period of stable operation in vacuum is from 1656 hours through the remainder of the graph (3700 hours). This period is characterized by low torque average and torque peak-to-peak values, and very low I/O race resistance values. No obvious relationship now exists between torque and I/O race resistance.

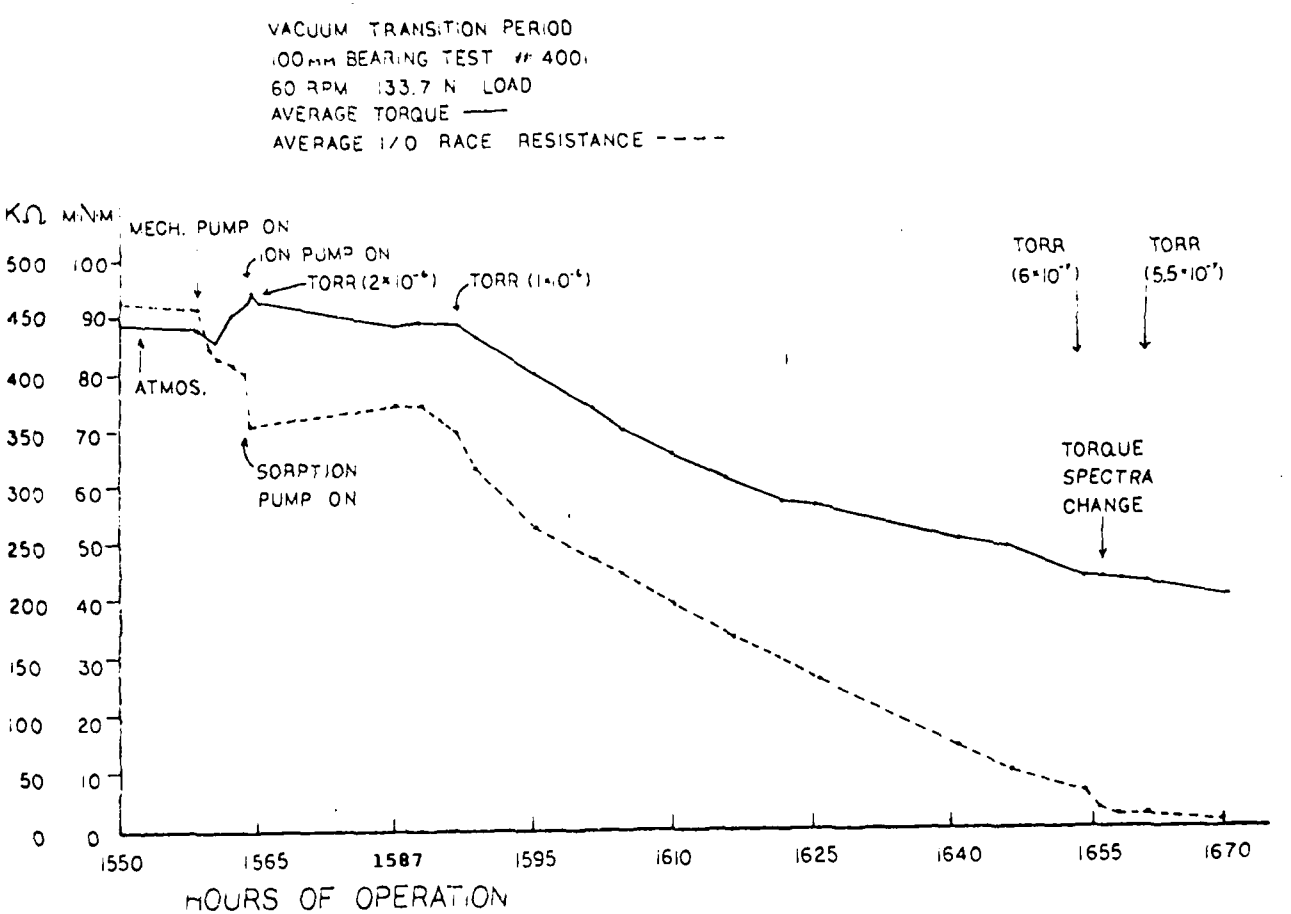

Figure 23. Vacuum Transition Period, Test 4001.

C. Frequency Spectra

The frequency spectrum of the parameters of torque and I/O race resistance are recorded at every data reading. Several spectra have been selected as typical and are presented as Figures 24 through 29. The spectra are generated by an FFT spectrum analyzer. At first, an X-Y plotter was used to record spectra, but it failed after only a few hours; and a strip chart recorder was substituted instead. For this reason the frequency scale (x-axis) in Figures 24 and 25 is linear, while the frequency scales of Figures 26, 27, 28, and 29 are not. However, the relative amplitude scales are correct among all figures. The spectra represent the frequencies present in the variable components of the signal and not the overall average level. For this reason there is not as great a magnitude change as might be expected in the amplitudes.

Figure 24 shows the initial torque spectrum at the start of the experiment (0 hours) and Figure 25 the initial I/O race resistance spectrum. Torque is dominated by a large peak near 1 Hz, representing the one revolution-per-second speed of rotation, and at 220 Hz by a peak initially thought to represent the mechanical resonant frequency of the system (as we shall see later, this was disproven). Smaller peaks at 91, 133, and 366 Hz are also present. The I/O race resistance spectrum of Figure 25 shows a broad band of frequencies of nearly equal amplitude except for a peak at 202 Hz. This band or white contact noise is typical of electric contacts as seen from the slip ring studies and extends up to 100 KHz which is as high a frequency as the equipment can measure. No torque frequencies have yet been detected above 400 Hz.

Figure 26 depicts torque and I/O race resistance at 213 hours as the wear-in period neared completion. Little change is seen in the torque spectra from the initial spectra except for a small reduction in amplitudes due to decreasing peak-to-peak values. The low frequency (1 Hz) torque has greatly reduced in amplitude. The I/O race resistance spectrum is essentially

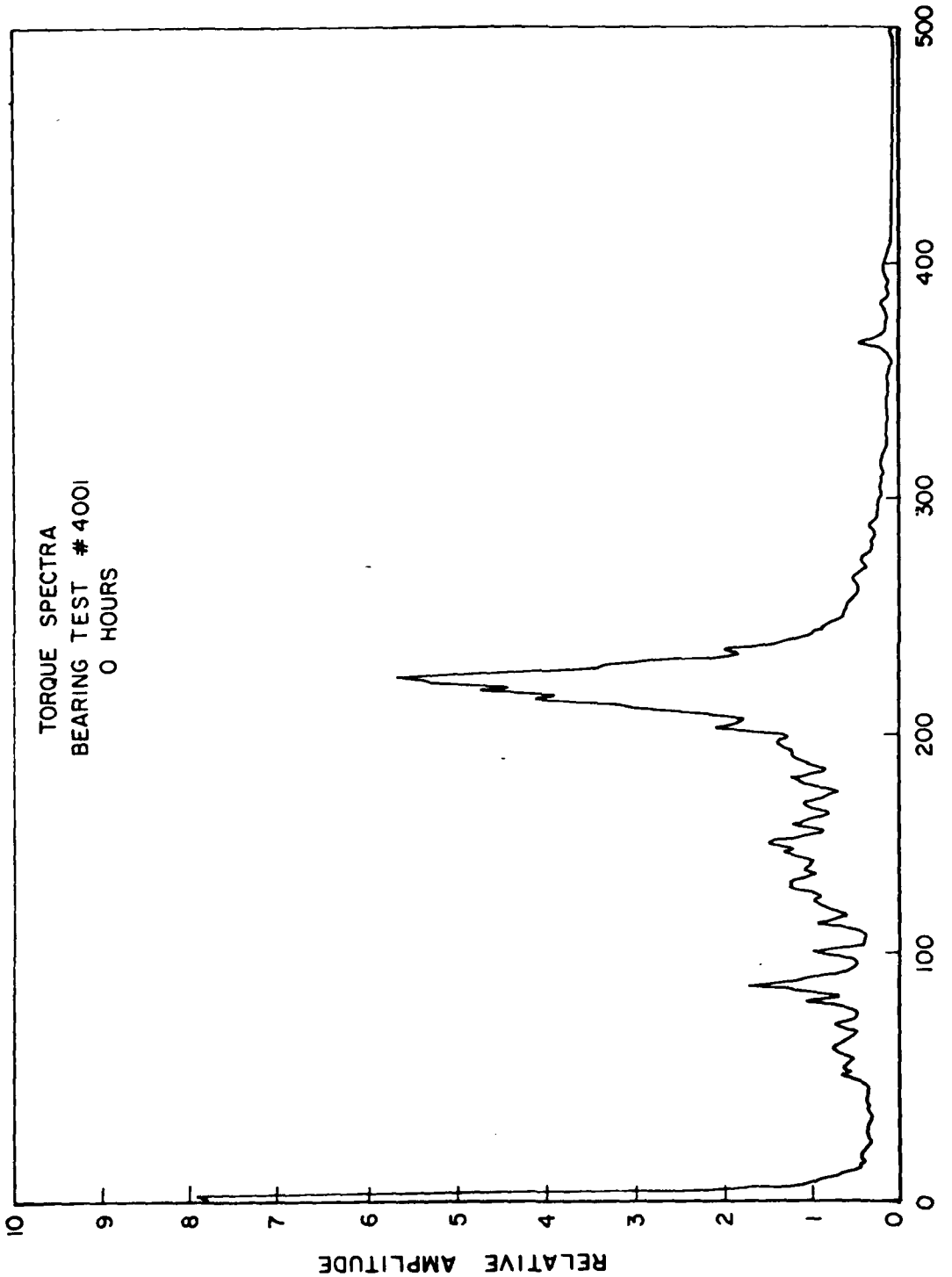

Figure 24. Initial Torque Spectra.

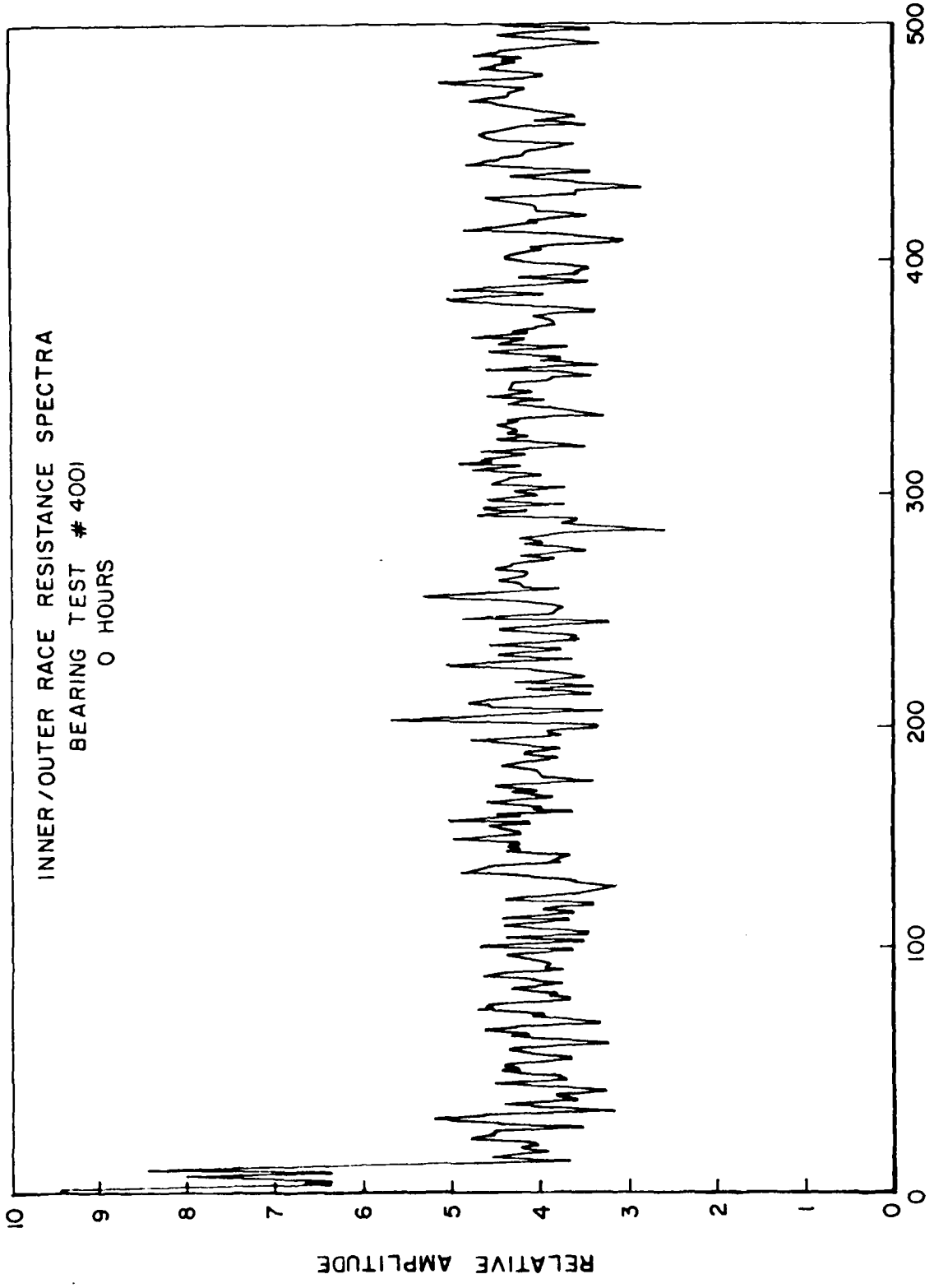

Figure 25. Initial I/O Resistance Spectra.

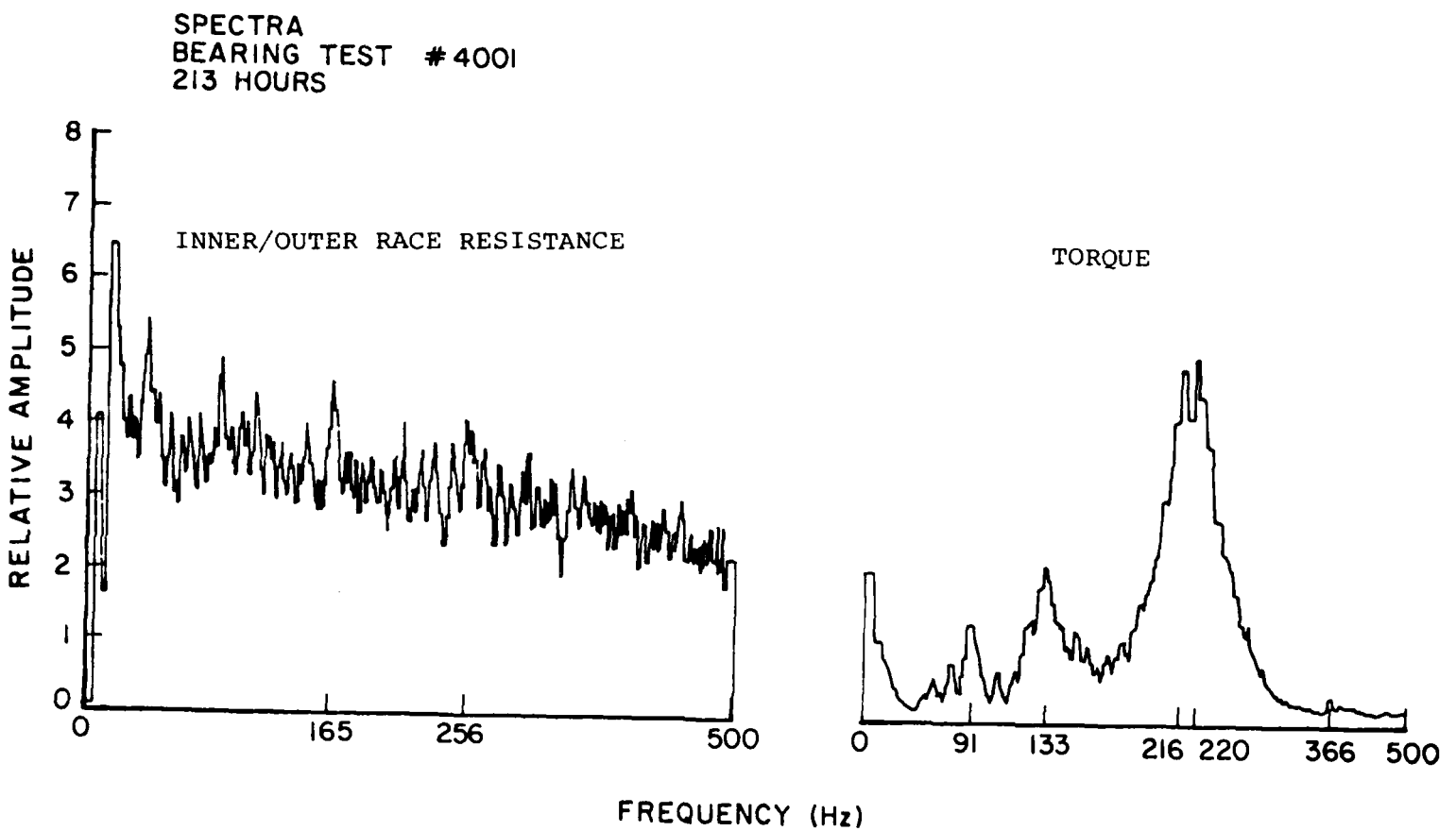

Figure 26. Torque and I/O Resistance Spectra at 213 Hours.

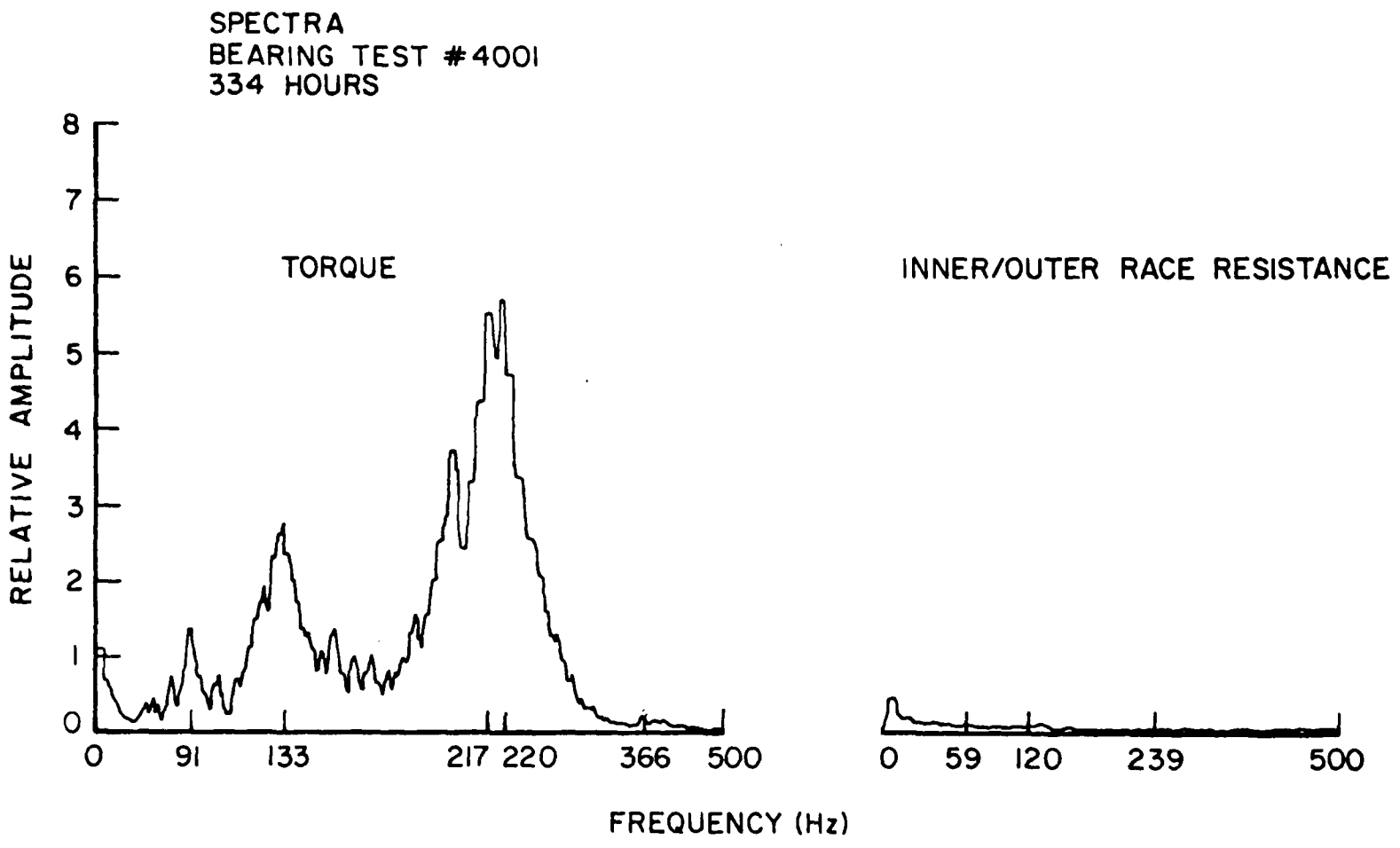

Figure 27. Representative Spectra of 334 thru 1654 Hours.

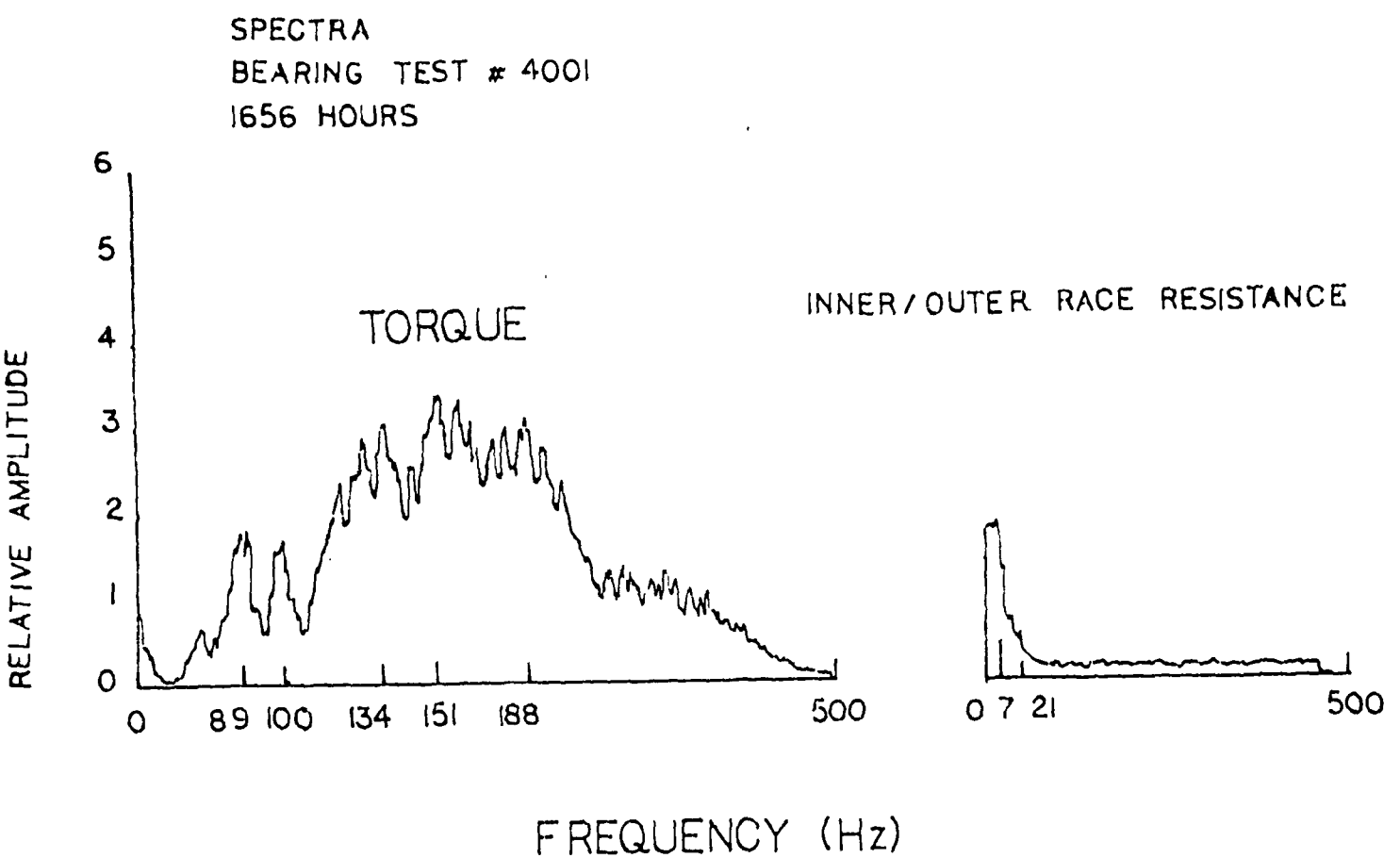

Figure 28. Spectra at 1656 Hours, Test 4001.

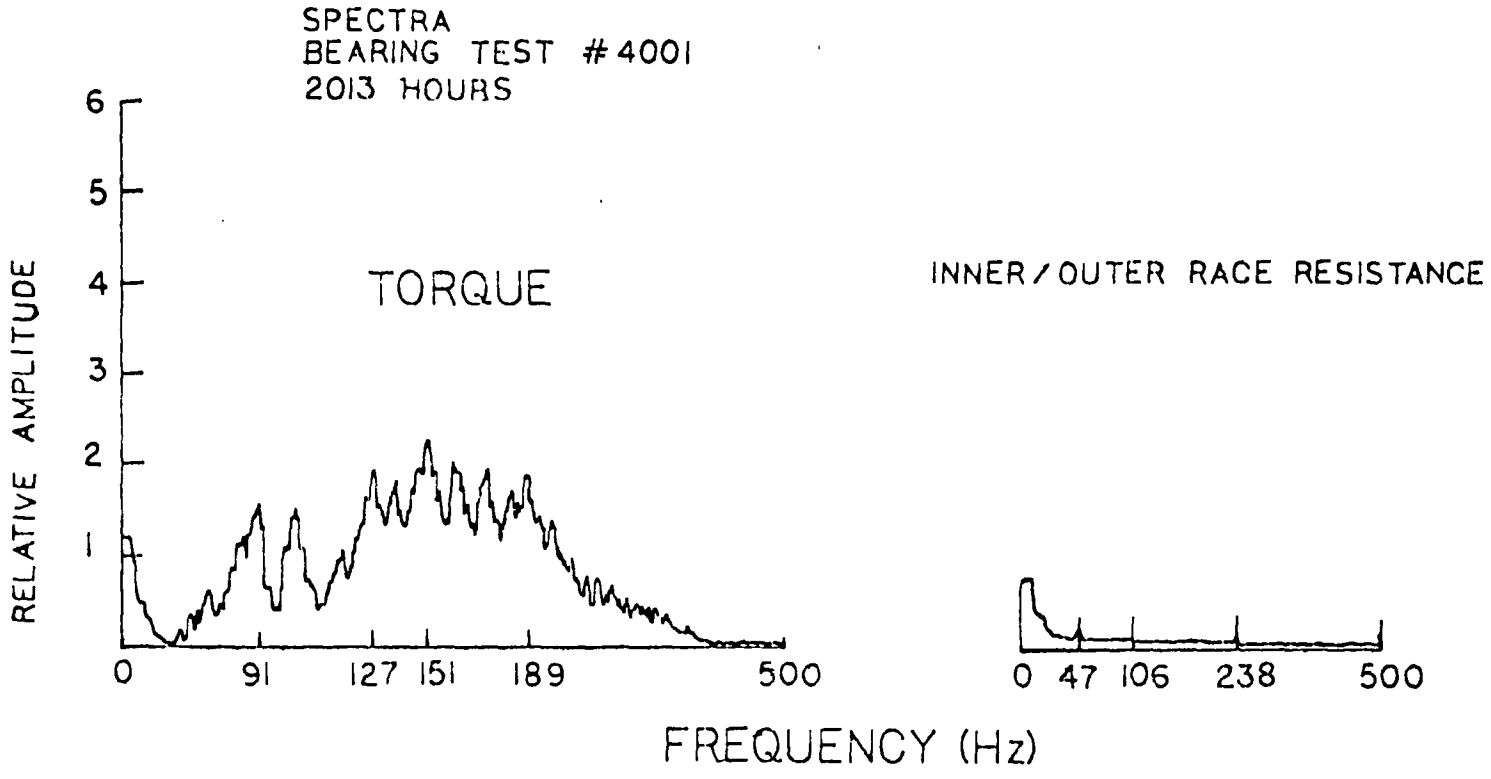

Figure 29. Spectra at 2013 Hours, Test 4001.

unchanged except for a slight decrease in amplitude of the high frequencies which is, perhaps, an indication that wear-in is near.

Figure 27, recorded at 334 hours is representative of all spectra of 334 thru 1654 hours. At the completion of wear-in, (334 hours) little change in torque spectra is indicated by Figure 27 except for the continued decreasing of amplitude at low frequencies. I/O race resistance spectra, however, has nearly vanished because the peak-to-peak values are now greatly reduced after wear-in. The only three frequencies of sufficient amplitude to record were apparently due to the 60 Hz power line frequency interference and its harmonics. This spectra did not change through 1654 hours, which is 90 hours after ion vacuum pump operation began at 1564 hours. During this 90-hour period, average torque decreased by 40%, but the amplitude and frequency characteristics of the torque variations held constant. Then by 1656 hours, the spectra had changed to that of Figure 28. Only two hours had elapsed since the spectra was as is shown in Figure 27. The vacuum pump pressure at 1656 hours was 5.5×10^{-7} torr. This spectra change may signal that the mechanisms which caused the vacuum torque drop were completed at this point. For this reason the spectral change was used to define the end of the vacuum transition period. These hours and points mentioned are also labeled on the vacuum transition graph of Figure 23. A later spectra of the torque parameter is shown in Figure 29. In Figures 28 and 29, note the shift to a lower frequency band in the torque spectra to a band centered around 158 Hz. The previous 220 Hz peak of Figure 27 has vanished. The shifting of this frequency probably indicates that the original 220Hz was not a mechanical resonant frequency of the system because resonant frequencies remain essentially constant. Also, the general amplitude has decreased from six to three to two units in Figures 26, 27, and 28, respectively.

The vacuum transition region is important because it may simulate the sudden pressure change experienced by a satellite

after launch into space. During this initial period, the first important changes may possibly occur in lubricant and bearing operation. Much more study of the transition region is needed.

D. Correlation Analysis

Bearing test #4001 data has been processed by the correlation program. All data is permanently stored in disk files and can be accessed at any time for further analysis, plotting, etc. For a more detailed explanation of the definition and use of correlation coefficients and curve fit equations, refer to Section II, part 3(A) and 3(B) of this report. Table 9 presents correlations between various pairs of bearing parameters, while Table 10 lists the corresponding curve fit equations' coefficients and other statistics generated by the program. Only four parameters have been processed by the correlation program at this time. Torque minimum, I/O race resistance minimum, I/O race resistance maximum, and vacuum pressure should be added to the program. Motor current was dropped from the correlations because it has no recognizable relationship to the test bearing parameters as was discussed in a previous section. Load, outer race rpm, and retainer rpm correlations were nearly zero, because they were held nearly constant by the experiment setup conditions. Although temperature is included, even its variation was only ± 3 or 4°C.

Table 9 lists all possible correlations between the four parameters for each of the four different periods or hour ranges of the experiment previously described. Any column/row combination can be read to determine corresponding correlation (RHO) and standard estimate of error (SE) values. The symbol N is the number of data points recorded in the hour range. In all hour ranges torque versus torque max contains the highest correlation values. This may indicate that the reduction of large torque peak values is perhaps a greater factor in average torque reduction than actual torque baseline changes, especially through 1656 hours. The best correlations for most parameters occurred in the vacuum transition region (1557-1656 hours). This

TABLE 9

BEARING TEST #4001 CORRELATION DATA

0-334 Hours
N = 47

	Torque Avg.	Torque Max.	I/O Race Resistance Avg.	Temperature
Torque Avg.		RHO = 0.98 SE = 3.74	RHO = -0.77 SE = 60.72	RHO = 0.20 SE = 0.52
Torque Max.	RHO = 0.98 SE = 3.74		RHO = -0.82 SE = 54.10	RHO = 0.20 SE = 0.52
I/O Race Resist. Avg.	RHO = -0.77 SE = 60.72	RHO = -0.82 SE = 54.10		RHO = -0.48 SE = 0.46
Temperature	RHO = 0.20 SE = 0.52	RHO = 0.20 SE = 0.52	RHO = -0.48 SE = 0.46	

335 - 1556 Hours
N = 67

	Torque Avg.	Torque Max.	I/O Race Resistance Avg.	Temperature
Torque Avg.		RHO = 0.90 SE = 1.97	RHO = -0.27 SE = 5.35	RHO = -0.37 SE = 0.82
Torque Max.	RHO = 0.90 SE = 1.97		RHO = -0.14 SE = 5.50	RHO = -0.43 SE = 0.80
I/O Race Resist. Avg.	RHO = -0.27 SE = 5.35	RHO = -0.14 SE = 5.50		RHO = -0.42 SE = 0.81
Temperature	RHO = -0.37 SE = 0.82	RHO = -0.43 SE = 0.80	RHO = -0.42 SE = 0.81	

1557 - 1656 Hours
N = 21

	Torque Avg.	Torque Max.	I/O Race Resistance Avg.	Temperature
Torque Avg.		RHO = 1.00 SE = 1.38	RHO = 0.97 SE = 37.07	RHO = 0.68 SE = 0.58
Torque Max.	RHO = 1.00 SE = 1.38		RHO = 0.97 SE = 31.47	RHO = 0.74 SE = 0.53
I/O Race Resist. Avg.	RHO = 0.97 SE = 37.07	RHO = 0.98 SE = 31.47		RHO = 0.80 SE = 0.47
Temperature	RHO = 0.68 SE = 0.58	RHO = 0.74 SE = 0.53	RHO = 0.80 SE = 0.47	

1657 - 3700 Hours
N = 83

	Torque Avg.	Torque Max.	I/O Race Resistance Avg.	Temperature
Torque Avg.		RHO = 0.81 SE = 2.61	RHO = -0.56 SE = 6.45	RHO = 0.52 SE = 1.41
Torque Max.	RHO = 0.81 SE = 2.61		RHO = -0.44 SE = 7.02	SE = 0.49 SE = 1.44
I/O Race Resist. Avg.	RHO = -0.56 SE = 6.45	RHO = -0.44 SE = 7.02		RHO = -0.24 SE = 1.61
Temperature	RHO = 0.52 SE = 1.41	RHO = 0.49 SE = 1.44	RHO = -0.24 SE = 1.61	

indicates that the dramatic changes seen in this period affected all parameters. Also, notice that all of the transition periods' correlations are positive and much different than those of the other three hour ranges. As expected, the torque versus I/O race resistance correlations are all negative (inverse) except for during the transition period. Of the inverse I/O resistance correlations, the one during wear-in was the best (0-334 hours). Temperature correlated best with I/O race resistance, perhaps indicating a relationship between temperature and the electrical conductivity of the oil. The total temperature change was only 3 or 4°C, however, so this correlation may not be accurate. As with most other results of this first bearing test, the usefulness of these statistics will be better known only when future test results are compared.

The equation tables of Table 10 can be used to define any of the parameter relationships in equation format. In general, relationships which have a high R-value and a low SE-value, compared with the mean value of the parameter, are of the best validity. These equations can be used as described in Section II part 3(B) to estimate or project one parameter's value from the measurement of another. However, additional bearing tests are needed to validate the equations as being true for bearings in the general case.

E. Accelerated Testing and Time Equations

One method to estimate or project future bearing performance or lifetimes is to establish a characteristic equation for each measured bearing parameter of a particular bearing. The computer program has generated equations of torque and I/O race resistance with respect to operational hours (time) for each of the four defined time periods of bearing operation in test #4001. These are presented in Table 11.

Given any hour point (time) within the hour range of each equation, the torque and I/O race resistance values of test #4001 can be determined to an accuracy of within one standard estimate of error (SE) value with a probability of 68%. Since the

TABLE 10

TEST #4001 CORRELATION EQUATIONS

0-334 HOURS N = 47

	X**0	X**1	X**2	STDEV	SE	X-MEAN	Y-MEAN	RHO
Torque Avg. vs. Torque Max.	-.3622E+02	0.1570E+01	-.1717E-02	18.785	3.739	*5.99	*2.30	0.98
Torque Avg. vs. I/O Race Resist. Avg.	0.2417E+04	-.3203E+02	0.1089E+00	94.713	60.719	*5.99	*4.86	-0.77
Torque Avg. vs. Temperature	0.2608E+02	-.2187E-01	0.1005E-03	0.529	0.518	*5.99	24.93	0.20
Torque Max. vs. I/O Race Resist. Avg.	0.2352E+04	-.2963E+02	0.9581E-01	94.713	54.098	*2.30	*4.86	-0.82
Torque Max. vs. Temperature	0.2603E+02	-.1933E-01	0.8252E-04	0.529	0.519	*2.30	24.93	0.20
I/O Race Resist. Avg. vs. Temperature	0.2506E+02	0.7593E-03	-.6147E-05	0.529	0.465	*4.86	24.93	-0.48

335-1556 HOURS N = 67

Torque Avg. vs. Torque Max.	-.3735E+03	0.9121E+01	-.4333E-01	4.510	1.968	95.06	*1.12	0.90
Torque Avg. vs. I/O Race Resist. Avg.	0.1797E+03	0.6080E+01	-.3329E-01	5.555	5.355	95.06	*6.11	-0.27
Torque Avg. vs. Temperature	0.4330E+02	-.3164E+00	0.1294E-02	0.888	0.825	95.06	24.94	-0.37
Torque Max. vs. I/O Race Resist. Avg.	0.6064E+03	-.2970E+01	0.1465E-01	5.555	5.500	*1.12	*6.11	-0.14
Torque Max. vs. Temperature	0.9499E+02	-.1326E+01	0.6247E-02	0.888	0.802	*1.12	24.94	-0.43
I/O Race Resist. Avg. vs. Temperature	-.9309E+02	0.1300E+01	-.3127E-02	0.888	0.806	*6.11	24.94	-0.42

*Number out of range

TABLE 10

TEST #4001 CORRELATION EQUATIONS

(Concluded)

	X**0	X**1	X**2	STDEV	SE	X-MEAN	Y-MEAN	RHO
1557-1656 HOURS N = 21								
Torque Avg. vs. Torque Max.	-.2406E+01	0.1175E+01	-.1063E-02	18.611	1.378	73.68	78.04	1.00
Torque Avg. vs. I/O Race Resist. Avg.	-.3518E+03	0.8900E+01	-.8582E-02	*4.362	37.066	73.68	*4.68	0.97
Torque Avg. vs. Temperature	0.1441E+02	0.3304E+00	-.2333E-02	0.786	0.575	73.68	25.36	0.68
Torque Max. vs. I/O Race Resist. Avg.	-.2667E+03	0.5575E+01	0.1344E-01	*4.362	31.474	78.04	*4.68	0.98
Torque Max. vs. Temperature	0.1266E+02	0.3620E+00	-.2423E-02	0.786	0.532	78.04	25.36	0.74
I/O Race Resist. Avg. vs. Temperature	0.2403E+02	0.1762E-01	-.3734E-04	0.786	0.472	*4.68	25.36	0.80
1657-3700 HOURS N = 83								
Torque Avg. vs. Torque Max.	0.3096E+02	-.4074E+00	0.2040E-01	4.410	2.607	32.41	39.47	0.81
Torque Avg. vs. I/O Race Resist. Avg.	0.1879E+03	-.1041E+02	0.1460E+00	7.807	6.451	32.41	5.78	-0.56
Torque Avg. vs. Temperature	0.2566E+02	-.1041E+02	0.8375E-02	1.657	1.414	32.41	23.87	0.52
Torque Max. vs. I/O Race Resist. Avg.	0.1967E+03	-.8993E+01	0.1040E+00	7.807	7.017	39.47	5.78	-0.44
Torque Max. vs. Temperature	0.1555E+02	0.2386E+00	-.6947E-03	1.657	1.441	39.47	23.78	0.49
I/O Race Resist. Avg. vs. Temperature	0.2422E+02	-.7076E-01	0.6871E-03	1.657	1.607	5.78	23.78	-0.24

*Number out of range

TABLE 11

TIME EQUATIONS

Torque Average (mN·m)

Hours	Equation	SE	Mean Value
0-334	$T_{avg} = 138.0 - 0.3415t + 0.000762t^2$	8.66	125.99
335-1556	$T_{avg} = 109.8 - 0.0264t + 0.00000886t^2$	1.77	95.06
1557-1656	$T_{avg} = -4960 + 6.818t - 0.00229t^2$	4.20	73.68
1657-3700	$T_{avg} = 35.03 + 0.0015t - 0.000001019t^2$	2.97	32.41

I/O Race Resistance Average (KΩ)

Hours	Equation	SE	Mean Value
0-334	$R_{avg} = 118.9 + 0.2091t + 0.00221t^2$	35.96	214.9
335-1556	$R_{avg} = 438 + 0.0473t - 0.0000250t^2$	4.51	456.1
1557-1656	$R_{avg} = 11210 - 9.246t + 0.001499t^2$	25.12	224.7
1657-3700	$R_{avg} = 58.32 - 0.0484t + 0.00001038t^2$	6.25	55.78

SE values are very low for this test, compared to the mean value of these parameters, the equations appear to be quite valid. The program can also be reversed to produce equations to estimate the hours at any given torque or I/O race resistance. The probability of a value being within two standard errors is 95% and to within three standard errors is 99.7%.

Similar equations with time will be developed for future bearing tests. Then these equations can be combined and correlated to arrive at a typical or "characteristic" equation for a particular bearing and operational condition. If a large enough data base can be developed by running many bearing tests to failure, it may be possible to predict extended bearing performance and possibly lifetime from these equations. For this to be possible, either the standard deviations must be very low between the equations, or they must be able to be dependably related by a scale factor or other conversion. Methods of accelerated testing must also be employed to shorten the time required to generate such a data base. Also, the accelerated results must be able to be related to normal operating conditions. Accelerated methods may include high load, high rpm, or degraded lubricants. In any event, now that the bearing rig test systems are completed, numerous coordinated tests are needed to generate and validate data and arrive at conclusive results.

SECTION IV
LUBRICANT DEGRADATION STUDIES

1. INTRODUCTION

Lubricant degradation has been studied as a potential mode of failure of Despin Mechanical Assemblies. Whether the lubricant degrades chemically or physically, it can affect the mechanical assembly's operation. The use of small amounts of lubricants in this application necessitates the use of sophisticated analytical techniques rather than conventional determinations of physical and chemical properties. Further, the amount of degradation of performance necessary to cause failure of a Despin Mechanical assembly is far less than in other lubricated assemblies. Minor torque variations can normally be accepted in other applications, but are totally unacceptable in space systems.

It is necessary to quantitatively analyze any changes which may occur during the lifetime of the system from storage to the operational life of the satellite. To do this, baseline data is required on the currently used lubricant materials. (This will allow possible application to in-situ sampling of materials from operating bearings or slip rings.)

The most commonly used lubricant is produced by Ball Aerospace Systems Division and is commonly called Vac Kote (BBRC 36233). The oil's basestock is Apiezon C, a low vapor pressure hydrocarbon oil used in vapor diffusion vacuum pumps. The oil contains five percent lead naphthenate concentrate as an antiwear agent. The concentrate contains approximately 88 percent lead naphthenates and 12 percent of a lower boiling hydrocarbon diluent. The third component is 1.5 percent p,p'-dioctyldiphenylamine.[8]

The approach taken was to analyze the components of the formulation individually as well as the formulated material, Vac Kote. Techniques have been developed for analysis of some of the materials, while analysis for others requires more effort.

2. METHODS OF CHEMICAL ANALYSIS OF VAC KOTE COMPONENTS

Sensitive methods of analysis are required in order to evaluate small changes in the chemical composition of the Vac Kote lubricant during artifical, accelerated, and 'real life' testing. Such methods must be capable of detecting chemical changes in both the basestock and additive package as well as detecting degradation products. To this end, the chromatographic methods lend themselves very well to these types of analyses because of their ability to resolve complex materials and to detect submilligram quantities. For this reason, both gas and liquid chromatography have been used as methods of analysis. Other methods include infrared and ultraviolet spectroscopy, thermogravimetric analysis, and x-ray photoelectron spectroscopy (XPS).

In order to aid in selection of the ultraviolet (UV) wavelength for the liquid chromatographic analysis, UV spectra of Vac Kote and its three components were run from 300 to 200 nm, the results are shown in Figure 30. The results are qualitative only and none of the compounds showed any significant absorption above 300 nm.

The following paragraphs outline specific methods and data generated for the characterization of the components of the Vac Kote.

A. Apiezon C Analysis

(1) Liquid Chromatography Analysis

Apiezon C, the basestock oil for the Vac Kote lubricant which comprises about 94 percent of the weight of the formulation, is a molecularly distilled mineral oil. It is one oil in a series of Apiezon oils (available from James G. Biddle Corporation) consisting of various molecular weight hydrocarbon fractions. Size exclusion liquid chromatographic analysis of Apiezon A, C, and K (Figure 31) illustrates the differences that exist in both the molecular weight and molecular weight distribution among these various distillation cuts. Such a method of

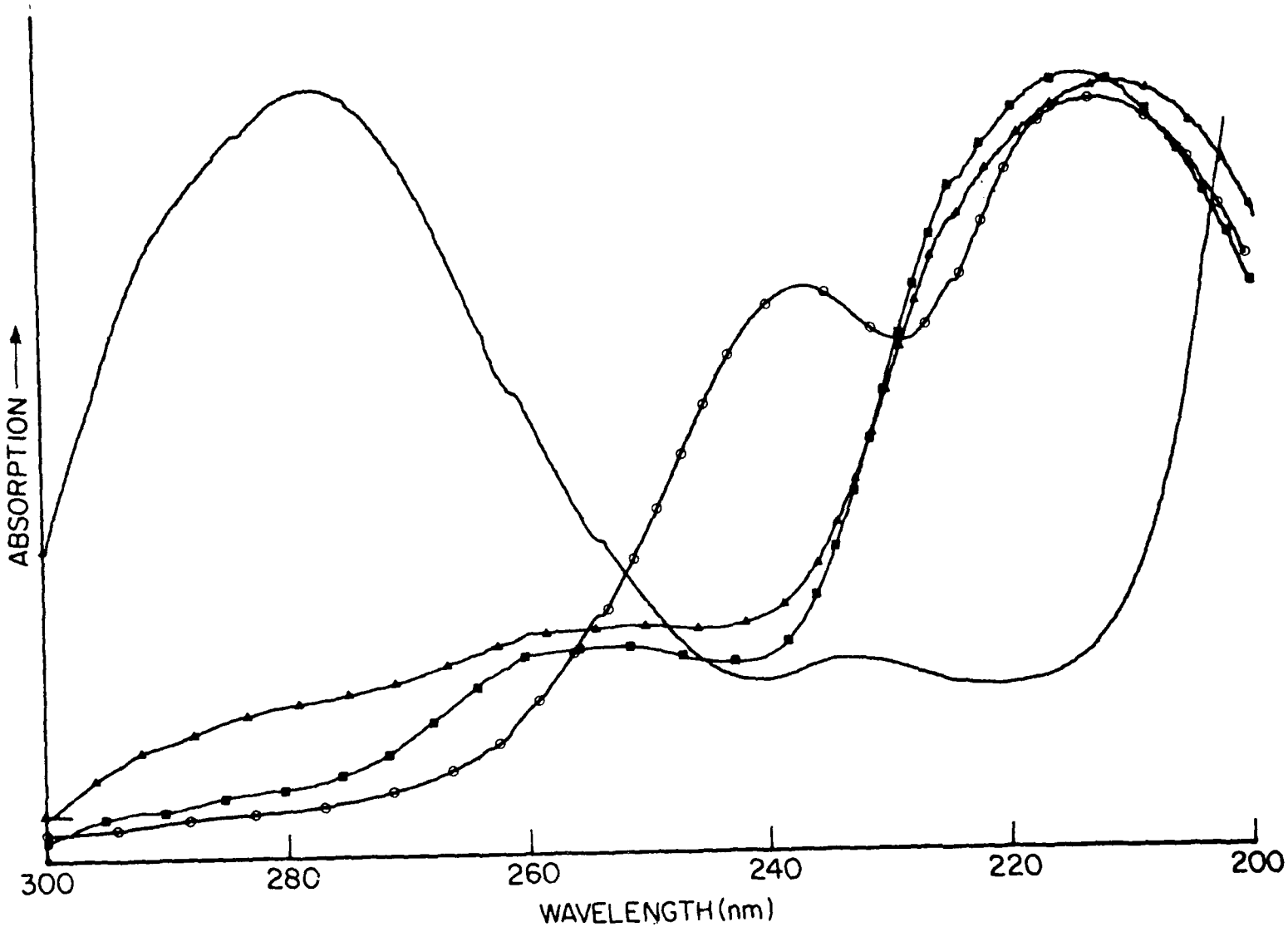

Figure 30. UV Absorption Spectra of Vac Kote and Its Components
——— dioctyldiphenylamine —o— lead naphthenate
—■— Apiezon C —▲— Vac Kote.

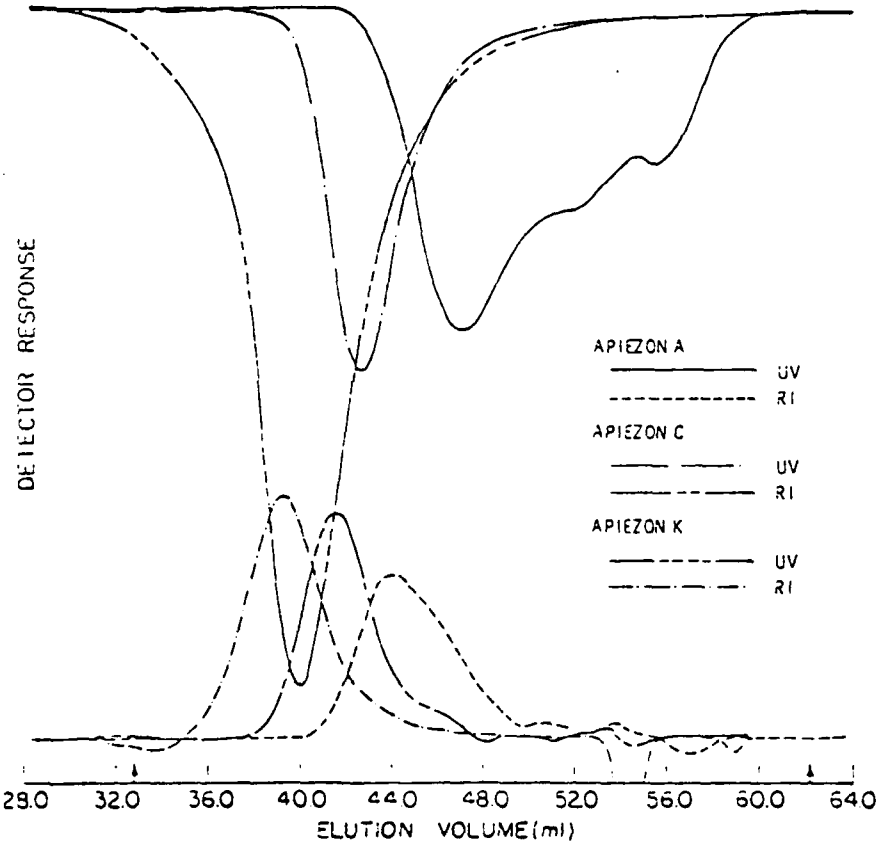

Figure 31. Size-Exclusion Chromatographic Comparison of Apiezon A, C, and K.

analysis is also capable of detecting lot to lot variance in the lubricant basestock. Figure 32 depicts the chromatographic overlays of Apiezon C lots obtained over a four year period. The chromatograms indicate a decrease in the peak maximum of the refractive index trace over this time span, but the breadth of the molecular distribution is approximately constant. This correlates with data bulletins from the supplier which indicated a reduction in the number average molecular weight of Apiezon C due to changes in the basestock supply.

Size exclusion chromatography is therefore a useful method for determining batch to batch variations in the Apiezon oils with its concurrent potential for the correlation of such data to performance in 'real life' testing. Similarily, such a method is capable of determining changes in the basestock oil during testing such as may be due to thermal or oxidative degradation and evaporative depletion.

(2) Gas Chromatographic Analysis

Analysis of Apiezon C by gas chromatography is somewhat hindered by its low volatility, the maximum temperature limits of column coatings, and the great complexity of this oil. Nevertheless, analyses were done using an SE-52 13 meter glass capillary column with a typical chromatogram shown in Figure 33. As can be seen the great complexity of the oil precludes baseline resolution of individual components. Although qualitative differences were seen among the various Apiezon C batches, the reporting of such data (peak retention times), even with the aid of the computer data station, is not very meaningful due to its complexity. But some indication of the quantitative differences can be obtained by listing the range of retention times for major peaks (>1 percent area), as is listed in Table 12. Such analyses may yield useful information regarding changes in the lubricant basestock during accelerated and 'real life' testing, particularly that due to evaporative depletion as one would expect relative depletion at earlier eluting (lower boiling) peaks.

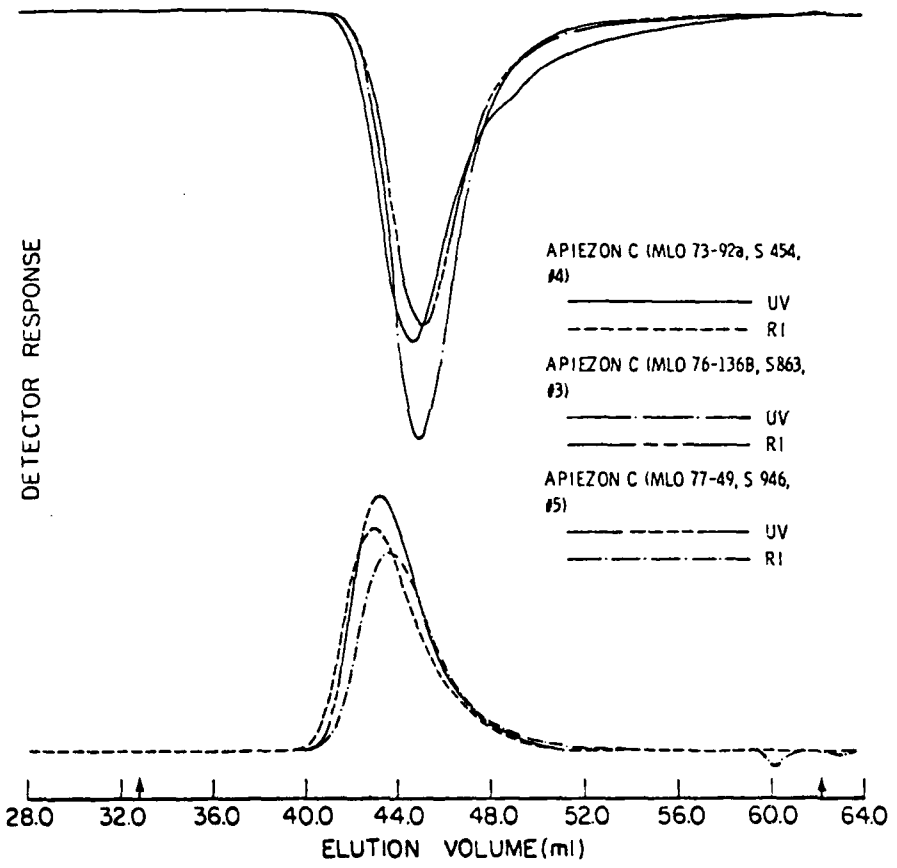

Figure 32. Size-Exclusion Chromatogram Illustrating Lot to Lot Variation for Apiezon C (Four Year Period).

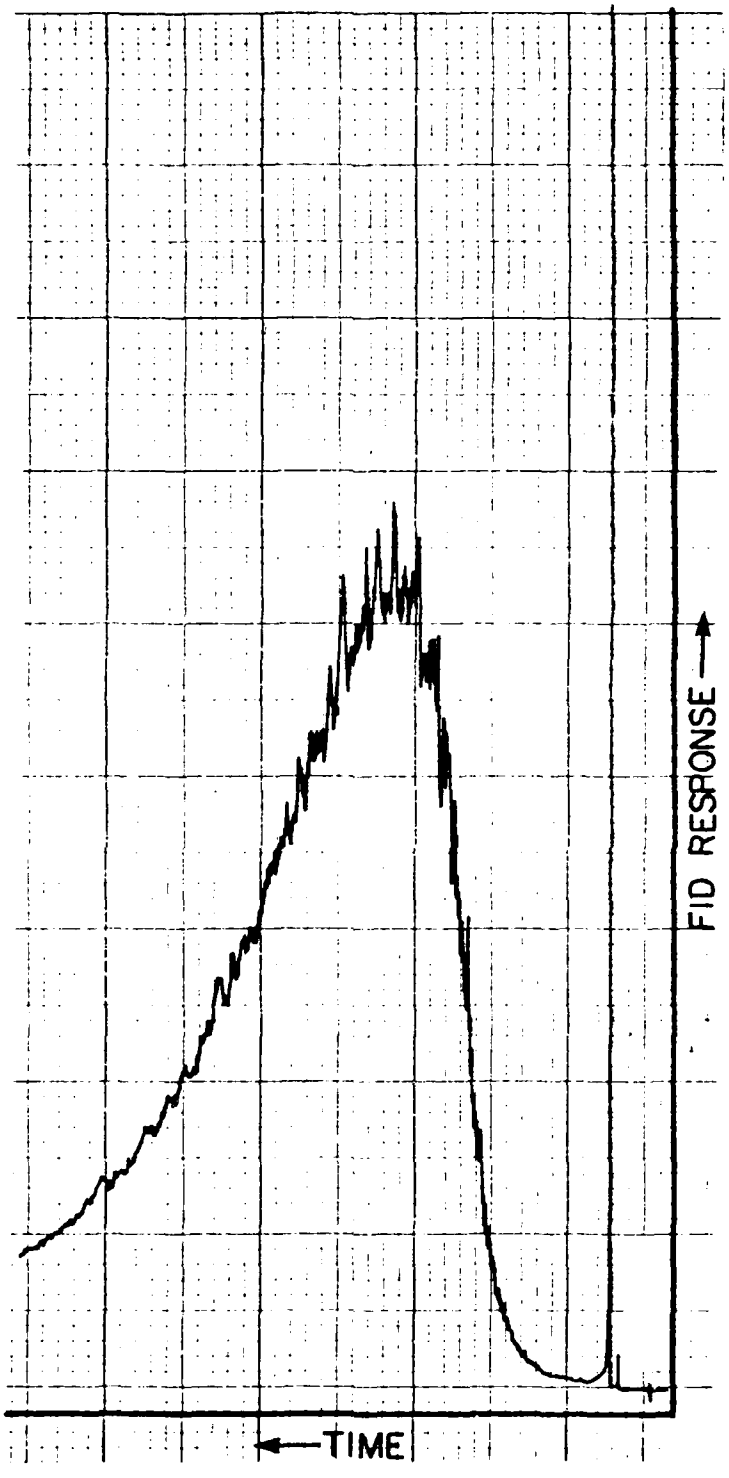

Figure 33. Gas Chromatogram of Apiezon C (MLO 76-136 B); 13m x 0.25mm Glass Capillary Column Coated with SE-52; Temperature Programmed 200 to 280°C at 8°C Per Minute; FID Detector.

TABLE 12

APIEZON C ANALYSIS

Apiezon C (Lot No.)	Retention Range (min., >1 percent area)
MLO 76-136 B, No. 3	10.3 - 25.2
MLO 73-92 A, No. 4	8.3 - 14.3
MLO 77-49, No. 5	10.5 - 20.5
MLO 77-49, No. 8	9.1 - 18.3
MLO 73-92 B, No. 4	9.1 - 20.8

B. Dioctyldiphenylamine Analysis

A simple method for the quantitative analysis of dioctyldiphenylamine (DODPA), the antioxidant present in Vac Kote, was developed using reverse phase liquid chromatography. Analysis was accomplished by the addition of an internal standard (diphenylamine) to a known weight of Vac Kote, chromatographing this mixture (UV detection), and calculating percent DODPA from the peak areas based on previously determined response factors. The following table shows the percent DODPA in various batches of Vac Kote.

Vac Kote Oil (Lot No.)	Percent DODPA
UDRI Formulation**	0.88
MLO 74-9, No. 5	0.52
MLO 74-9, No. 8	0.71
MLO 76-37, No. 8	1.40
MLO 73-91, No. 4	1.39

**Consisting of 93.2 percent Apiezon C, 5.9 percent lead naphthenate, and 0.92 percent DODPA.

The data shows a wide range of DODPA levels in the Vac Kotes. Furthermore, the Vac Kote samples with relatively depleted levels of DODPA show an additional peak in the Apiezon C elution region that is not present in Vac Kote samples with higher levels (1.4 percent). Figure 34 represents the chromatograms of two such samples overlayed. The first peak is the internal standard, the second is the DODPA (with the two small peaks in between being impurities from the DODPA), and the third is the Apiezon C basestock oil. The Vac Kote MLO 74-9, #5 shows a depleted level of the DODPA (0.52 percent) as well as the appearance of the sharp peak in the Apiezon C region relative to Vac Kote MLO 76-137, No. 8 (1.4 percent DODPA). Also, there is a considerable color difference between the two Vac Kotes as the MLO 76-137, No. 8 is a dark yellow while MLO 74-9, No. 5 is a deep reddish brown. Since neither the color change or the additional peak have been seen in Apiezon C samples, the interpretation of this data is that an oxidative process may be occurring during storage of the Vac Kote which depletes the antioxidant, forming some sort of adduct which elutes later in the chromatogram.

C. Lead Naphthenate Analysis

Lead naphthenate, an antiwear additive comprising about 5 percent of the Vac Kote, is a lead salt of naphthenic acids, which are a complex mixture of carboxylic acids, mostly cyclic and polycyclic aliphatics.[9] Attempts were made to analyze this compound by chromatographic techniques. Size exclusion liquid chromatography did not prove to be useful as the similar molecular sizes of the Apiezon C and lead naphthenate prevented separation, even with the smallest pore size columns. Some success was achieved with reverse phase liquid chromatography, but sample component resolution could not be achieved and the low UV absorbance of the naphthenate moiety makes UV detection difficult if one is working with very small sample sizes. The low volatility of lead naphthenate makes it unsuitable for gas chromatographic analysis. With these limitations, attention was turned toward derivatization of the naphthenate moiety.

AD-A113 766 DAYTON UNIV OH RESEARCH INST F/G 17/2
ACCELERATED LIFE PREDICTION TECHNIQUES.(U)
NOV 81 K DAVIS, M KELLER, R MARTIN F33615-78-C-5107
UNCLASSIFIED UDR-TR-81-90 AFWAL-TR-81-4137 NL

2 OF 2
AD A113766

END
DATE FILMED
5-82
DTIC

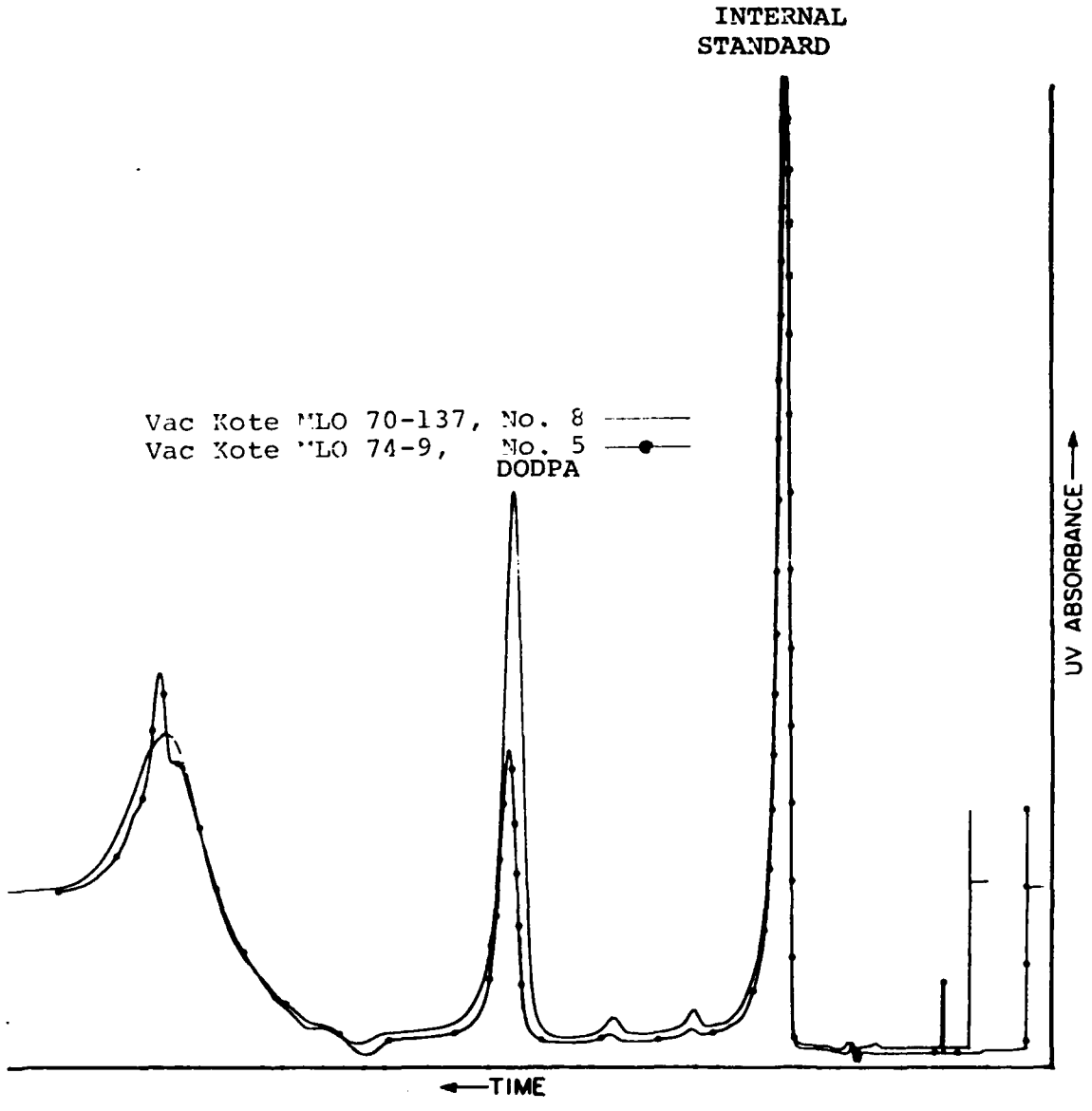

Figure 34. Reverse Phase Liquid Chromatogram of Vac Kote: U-Bondapak C-18 Column (30 cm), Gradient Elution, THF/H_2O, 70/30 to 85/15, 15 minutes; 1.0 ml/min Flow rate; UV Detector at 280 nm, 1.0 AUFS.

Sample derivatization is a common technique used in chromatography which yields two important advantages: 1) it can increase the chromatographability of a compound (particularly gas chromatography), and 2) it can increase the detectability of a compound via introduction of a functional group to which a particular detector is sensitive (such as a phenyl group for UV detection). A method was reported in the literature for the derivatization of fatty acids to their phenacyl esters and subsequent analysis by high pressure liquid chromatography.[10] Although the method was developed for carboxylic acids, it proved to work well on lead carboxylates with only minor modifications. The method involves a 30 minute reflux of triethylamine/phenacyl bromide/lead carboxylate in an equivalent ratio of 2/2/1 (in methylene chloride), with direct chromatographic analysis of this solution after filtering the precipitate (a lead salt). After derivatization of lead octoate (a solution of lead 2-ethyl hexanoate, 24 percent Pb, Alfa products), an IR of this solution showed complete disappearance of the carboxylate band at 1540 cm^{-1}, and the subsequent appearance of an ester carbonyl at 1745 cm^{-1}. Derivatization of lead naphthenate yielded the same results. Finally, the derivatization of the lead naphthenate in Vac Kote was accomplished using samples as small as 50 mg. The analysis of the solution was accomplished using reverse phase liquid chromatography. Figures 35 and 36 show the effects of derivatization on the UV detection of lead naphthenate (before and after derivitization respectively) in Vac Kote. Figure 36 shows greatly increased detectability of the naphthenate moiety due to derivatization relative to the lead naphthenate. Unfortunately, derivatization did not appreciably increase the chromatographability of the naphthenate and baseline resolution of individual components could not be accomplished. It would appear, then, that the limited efficiency of LC columns makes it impossible to resolve such a complex mixture of compounds, and only a fingerprint analysis is possible. Gas chromatographic capillary columns have the necessary efficiency, but a better derivative (such as methyl or trimethylsilyl esters) should be investigated.

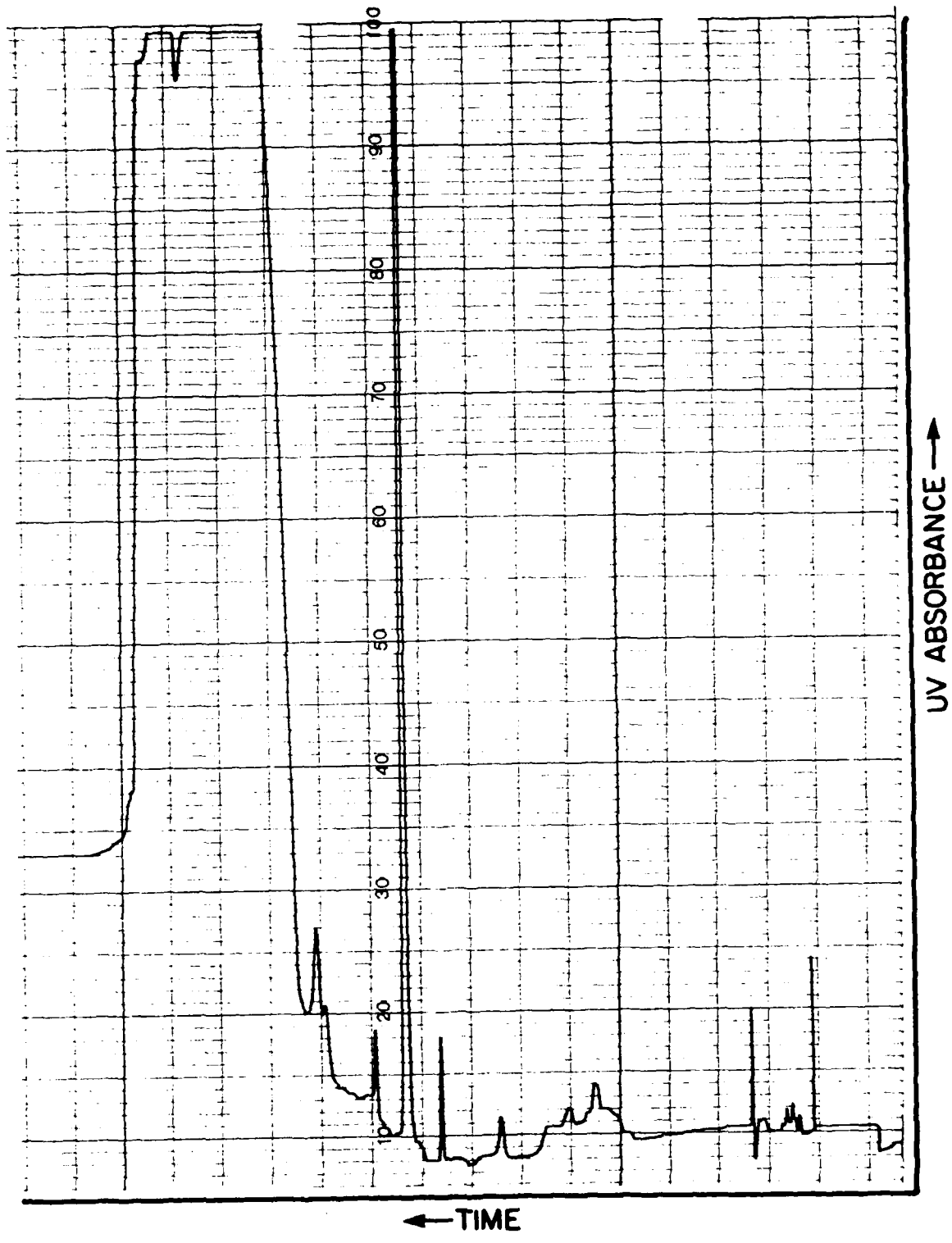

Figure 35. Reverse Phase Liquid Chromatogram of Vac Kote (MLO 76-137, No. 8); μ-Bondapak C-18 Column (30 cm); Gradient Elution, Acetonitrile/Water/Chloroform; 2.0 ml/minute Flow Rate; UV Detector at 254 nm at 0.1 AUFS; 4.0 μl Injection of 2.5 Percent Solution in Methylene Chloride.

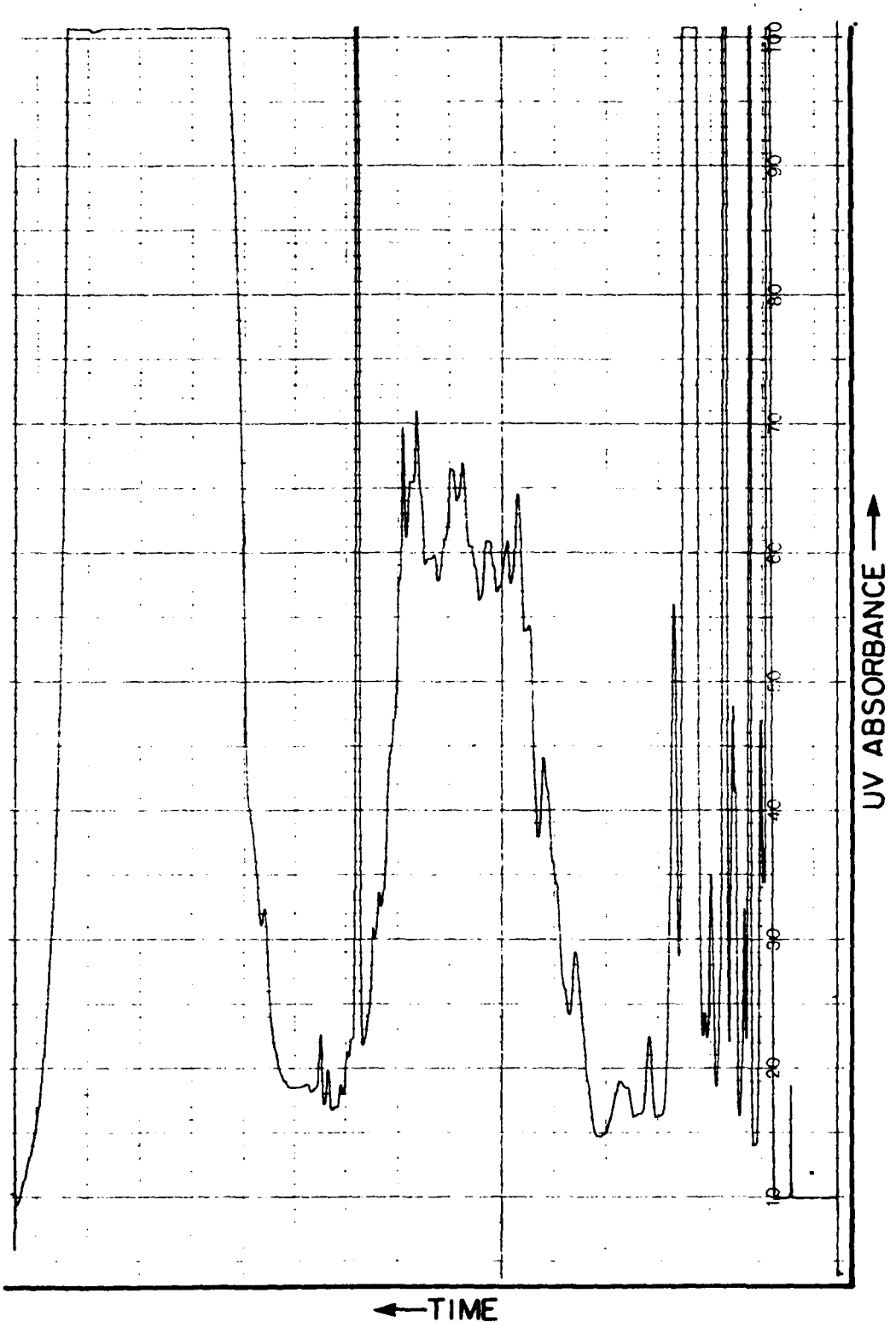

Figure 36. Reverse Phase Liquid Chromatogram of Derivatized Vac Kote (MLO 76-137, No. 8) Conditions same as Figure 35.

3. THERMAL DEGRADATION

Samples of Vac Kote, Apiezon C, and lead naphthenate were heated in stainless steel bombs under nitrogen for specified times and temperatures and then analyzed by the previously mentioned methods.

A. Micro Scale Degradation

Two gram samples of Vac Kote (MLO 74-9, No. 8), Apiezon C (MLO 73-92 B), and lead naphthenate (MLO 80-43) were placed in an oven at 300°C (572°F) for 6 hours. Analysis of the sealed (N_2 inerted) samples yielded the following results. The Apiezon C sample showed a slight yellowing as well as a light sulfur-like odor. However, there were no detectable changes in the IR spectra (Figure 37), the size exclusion liquid chromatographic or gas chromatographic chromatograms relative to those of unstressed Apiezon C. The Vac Kote sample darkened and contained a small amount of a fine black precipitate. But again there were no qualitative differences in the IR spectra (Figure 38) or the size exclusion liquid chromatograph relative to the unstressed Vac Kote. Analysis of DODPA found a level of 0.90 percent compared to 0.73 percent found in the unstressed sample. The reasons for an increase in the level of DODPA after stressing are not obvious.

The lead naphthenate sample showed the same small amount of a fine black precipitate as was found in Vac Kote as well as a slight darkening of the compound. Its IR spectra (Figure 39), relative to the control sample (Figure 40), shows the appearance of a small peak at about 1730 cm^{-1}, which indicates formation of a monomeric carboxylic acid.

B. Full Scale Degradation

Twenty gram samples (Sealed, N_2 inerted) of Vac Kote (MLO 76-137, No. 8) and lead naphthenate (MLO 80-43) were placed in an oven at 371°C (700°F) for 24 hours. The thermally degraded lead naphthenate consisted of a dark, low viscosity oil and a black tarry precipitate. An infrared spectra (Figure 41) of the oil

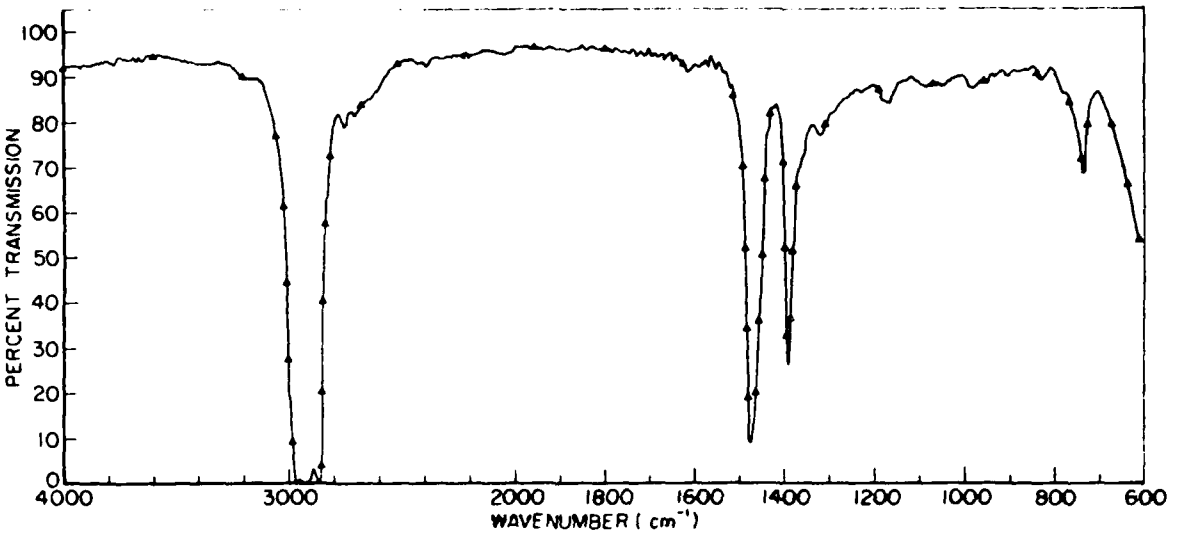

Figure 37. Thermally Stressed Apiezon C (MLO 73-92 B).

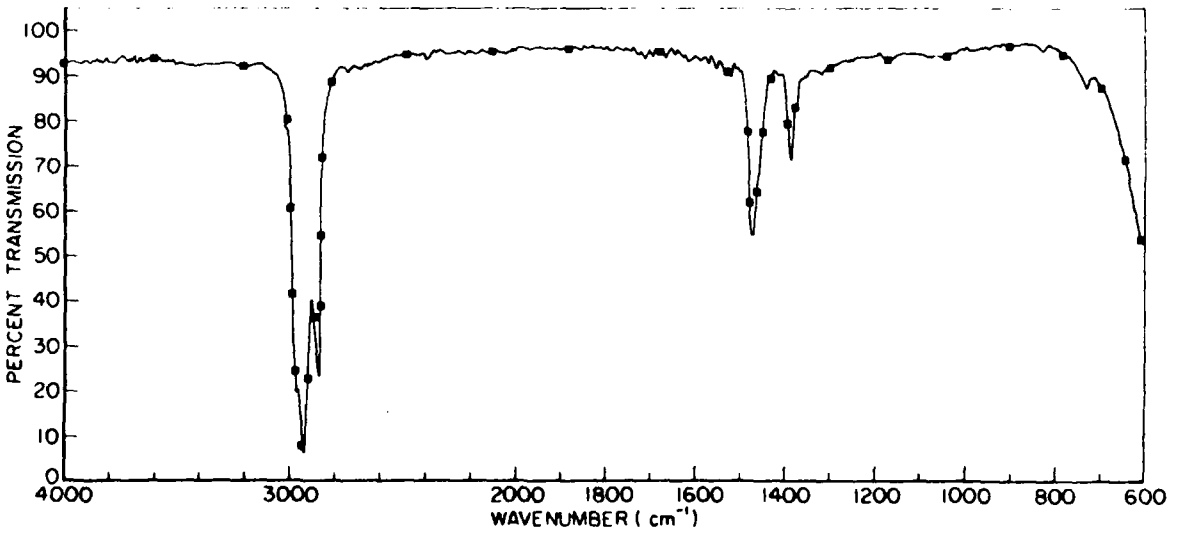

Figure 38. Thermally Stressed Vac Kote (MLO 74-9, No. 8).

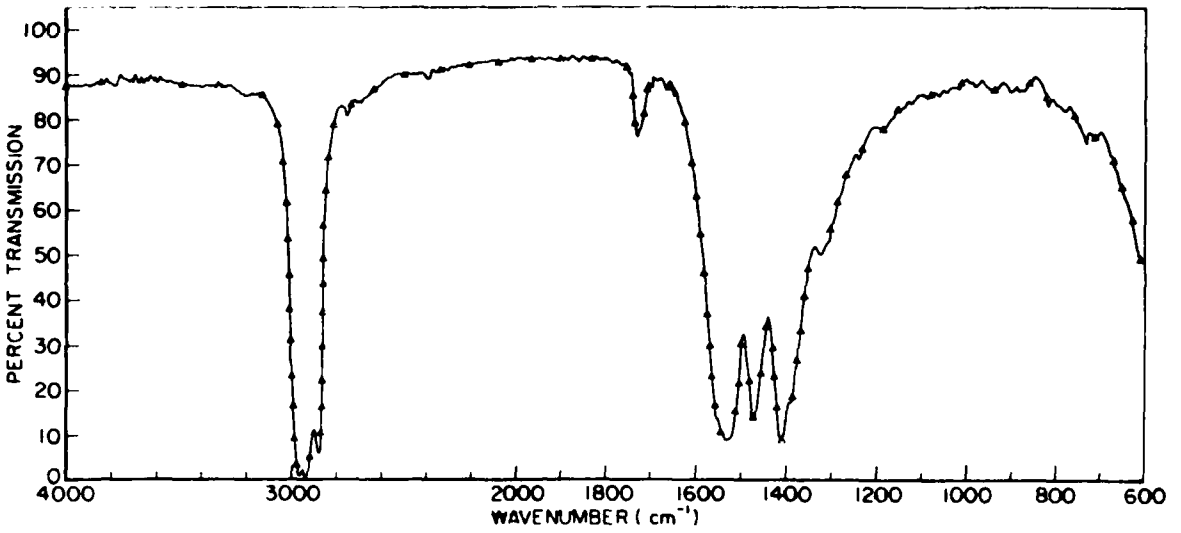

Figure 39. Thermally Stressed Lead Naphthenate (MLO 80-43).

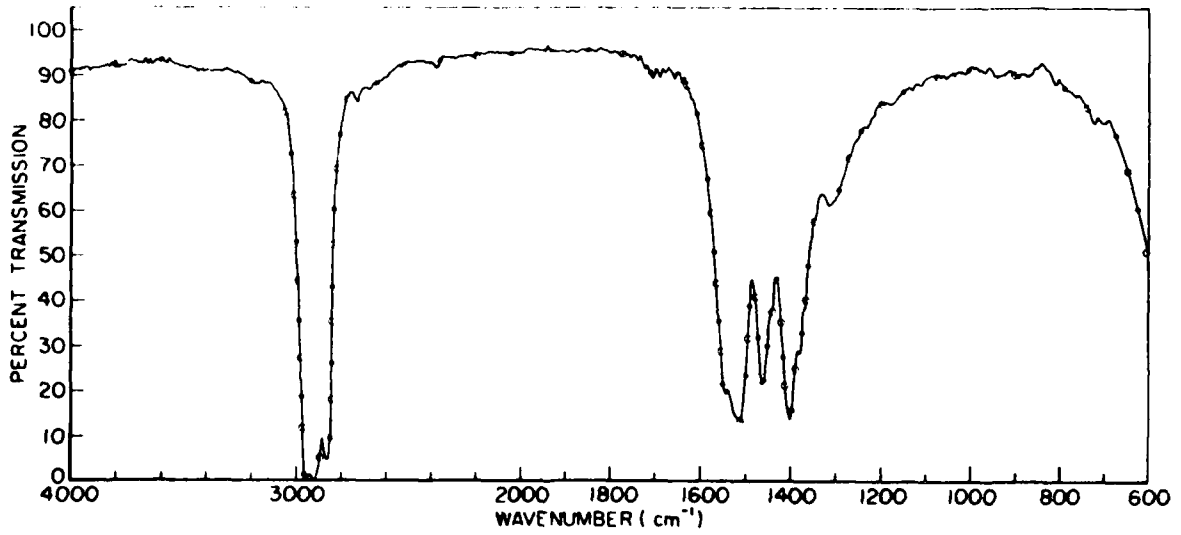

Figure 40. Unstressed Lead Naphthenate (MLO 80-43).

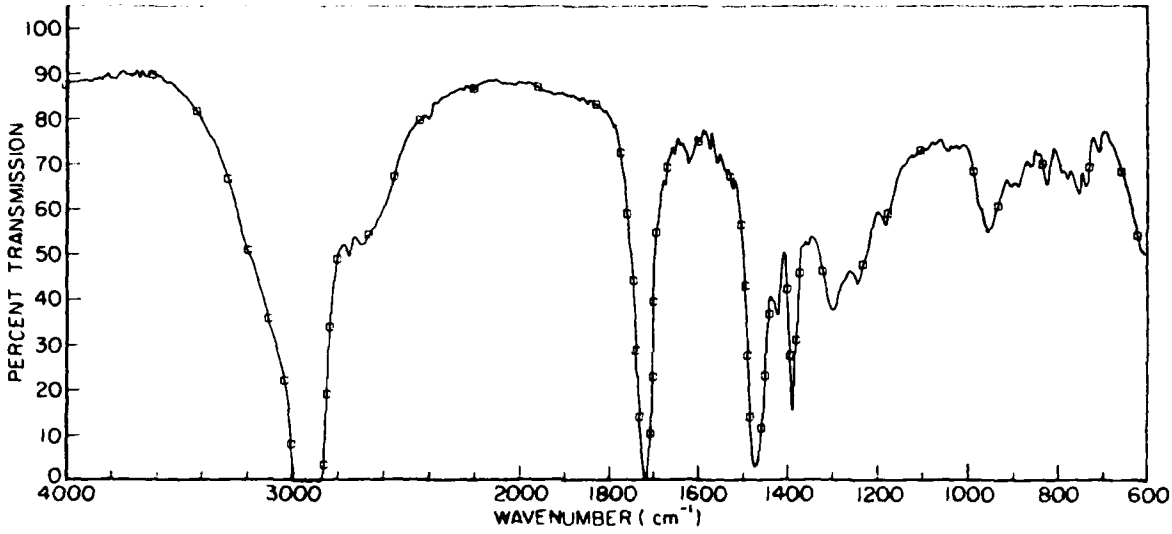

Figure 41. Stressed Lead Naphthenate (MLO 80-43) at 700°F, 24 Hours.

revealed a spectra consistent with naphthenic acids (carbonyl band at 1710 cm^{-1} and a broad OH at 3000 cm^{-1}) along with a few small unidentified absorptions in the 900 to 700 cm^{-1} range, while the carboxylate peak at 1550 cm^{-1}, typical of lead naphthenate, (Figure 40) totally disappeared. Washing of the tarry precipitate with methylene chloride yielded a dark oil and a fine black powder. An IR of the dark oil showed a spectrum consistent with a mixture of naphthenic acids and lead naphthenate (absorptions at 1715 cm^{-1} and 1550 cm^{-1}). The fine black powder obtained was found to be insoluble in acidic or basic solutions as well as all organic media, with the exception that the powder swelled up and formed a thick gel-like solution in boiling heptane. An IR spectra, run at 1 percent in KBr, revealed a blank spectra, apparently due to the high absorbance of the black powder. A sample of the material was submitted for surface analysis. An XPS scan (Figure 43) showed the presence of carbon, hydrogen, oxygen, and about 1 atom percent of lead. An X-ray diffraction analysis gave a pattern that could be explained by one or more of eight possible carboxylic acids, but no lead was present in any stable compound greater than 5 percent. It should be noted that the XPS scan is a surface technique, and its analysis may not be consistent for the whole particle. Its lack of solubility in any solvent and its tendency to form a gel in heptane, though, indicate that the black powder may be a very high molecular weight or crosslinked polymer. A Thermogravimetric Analysis run in nitrogen showed the loss of about 11 percent of weight between 330°C and 450°C and a stable baseline to 750°C.

The thermally degraded Vac Kote had darkened considerably, had a strong sulfur-like odor, and had a small amount of a dark sludgy precipitate. The only major changes in the IR spectra (Figures 44 and 45) of the oil were the appearance of a band at 1715 cm^{-1}, which is probably due to naphthenic acids, and the disappearance of the small band at 1550 cm^{-1}, which is due to the lead naphthenate.

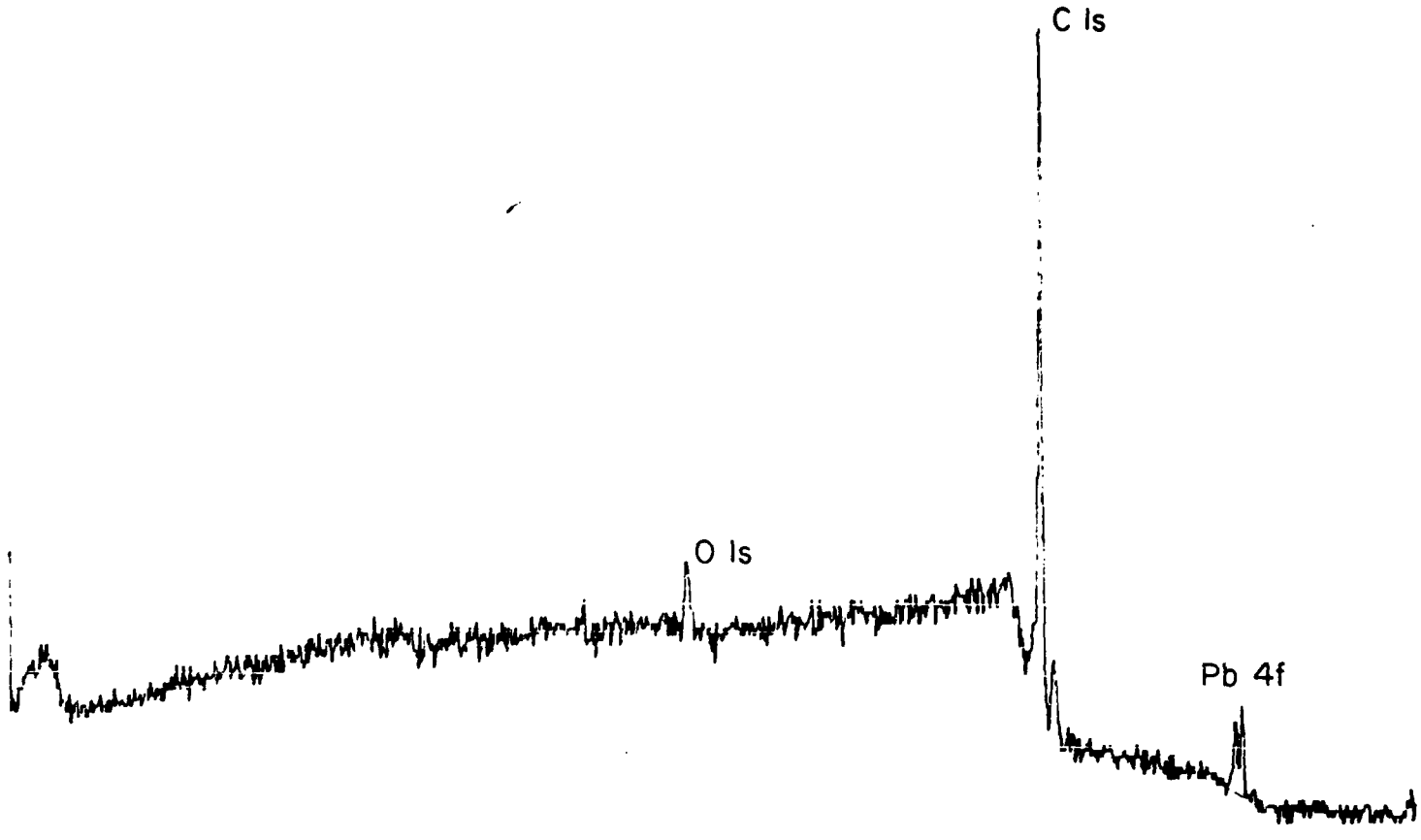

Figure 42. X-Ray Photoelectron Spectroscopy Analysis of Black ppt from Stressed Lead Naphthenate Scan Size 1000 eV; Initial K.E. 150 eV; Energy Increment 1.0 eV.

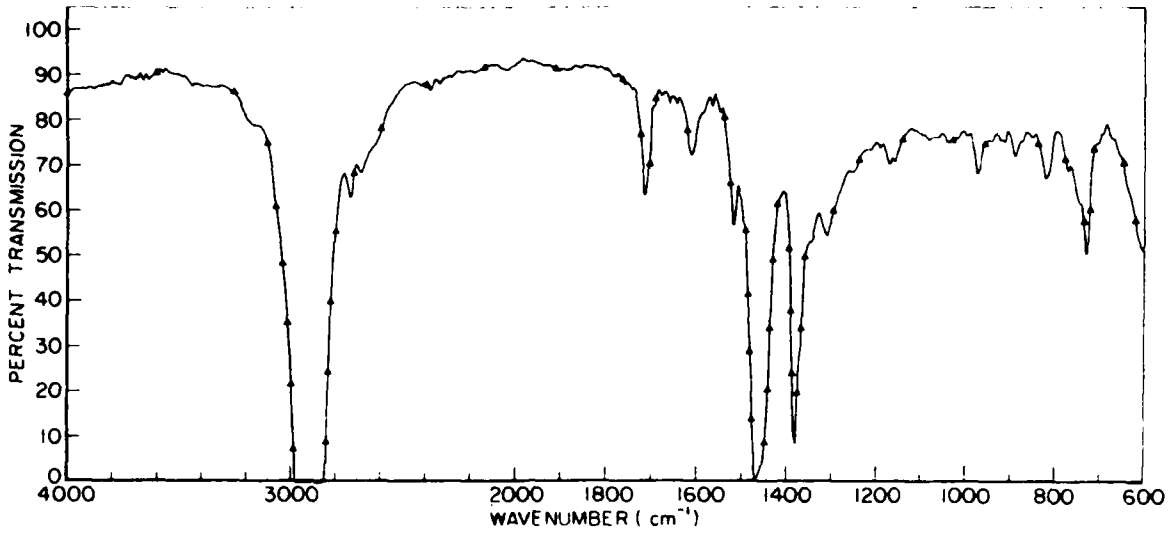

Figure 43. Stressed Vac Kote (MLO 76-137) at 700°F, 24 Hours.

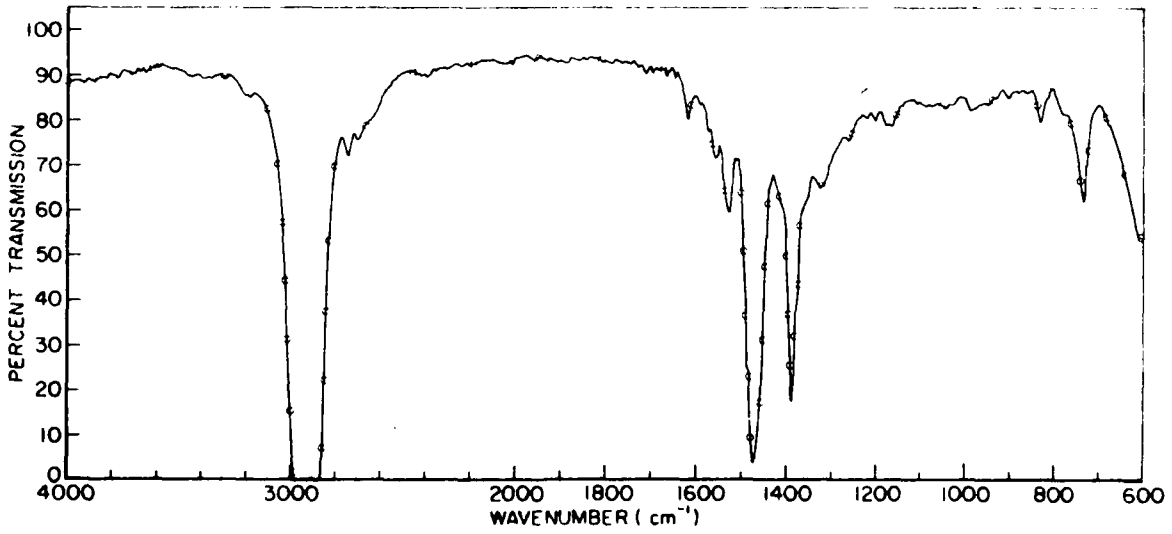

Figure 44. Unstressed Vac Kote (MLO 76-137).

The stressed Vac Kote was analyzed by size exclusion chromatography using three Du Pont PSM 60-0 columns in the Varian 5000 liquid chromatograph. Detection was by both UV absorbance at 254 nm and by infrared at 3.4 microns (2940 cm^{-1}) for detection of C-H using the DuPont liquid chromatograph infrared spectrophotometer. The chromatograms show a considerable increase in peak retention time for the UV absorbant material (Figure 46) of Apiezon C (from 14.32 to 15.01 minutes) as well as some shoulders which indicate degradation to lower molecular weight products. The infrared detection (Figure 47), however, shows virtually no change in the peak retention times of stressed and unstressed Vac Kote but does show a large (later eluting) shoulder on the main peak. This might indicate that the thermal degradation is more selective for the UV absorbant (aromatic containing) hydrocarbons than for the aliphatic (non-UV absorbing) hydrocarbons.

After derivatization to their respective phenacyl esters, both the unstressed and stressed Vac Kote were analyzed by gas chromatography. With a temperature gradient of 100 to 280°C at 5°C/minute, the chromatograms of stressed (Figure 48) versus unstressed Vac Kote (Figure 49) are substantially different. The stressed Vac Kote shows a large relative decrease in the Apiezon C elution region peaks as well as a tremendous number of earlier eluting degradation products. This data confirms the speculation of thermal degradation of the basestock as found in the size exclusion liquid chromatographs.

4. CONCLUSIONS

Size exclusion liquid chromatography has been demonstrated as a method of "fingerprinting" the various Apiezon base stocks as well as determining batch to batch variations. Gas chromatography has a potential to identify base stocks, but is currently limited by its resolution. A method was developed to use reverse phase liquid chromatography to quantitatively analyze formulations for the antioxidant (p,p'-dioctyl-diphenylamine). Lead naphthenate

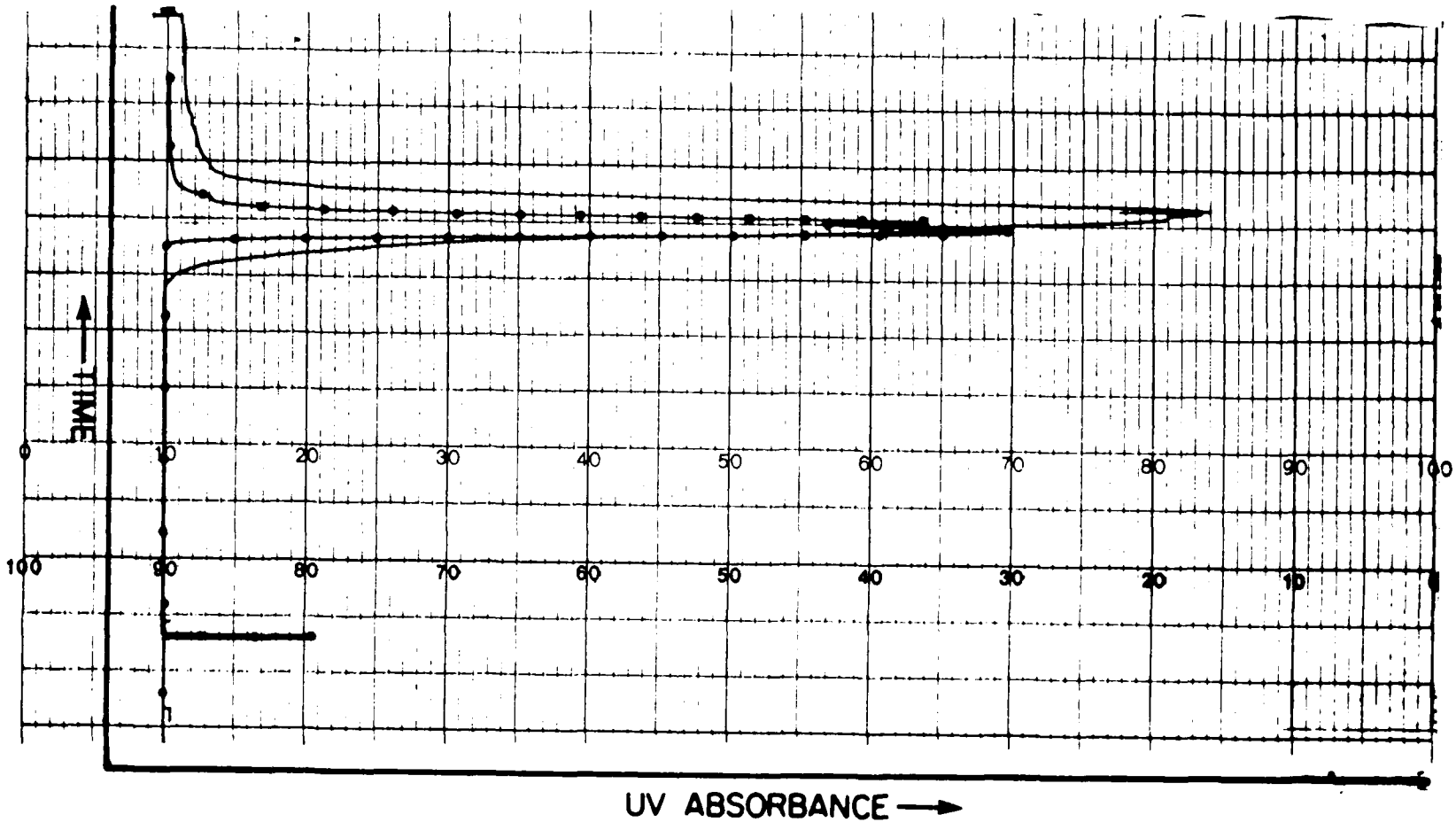

Figure 45. Size Exclusion Chromatogram of Stressed and Unstressed Vac Kote (MLO 76-137)——o—— Unstressed, ——— Stressed; 3 Zorbax 60-S (DuPont) Columns, THF Mobile Phase, 2.0 ml/minute; 254 nm UV 1.0 AUFS.

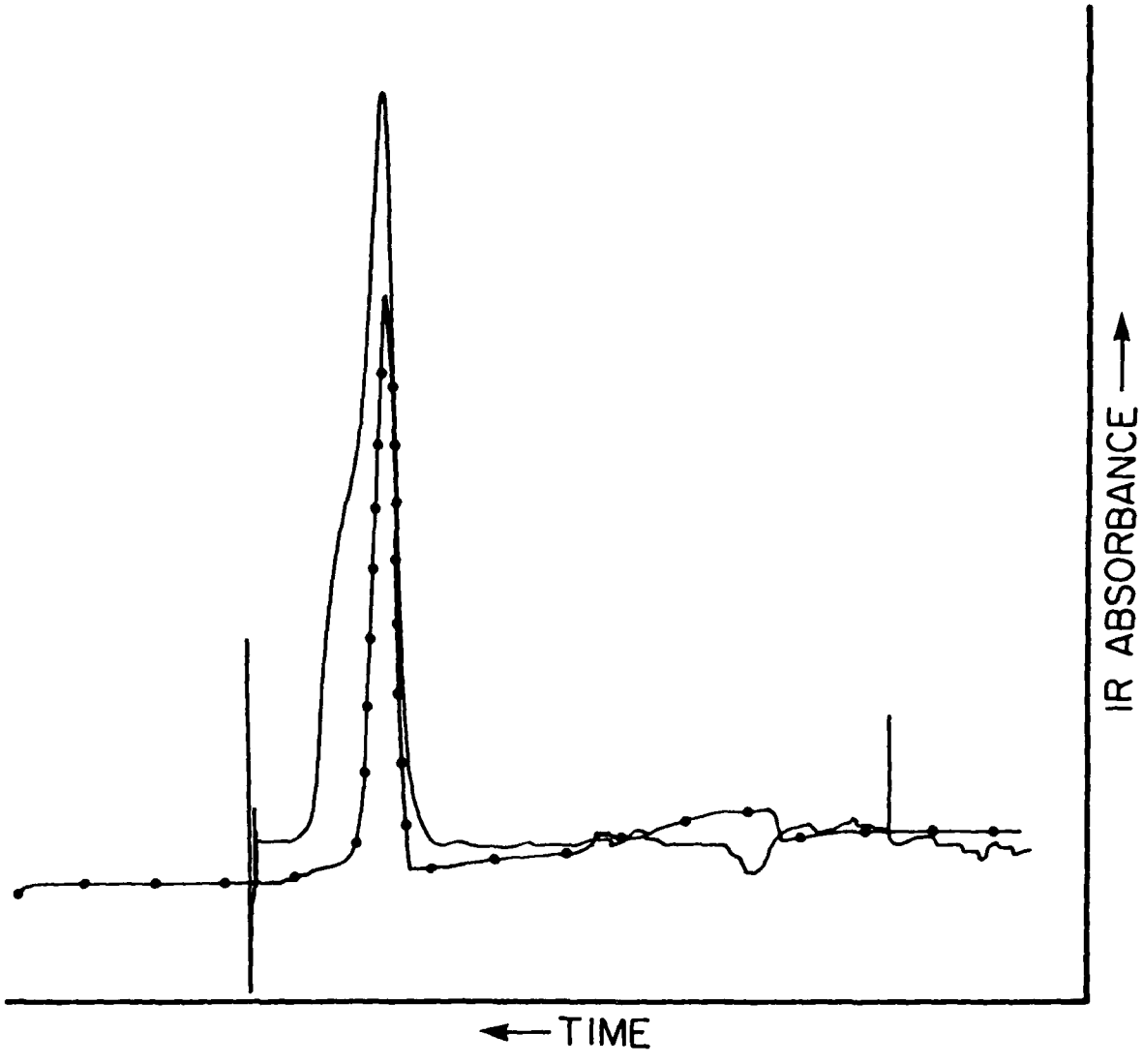

Figure 46. Size Exclusion Chromatogram of Stressed and Unstressed Vac Kote (MLO 76-137) ——o—— Unstressed, ———— Stressed; 3 Zorbax 60-S (DuPont) Columns, THF Mobile Phase, 2.0 ml/minute; 3.4 Microns IR, 0.1 AUFS.

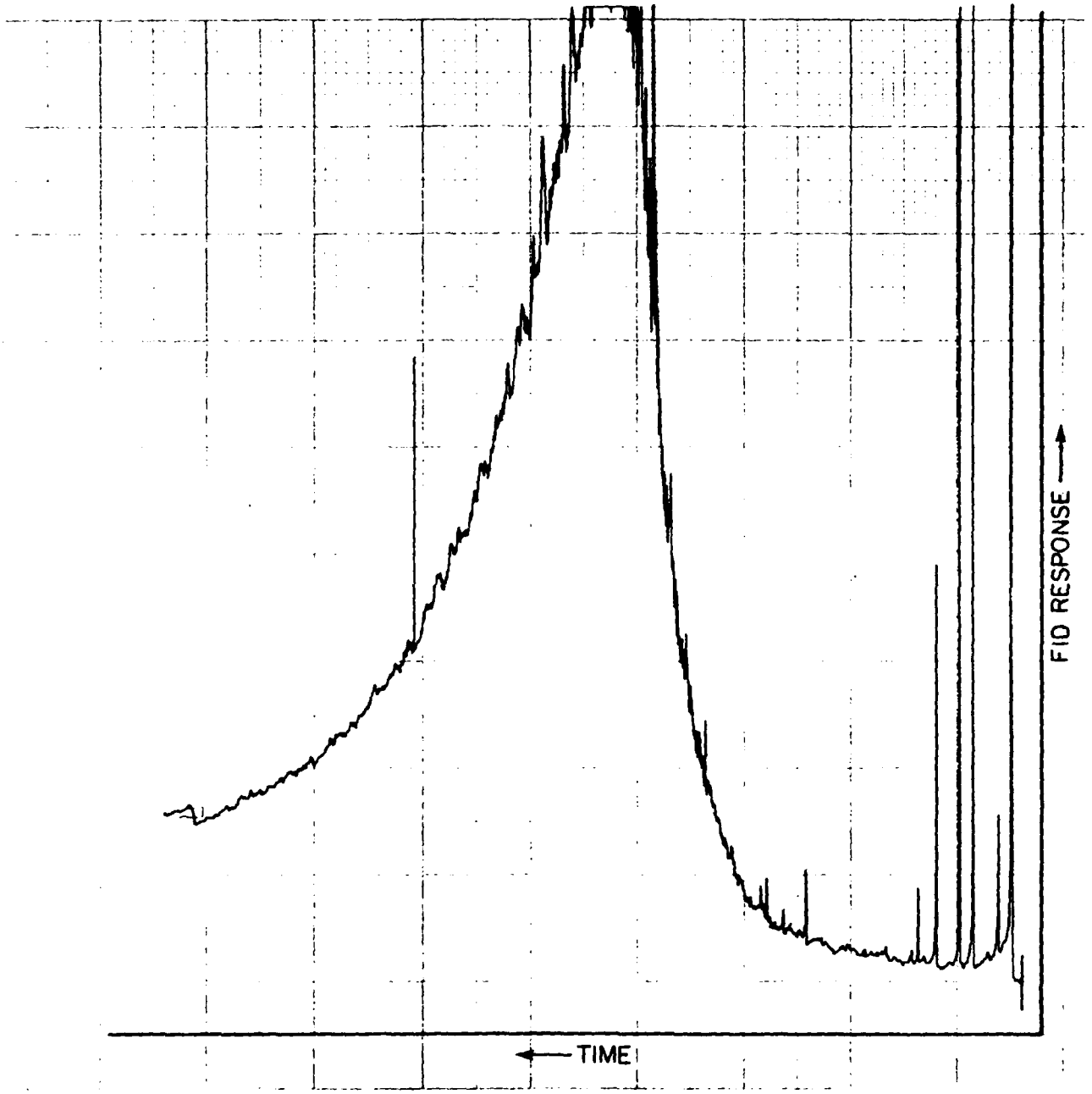

Figure 47. Gas Chromatogram of Unstressed Vac Kote (MLO 76-137); 13 MX 0.25 mm ID Glass Capillary Column Coated with SE-52; Temperature Gradient of 100 to 280°C at 5°C/ Minute; FID Detector, 1.0 µl of 50% Solution in $CH_2 Cl_2$, 10^{-12}A/mv, Attenuation 32.

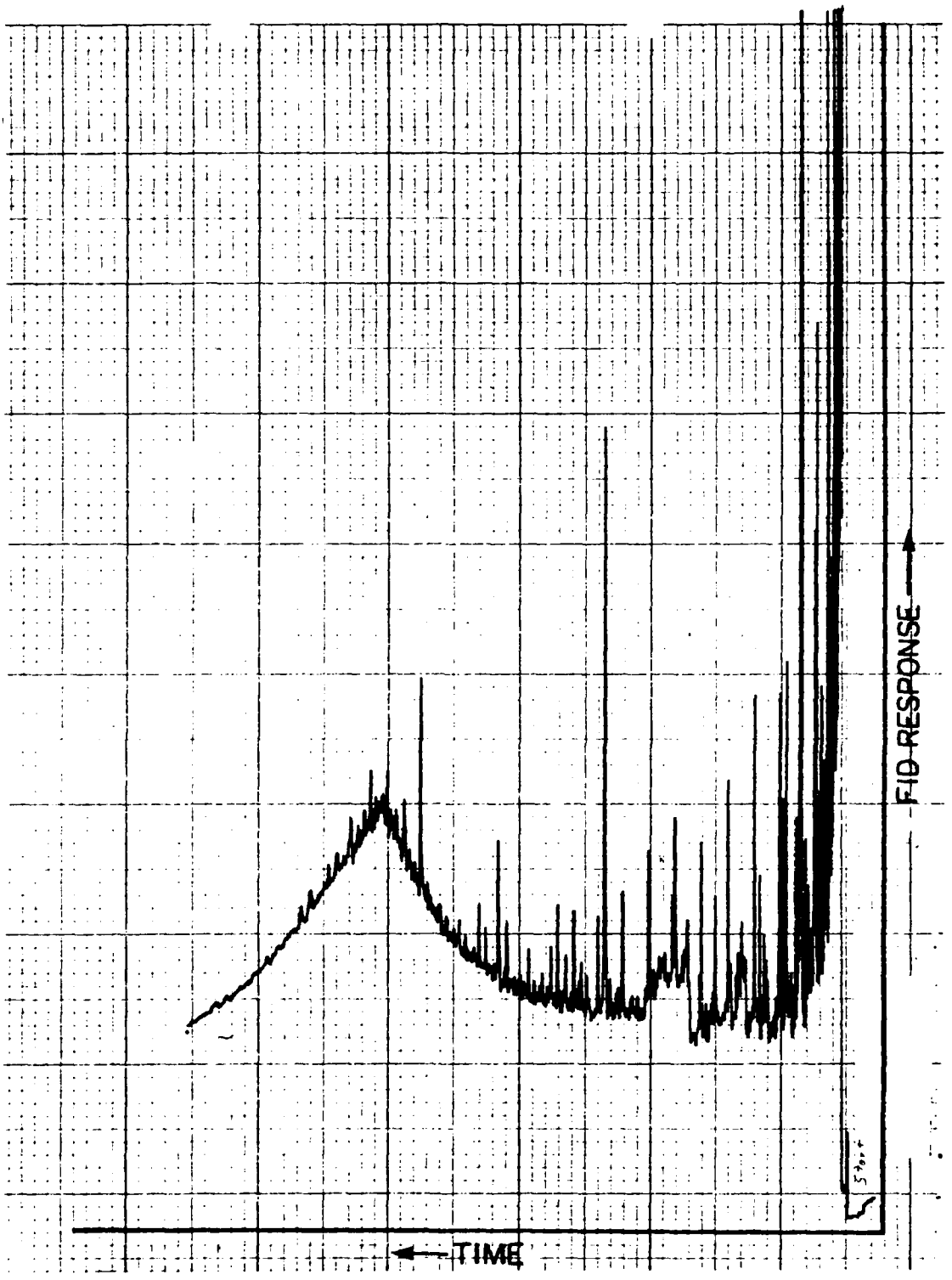

Figure 48. Gas Chromatogram of Stressed Vac Kote (MLO 76-137); Conditions same as in Figure 48.

is difficult to analyze primarily because it is composed of a mixture of acid moieties which defy resolution. Derivatization has been shown to increase the sensitivity of naphthenic acids by liquid chromatography, but still lacks the resolution required. Thermal stressing of Vac Kote and its components under these conditions is a method of simulating the chemical processes that may occur in the lubricant due to the high temperature that can occur in the metal to metal contact points of bearings. From the data gathered, it appears that the basestock oil (Apiezon C) is fairly resistant to thermal degradation as would be expected given the stability and relative non-reactivity of hydrocarbons. Very severe conditions are needed (700°F, 24 hours) before degradation is observed, and then it appears that the UV active species in the Apiezon C are less stable than the aliphatic (non-UV active) species. The thermal decomposition of the lead naphthenate occurs under much milder conditions and is noted by the formation of naphthenic acids and an unidentified black precipitate which appears to be a polymeric material.

5. RECOMMENDATIONS

A. Analytical Methods Development

The analysis of Apiezon C by capillary gas chromatography yielded data that was difficult to handle and interpret. A more useful analysis may involve the use of the simulated distillation technique. In this method, a short packed tubular column is used to analyze the boiling point distribution of a sample by calibration with appropriate standards. Such data would be much more quantitatively meaningful than the GC detection methods already developed as it would be more easily interpreted with respect to influences upon the physical properties (i.e. viscosity) and thus performance of the lubricant in 'real life' testing.

Other methods of derivatization of the naphthenate moiety (from the lead naphthenate) for the purpose of analysis by capillary gas chromatography should be developed. Efforts at

this approach are hindered somewhat by the almost total lack of reported methods for the analysis of lead carboxylate type compounds in either the literature or from discussions with application chemists at various companies contacted. Nevertheless some candidates for trial include the methyl, trimethylsilyl, and pentafluorobenzyl esters (the latter detectable by an Electron Capture Detector). As other candidate lubricants (such as synthetic hydrocarbons) are submitted for evaluation, analytical methods will require development.

B. Accelerated Testing of Lubricant

Present and future methods of analysis of Vac Kote and other candidate lubricants will be required to evaluate chemical changes in the lubricant during artifical, accelerated, and 'real life' testing. Thermal stressing of Vac Kote and its' components will be required in order to further elucidate thermal degradation mechanisms, particularly of the lead naphthenate additive. Effects of evaporative depletion on Vac Kote should be attempted by distillation of 5, 10, and 15 percent of Apiezon C, and back formulating the additives to produce an 'evaporatively depleted' Vac Kote. Hopefully such work will result in the production of Vac Kote samples of known degradation for testing in despin mechanical assembly rigs. Finally, chemical analysis of 'real life' tested lubricants in despin mechanical assembly and slip ring rigs is required.

REFERENCES

1. Martin, R.W. and Brooks, F.C., "Instrumentation for Long-Term Slip Ring Experiments," Instrumentation in the Aerospace Industry, Volume 26, ISA 87664-473-6, Instrument Society of America, 67 Alexander Drive, Research Triangle Park, NC 27709, 1980, pp 485-492.

2. Martin, R.W., "Long-Term Slip Ring Data and Analysis," Interim Technical Report, UDR-TR-81-86, August 1981, pp 2-9.

3. Beitel, F.E., "Users Guide, Long-Term Brush Rig Software," Special Technical Report, UDR-TM-79-22, September 1979.

4. Op. cit., Ref. (2), pp 11-30.

5. Arkin, H. and Colton, R.R., "Statistical Methods," Barnes and Noble, Inc., New York, NY, 1971.

6. Op. cit., Ref. (2), pp 30-63.

7. Rosen, C., "System Transmission Parameters Design for Threshold Performance", Tutorial Program Fundamentals of Aerospace Instrumentation, Volume 12, ISA 87664-474-4, Instrument Society of America, 67 Alexander Drive, Research Triangle Park, NC, 27709, 1980, pp 1-38.

8. Tyler, J.C., Carper, H.J., Brown, R.D. and Ku, P.M., "Analysis of Film Thickness Effect in Slow-Speed Lightly Loaded Elastohydrodynamic Contacts," AFML-TR-74-189, Part I, December 1974.

9. Dictionary of Scientific and Technical Terms, McGraw Hill, Inc., New York 1974.

10. Borch, R.F., Anal. Chem., 47, 2437 (1975).